FITTING OF POTENTIAL-ENERGY CURVES AND SURFACES AND DYNAMICS OF A MODEL SIX-CENTER EXCHANGE REACTION

by

SUKARMA RANI THAREJA

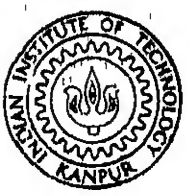

DEPARTMENT OF CHEMISTRY

INDIAN INSTITUTE OF TECHNOLOGY KANPUR

DECEMBER, 1985

FITTING OF POTENTIAL-ENERGY CURVES AND SURFACES AND DYNAMICS OF A MODEL SIX-CENTER EXCHANGE REACTION

A Thesis Submitted
in Partial Fulfilment of the Requirements
for the Degree of

DOCTOR OF PHILOSOPHY

by

SUKARMA RANI THAREJA

to the

DEPARTMENT OF CHEMISTRY

INDIAN INSTITUTE OF TECHNOLOGY KANPUR

DECEMBER, 1985

To my husband

STATEMENT

I hereby declare that the matter embodied in this thesis is the result of investigations carried out by me in the Department of Chemistry, Indian Institute of Technology, Kanpur, India, under the supervision of Professor N. Sathyamurthy.

In keeping with the general practice of reporting scientific observations, due acknowledgement has been made wherever the work described is based on the findings of other investigators.

Sukarma Rani Thareja

December 4, 1985

Sukarma Rani Thareja
Candidate

DEPARTMENT OF CHEMISTRY
INDIAN INSTITUTE OF TECHNOLOGY KANPUR, INDIA

CERTIFICATE I

This is to certify that Ms. Sukarma Rani Thareja has satisfactorily completed all the courses required for her Ph.D. Degree programme. These courses include:

Chm 500	Basic Course in Mathematics I
Chm 521	Chemical Binding
Chm 524	Modern Physical Methods in Chemistry
Chm 541	Advanced Inorganic Chemistry I
Chm 800	General Seminar
Chm 801	Graduate Seminar
Chm 900	Research

Ms. Sukarma Rani Thareja was admitted to the candidacy of the Ph.D. Degree in May 1982 after she successfully completed the written and oral qualifying examinations.

P.T. Narasimhan 4/12/85
(P.T. NARASIMHAN)
Head,
Department of Chemistry,
IIT KANPUR

P C Nigam
(P.C. NIGAM)
Convenor,
Departmental Post-Graduate
Committee
Department of Chemistry,
IIT KANPUR

4-12-85

CERTIFICATE II

Certified that the work contained in this thesis entitled, "FITTING OF POTENTIAL-ENERGY CURVES AND SURFACES AND DYNAMICS OF A MODEL SIX-CENTER EXCHANGE REACTION" has been carried out by Ms. Sukarma Rani Thareja under my supervision and the same has not been submitted elsewhere for a degree.

N Sathyamurthy

(N. SATHYAMURTHY)
Thesis Supervisor
Professor of Chemistry
IIT KANPUR

Kanpur

December 4 , 1985

ACKNOWLEDGEMENTS

It is a great pleasure to express my sincere gratitude and appreciation to my thesis supervisor Professor N. Sathyamurthy for his constant guidance and encouragement through out this research work.

I take immense pleasure in dedicating this thesis to my husband, Dr. Raj Kumar Thareja.

I am thankful to my daughter Prachi, my parents Mrs. and Mr. Satyananda Talwar, my mother-in-law and Mr. K.C. Thareja for their constant moral support.

I am thankful to all the members in our laboratory and in particular to Raghavan for many discussions during the course of this work.

I sincerely thank the staff of the Computer Center for their co-operation and help.

Finally I thank Mr.R.K. Bajpai for drawing the figures and Mr. U.S. Mishra for his excellent typing of this thesis.

Sukarma Rani Thareja

ABSTRACT

In this thesis we report the results of a study of fitting of repulsive potential-energy (PF) curves for a few diatomic species and the ground and the first excited state surfaces for H_3 and of a quasiclassical trajectory (QCT) study of a model six-center exchange reaction.

We have made a comparative study of various analytic functions for fitting repulsive curves, using $H_2(^3\Sigma_u^+)$ as a test case. Exponential-poly function is found to be the best. Although the anti-Morse function is not as good as the exponential-poly, the former offers an advantage over the latter in that it could be extended to higher dimensions. We have found the rotated-anti-Morse-curve-spline to give a good representation of the potential-energy surface (PES) for H_3^* for linear as well as fixed nonlinear geometries.

We have tested the utility of the Sorbie-Murrell (SM) function to fit the ground and the first excited state PES of H_3 using the chemically accurate PE values of Siegbahn and Liu for the ground state and slightly less accurate values of Nager and Jungen for the excited state. Static properties like minimum-energy-path, classical barrier height, force constant etc. of the ground state SM surface are in good agreement with those of the Truhlar-Horowitz (SLTH)

fit. Results of time-dependent quantum mechanical scattering calculations for the collinear geometry using the SM surface are also in accord with the results obtained on the SLTH surface.

We report, for the first time, results of a quasiclassical trajectory study of a model six-center exchange reaction

$$H_2...H_2 + H_2 \rightarrow H_2 + H_2 + H_2$$

over a wide range of relative translational energies (E_T) and for different vibrational states (v). We find that at low E_T (90-130 kcal.mol^{-1}), a four-center exchange reaction takes place with one of the molecules of the dimer acting as a mediating partner. At relatively higher E_T (135-155 kcal.mol)$^{-1}$ for v = 8-11 of the dimer and the non-dimer molecules, a 'proper' six-center exchange reaction, with three/two/one stable molecule(s) as the products is observed. On the whole, we find that v is more effective than E_T in causing the reaction.

CONTENTS

LIST OF ABBREVIATIONS

c.m.	Center of mass
ER	Extended Rydberg
LCAO-MO-SCF	Linear combination of atomic orbitals-molecular orbitals-self consistent field
LEPS	London-Eyring-Polanyi-Sato
MEP	Minimum energy path
PE	Potential energy
PES	Potential-energy surface
QCT	Quasiclassical trajectory
RAMCS	Rotated-anti-Morse-curve-spline
RMCS	Rotated-Morse-curve-spline
SM	Sorbie Murrell
SLTH	Siegbahn-Liu-Truhlar-Horowitz
TDQM	Time-dependent quantum mechanical
VDW	van der Waals
1D	One dimensional
2D	Two dimensional
3D	Three dimensional
4C	Four-center
6C	Six-center

LIST OF SYMBOLS

b	Impact parameter
E_a	Activation energy
E_b	Classical barrier height
E_{int}	Internal kinetic energy
E_{rot}	Rotational energy
E_T	Relative translational energy
E_{th}	Threshold energy
E_{TOT}	Total internal energy
E_{vib}	Vibrational energy
I	Moment of inertia
k	Specific rate constant
M_{ij}	Internal angular momentum for the i-j pair
P	Total linear momentum
P^R	Reaction probability
P_v	Vibrational momentum
r_{ij}	Internuclear distance between i and j pair
R_s	Reaction shell radius
TA	Range factor
v	Vibrational quantum number
γ	Apex angle defined as HγH
μ	Reduced mass
ω	Angular velocity
σ^R	Reaction cross section
Θ	Rotating angle used in RAMCS.

CHAPTER ONE

INTRODUCTION

Any molecular dynamical calculation[1-4] is carried out by solving quantal or classical equations of motion for the nuclei on an adiabatic potential-energy surface (PES) and hence requires a detailed knowledge of the interaction potential. This is obtained by solving the electronic Schrödinger equation, within the Born-Oppenheimer approximation, for a series of nuclear geometries, on an electronic computer. Although this can be achieved almost routinely by using some of the readily available software packages[5] like Gaussian 80 for a variety of systems, the enormity of the task of getting an ab initio PES of chemical accuracy ($\pm$ 1 kcal.mol^{-1}) can be realised from the fact that the number of systems for which such surfaces are available (for example, see ref. 6-9) can be counted by the fingers in one hand. Further, results of such calculations are available in the form of tables of numbers and for any subsequent dynamical calculation, these numbers have to be interpolated (and extrapolated if necessary) so that the potential and its derivative(s) may be computed at any arbitrary geometry during the simulation of the molecular collision. Here lies a 'bottle neck' in going from an ab initio electronic structure calculation to a molecular reaction dynamical study.

To fit the potential energy (PE) values in one dimension (1D - one independent variable, for instance, bond distance for a diatom) is fairly straightforward. The variety of analytical functions and numerical methods that are available in the literature have been reviewed elsewhere[10,11]. Yet, one finds that fitting a PE curve with no minimum in it can be frustrating. Therefore, we have undertaken[12] a comparative study of various different repulsive analytic functions using $H_2^*(^3\Sigma_u^+)$[13] as a test case. We have also tried the different functional fits for the ab initio potential data for Fe_2[14], HeH[15] and NaLi[16]. Details of the different functions used and a summary of our findings are given in Chapter 2.

Fitting PE values as a function of two independent variables (two dimensions : 2D) is more difficult than fitting a function to data in 1D. The choice of the functional form to be used for fitting is decided by the nature of the problem and the coordinates in which the data are available. The PE values for collinear and fixed nonlinear geometries were available[17] for H_3^* (2pE') in rotated-Morse-curve-spline (RMCS) coordinates. Therefore we have tested the utility of a rotated-anti-Morse-curve-spline (RAMCS) approach to fit the purely repulsive potential H_3^* (2pE'). Details of the fitting procedure and the parameters of the resulting fits are included in Chapter 2.

Fitting data in three dimensions (3D) is a much more difficult task and the state of the art is presented elsewhere[10,11]. We only wish to point out here that the Sorbie-Murrell (SM) function[18] has been found to be successful in fitting ab initio PES for several systems: H_3[19], H_2O[20,21], LiFH[22], FH_2[22], NH_2^+[23], CH_2^+[24] and HeH_2^+[25].

Interestingly, its utility in fitting the most accurate ab initio PES of Siegbahn and Liu[6-8] for H_3 has not been tested. While it is true that Truhlar and Horowitz[26] have provided an excellent analytical representation of the surface and that its quality of fitting, with a root-mean-square (rms) deviation of 0.17 kcal.mol^{-1} may remain unsurpassed for some time to come, it would be admitted that it is not general in nature. Therefore, we have undertaken to test the utility of the SM function in fitting the Siegbahn-Liu PES. We have also tried to use it in fitting the PES for the lowest excited state (2pE') of H_3 by using the ab initio data of Nager and Jungen[27]. We have scrutinised the quality of the ground state fit by examining static properties like, barrier height, saddle point location, minimum energy path etc and also by comparing the results of a time-dependent quantum mechanical (TDQM) calculation of the probability for the collinear reaction

$$H + H_2 \rightarrow H_2 + H \qquad (R1)$$

on the SM surface with those on the Siegbahn-Liu-Truhlar-

Horowitz (SLTH) PES. The details are given in Chapter 3.

The original aim of the present study was also to use the approach of Varandas and Murrell[19] via the SM function to obtain a double-valued functional representation of the PES for the ground and the first excited state of H_3. Some aspects of this attempt are included in Chapter 3.

Traditionally, reactions like

$$H_2 + I_2 \rightarrow 2HI \qquad (R2)$$

were thought to go via a four-center (4C) transition state. But this picture started changing in the 60's. The above reaction was shown[28] to proceed via an atomic mechanism. For the hydrogen-deuterium exchange reaction

$$H_2 + D_2 \rightarrow 2HD \qquad (R3)$$

shock-tube studies[29-32] yielded an activation energy (E_a) of 42 kcal.mol^{-1}. The results were explained by a 4C mechanism postulating a vibrational excitation of the reactant molecules, but the recent laser-beam experimental study[33] of the reverse reaction

$$HD + HD \rightarrow H_2 + D_2 \qquad (R4)$$

has shown that this 4C reaction does not occur even when one of the reactant molecules is excited up to the vibrational state v = 5.

Extensive ab initio calculations (for example, see ref.[34] and references therein) yielded a classical barrier height (E_b) for the 4C reaction that was larger than the bond dissociation energy of H_2. Detailed quasi-classical trajectory (QCT) calculations of Brown and Silver[35] also failed to produce any exchange products via the 4C pathway.

Woodward-Hoffman rules[36] also suggested that the reactions (R2) and (R3) may not proceed through a 4C transition state. For such a pathway, the electronic ground state of the reactants is not correlated with the electronic ground state of the products and as a result, a large barrier for the reaction may result. Wright[37,38] suggested a six-center (6C) mechanism as an alternative as his LCAO-MO-SCF calculations yielded an E_b of 90 kcal. mol^{-1} significantly below the dissociation energy of H_2. Thompson and Suzukawa[39] used a semiempirical approach and obtained an E_b of 88 $kcal.mol^{-1}$ for the 6C pathway. Dixon et al[40] used a large basis set for their ab initio calculation and obtained an E_b of 69 $kcal.mol^{-1}$. With a still larger basis set, the E_b of the reaction may get lower still!

Crossed molecular beam experiments of Dixon and Herschbach[41,42] gave further support to the 6C mechanism.

The reaction

$$Cl_2 + Br_2 \rightarrow 2\ BrCl \qquad (R5)$$

did not occur at collision energies (E_T) around 25 kcal.mol^{-1}. However, at high pressures and low temperatures in the supersonic nozzle expansion, where there was a high concentration of $(Cl_2)_2$ they found the reaction to proceed at E_T as low as $\simeq$ 3 kcal.mol^{-1}. They attributed their results to

$$Cl_2....Cl_2 + Br_2 \rightarrow Cl_2 + 2\ BrCl$$
$$\rightarrow BrCl....Cl_2 + BrCl \qquad (R6)$$

involving a 6C transition state.

We have undertaken a detailed QCT study of a model 6C exchange reaction. We have used the diatomics-in-molecules approach to construct the PES. The parameters were adjusted so that E_b has the same value as reported by Dixon et al.[40] We have computed the reaction cross section (σ^R) over a wide range of E_T: 90-135 kcal.mol^{-1} for different v states of the diatoms. Details of the method and the results are given in Chapter 4.

A summary of our work and the conclusions are presented in Chapter 5.

CHAPTER TWO

FITTING REPULSIVE POTENTIAL-ENERGY CURVES AND SURFACES

2.1 Repulsive Curves

The first attempt to represent a repulsive PE curve was perhaps by Sato[43] and was for the triplet state ($^3\Sigma_u^+$) of H_2. He had used an anti-Morse function of the form

$$V = \frac{D}{2}\{\exp(-2\beta\rho) + 2\exp(-\beta\rho)\}, \rho = r - r_e \qquad (1)$$

where D, r_e and β are the bond dissociation energy, equilibrium bond distance and the curvature parameter respectively for the ground state ($^1\Sigma_g^+$) of H_2 and have no such physical meaning for the triplet state.

Pedersen and Porter[44] had extended the function by matching it with an exponential function at a longer range

$$\begin{aligned} V &= A\{e^{-2\beta\rho} + 2e^{-\beta\rho}\}, r < 1.6 \text{ au} \\ &= b(r+c)e^{-\alpha r}, r > 1.6 \text{ au} \end{aligned} \qquad (2)$$

and were able to fit the ab initio potentials for H_2 and H_2^+ ($^2\Sigma_u^+$).[45,46] Kuntz and Roach[47] modified the anti-Morse function further by allowing β to be a variable:

$$\beta = \beta(1 + \gamma\rho + \delta\rho^2) \qquad (3)$$

and fitted the potentials for H_2 and H_2^+ successfully.[45,48] Berces[49] has shown that

$$V = (D/\alpha)\ \exp\ (-2\beta\rho)\ \{1 + (\beta\rho)^{2\alpha}\} \qquad (4)$$

is also more flexible than the anti-Morse in fitting the triplet PE curve of H_2, HI and I_2. Kafri and Berry[50] used an exponential with a polynomial exponent for fitting the ab initio data of Kolos and Wolniewicz[45]

$$V = \exp(-(a_o + a_1 r + a_2 r^2 + a_3 r^3 + a_4 r^4 + a_5 r^5)) \qquad (5)$$

Stine and Muckerman[51] used 1D spline[52] for fitting the PE curve for $H_2^+(^2\Sigma_u^+)$. Sonneleitner and Beckel[53] have shown that rational fractions can be used to reproduce the potential for $H_2^+(2p\sigma_u)$[54].

More recently Varandas and Brandão[55] have proposed the use of an exponential multiplied by an r^{-1}

$$V = A\ r^{-1}\ \exp(-b\rho) \qquad (6)$$

for alkali dimers in their $^3\Sigma$ state. Almost a decade ago Murrell and Sorbie[56] had proposed the use of an extended Rydberg (ER) function

$$V = -D\ \exp\ (-a_1\rho)\ \{1 + a_1\rho + a_2\rho^2 + \ldots\} \qquad (7)$$

for fitting potentials with a single minimum. But there is no reason why it cannot be used to fit a repulsive curve in the same way as an anti-Morse function. Huxley et al[57] have reported recently that an appended ER function

$$V = A\ (1 + a_1 r + a_2 r^2 + a_3 r^3)\ \exp(-a_4 r) - \tanh\ (r - r_m/2) \times (C_6 r^{-6} + C_8 r^{-8} + C_{10} r^{-10}) \qquad (8)$$

performs better than the ER in fitting a repulsive potential with a van der Waals minimum for a large number of diatomic species. In principle, given adequate data, the PE values can be fitted by a polynomial or better still by a 1D spline or Akima[58] interpolation. In practice, one prefers a simple analytic function with a few parameters to be determined.

To the best of our knowledge, no comparative study has been made of the validity of these various functions in fitting the data for a single system. The obvious choice for a test case would be the $^3\Sigma_u^+$ state of H_2 for which accurate ab initio values are available[45]. We have undertaken such a study and the results are summarized below. We must mention that we have only considered global functions in this study and not considered the use of piecewise interpolation methods. We have specifically considered only the anti-Morse[43], Berces[49], exponential-poly,[50] modified exponential[55] and the ER[56] functions as we are interested in functions which require only limited input data and also are extendable to higher dimensions.

Ab initio values[45] of lnV for H_2 ($^3\Sigma_u^+$) are plotted against r in fig. 1 and for comparison, the different analytically fitted potentials are shown in the same graph.

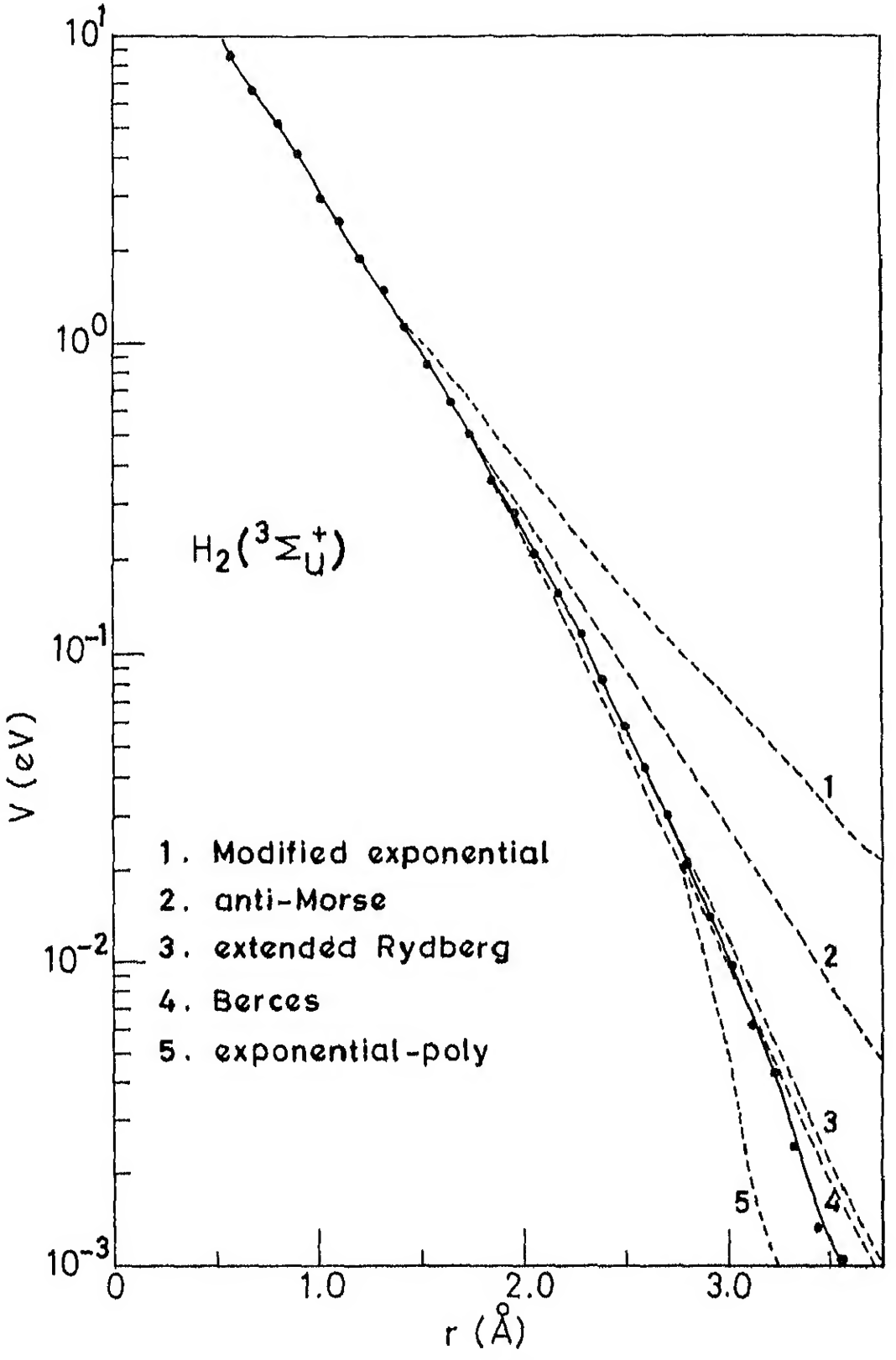

Fig.1 Comparison of different analytic fits to the ab initio data for $H_2(^3\Sigma_u^+)$. The ab initio PE values are connected by a solid line. The dashed lines represent the different functional fits.

The parameters for each function were determined by a nonlinear least squares fit of the ab initio data using the E04FCF program of NAG library[59]. The rms and the maximum deviation for each function are listed in Table 1.

The anti-Morse function fits the potential adequately at short range. The modification introduced by Berces improves the fit dramatically - but at the expense of adding a parameter. The exponential-poly function deviates much more than the Berces function at long range. But the former gives the best overall fit as is illustrated with the aid of a residual plot in fig. 2. The ER functional fit is only slightly inferior to the Berces, but involves as many parameters as the exponential-poly fit. The modified exponential function gives the poorest fit.

We have tried the different functional fits for the ab initio potentials for He_2, HeH and NaLi.[14-16] The results summarized in Table 1 show that while the anti-Morse fuction fits the potential reasonably, the exponential-poly gives a better fit for all the systems. The quality of the fit obtained by using the extended Rydberg function is comparable to that of the exponential-poly for He_2 and NaLi. Berces gives the worst fit for NaLi and extended Rydberg that for HeH. If a large number of potential-energy values are available and the number of parameters can be as large as six, the exponential-poly fit is obviously the best or close to being

TABLE 1 : Quality of fit of different analytic functions to the ab initio potential of a few selected diatomic systems

System	ref. for the ab initio data	range of r values /Å	range of V values /eV	Deviation[b,c] /eV				
				anti-Morse	Berces	exponential-poly	modified exponential	extended Rydberg
H_2	45	0.53-5.29 (85)	-0.002 -+10.30	3.6(-2) 14.4(-2)	1.5(-2) 3.8(-2)	0.4(-2) 1.2(-2)	10.1(-2) 28.6(-2)	2.3(-2) 17.9(-2)
He_2	14	1.58-5.29 (26)	-0.001 -(+)0.32	1.9(-3) 3.0(-3)	1.2(-3) 1.9(-3)	0.66 (-3) 1.0(-3)	1.7(-3) 2.7(-3)	0.7(-3) 1.1(-3)
HeH	15	2.64-4.76 (7)	0.00001 -(+)0.013	1.5(-5) 3.0(-5)	1.7(-5) 2.0(-5)	1.1(-5) 15.0(-5)	1.7(-5) 2.9(-5)	9.8(-5) 16.0(-5)
NaLi	16	2.65-7.98 (10)	0.0-0.65	6.4(-4) 10.0(-4)	18.0(-4) 39.0(-4)	1.6(-4) 3.4(-4)	5.0(-4) 8.0(-4)	1.4(-4) 2.3(-4)

[a] Values in parantheses give the number of r values.

[b] First row gives the r.m.s. deviation and second row the maximum deviation for each function.

[c] Values in parentheses give the powers of ten.

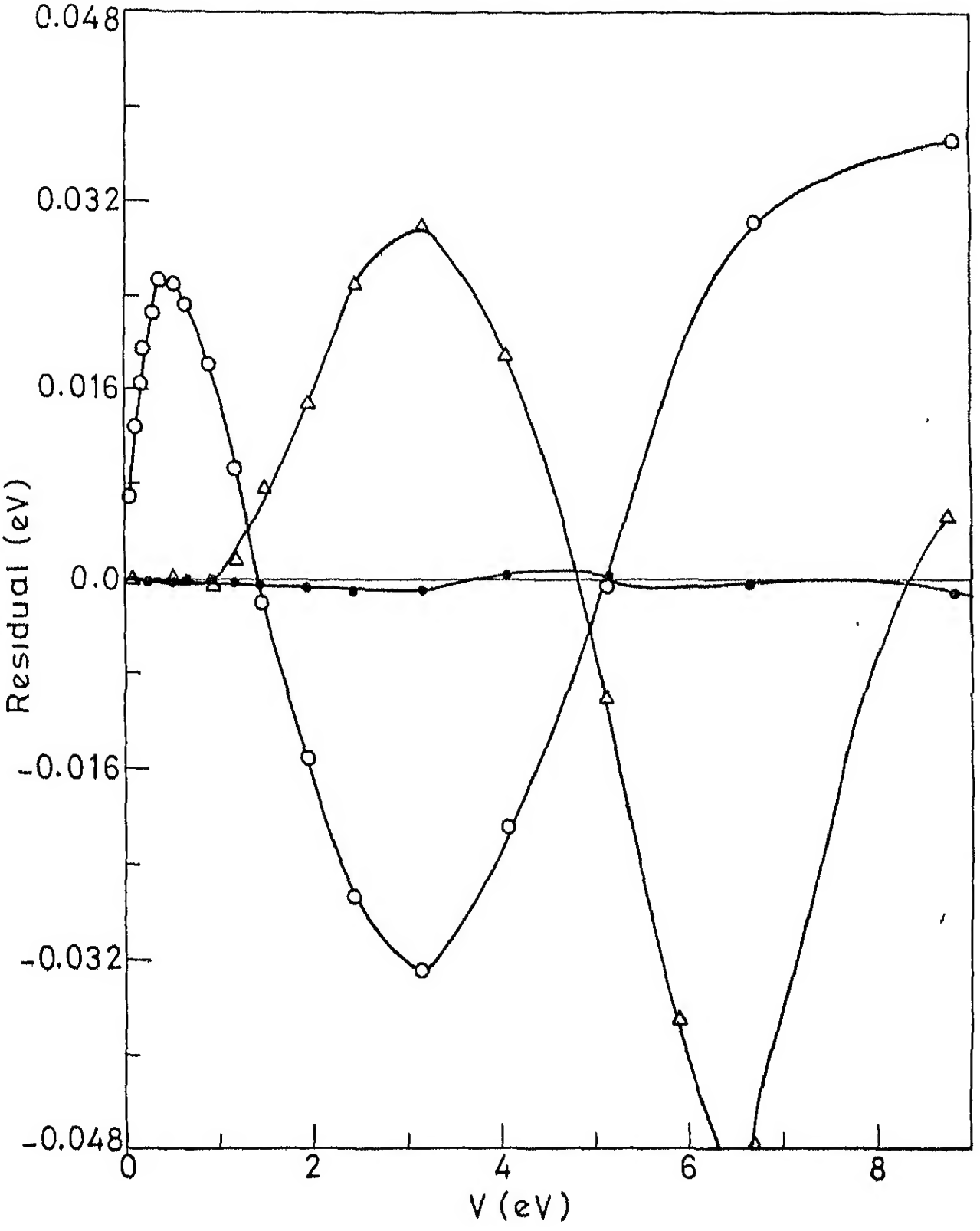

Fig.2 Residual plots comparing the performance of Berces (o) extended Rydberg (Δ) and exponential-poly (•) functions.

the best.

It also offers the advantage that lnV can be fitted to a polynomial by a linear-least-squares fit to yield an excellent set of initial guess parameters for carrying out a nonlinear-least-squares fit-an important practical advantage over the other functional approaches. On the other hand, if the number of parameters has to be as low as three, the anti-Morse function yields reasonable results and it also promises to be the candidate when PE values involving more than one independent variable are to be fitted.

2.2 Repulsive Surfaces

As a test case of a repulsive PES in 2-3 independent variables, we have examined the possibility of fitting the PES for H_3^* $(2pE')$ in its D_{3h} geometry . This surface is needed in the study of the spectroscopy of the transition state in predicting the wings to the Lyman-α line in $H + H_2$ collisions[60]. The amount of ab initio information available on this surface is scanty[61]. Therefore, at our request, Raynor[17] has computed a diatomic-in-molecules PES in rotated Morse coordinates[62] (ℓ, θ) (illustrated in fig.3) for linear as well as nonlinear geometries: three PE values along each ray, for θ = 0, 10, 20, 30, 35, 40, 42, 43, 44, 45° and hence by symmetry at θ = 46, 47, 48, 50, 55, 60, 70, 80, 90° for the bending angle γ = 60, 90, 120 and 180° .

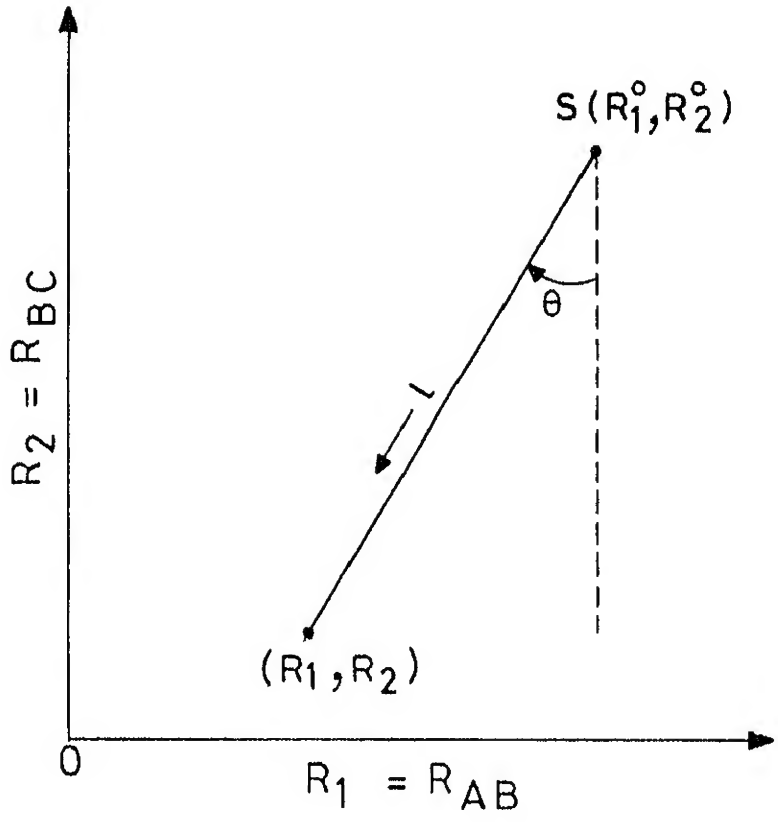

Fig. 3 Rotated - Morse-curve coordinates.

The idea of using a rotated Morse coordinate is that for $\theta = 0^{o}$, we have the PE curve for the reactant diatom and by rotating it about the swing point $S(R_1^o, R_2^o)$ through θ yields the PES, the $\theta = 90^{o}$ limit providing the PE curve for the product diatom. In principle, the Morse curve representation can be replaced by any other suitable representation. For H_3^*, only three data points are available along each ray and therefore, we were constrained to use only 3-parameter functions in our rotated-function approach. We tried to use

$$V = \exp(a_o + a_1\rho + a_2\rho^2) \qquad (9)$$

and

$$V = D\ell \exp(-a_1\ell)\{a_1 + a_2\ell\} \qquad (10)$$

which are the truncated and modified forms of the exponential-poly and ER functions respectively. We did not obtain satisfactory fits at low energies using eq. (9). Although eq. (10) gave a good fit along each ray, the variation of the parameters (D, a_1, a_2) with θ was not smooth. Hence we were not in a position to fit the H_3^* potential successfully using these two functions.

For the collinear geometry of H_3^*, the θ dependence of D, β and ℓ_e are shown in fig.4. These were subsequently fitted by 1D spline interpolation to obtain the overall fit.

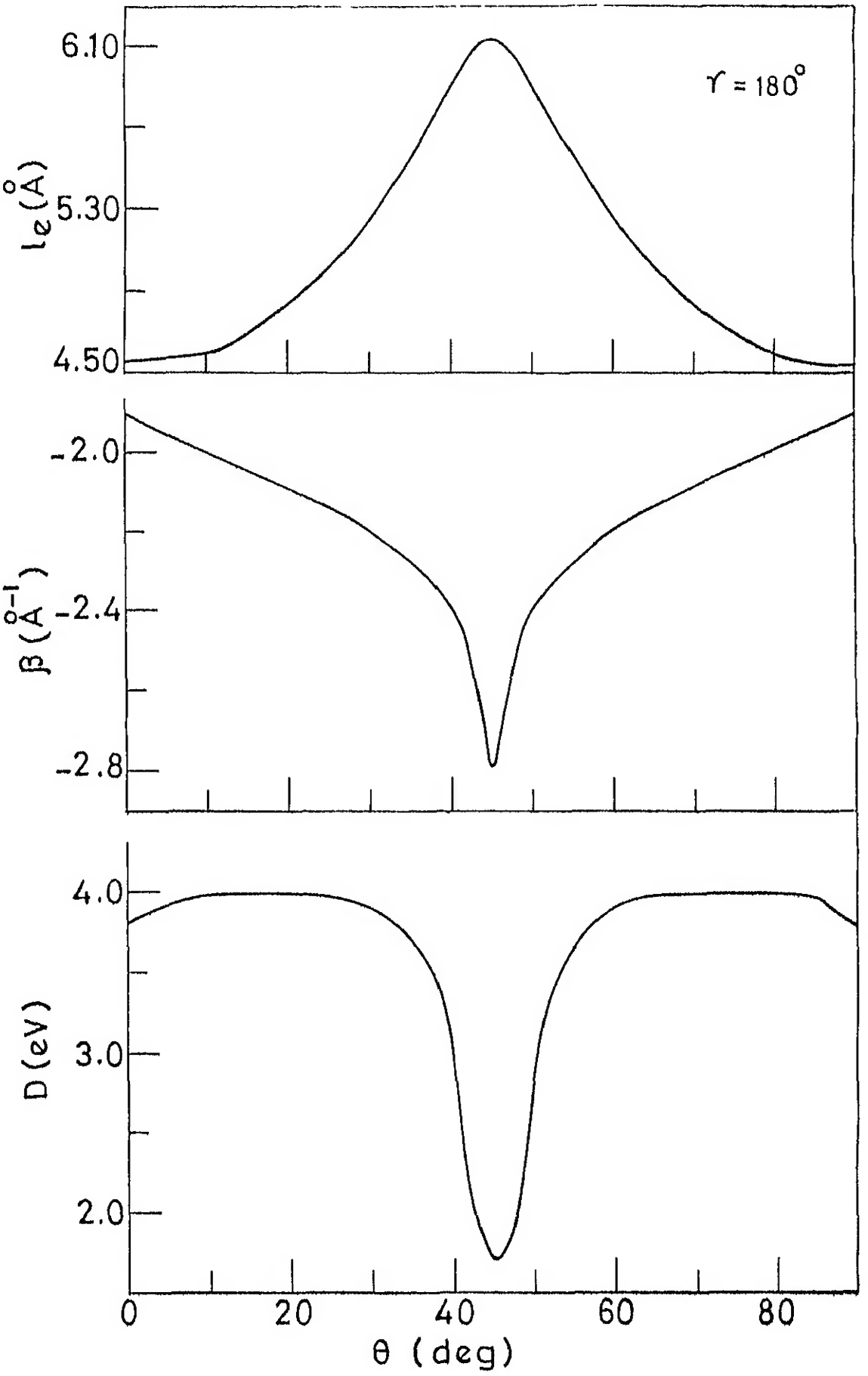

Fig.4 Dependence on θ of the anti-Morse parameters for collinear H_2^*

The resulting PES is illustrated with the aid of PE contours in fig.5. We were also able to obtain a similar fit to the potential for bent geometries The Θ-dependence of the parameters for γ = 120, 90, 60^{o} is illustrated in figs. 6-8 and it is comparable to that of γ = 180^{o} except for a double hump in $\ell_e(\theta)$ for γ = 60^{o}. The overall fit for γ = 120, 90, 60^{o} is illustrated with the aid of PE contours in figs. 9-11.

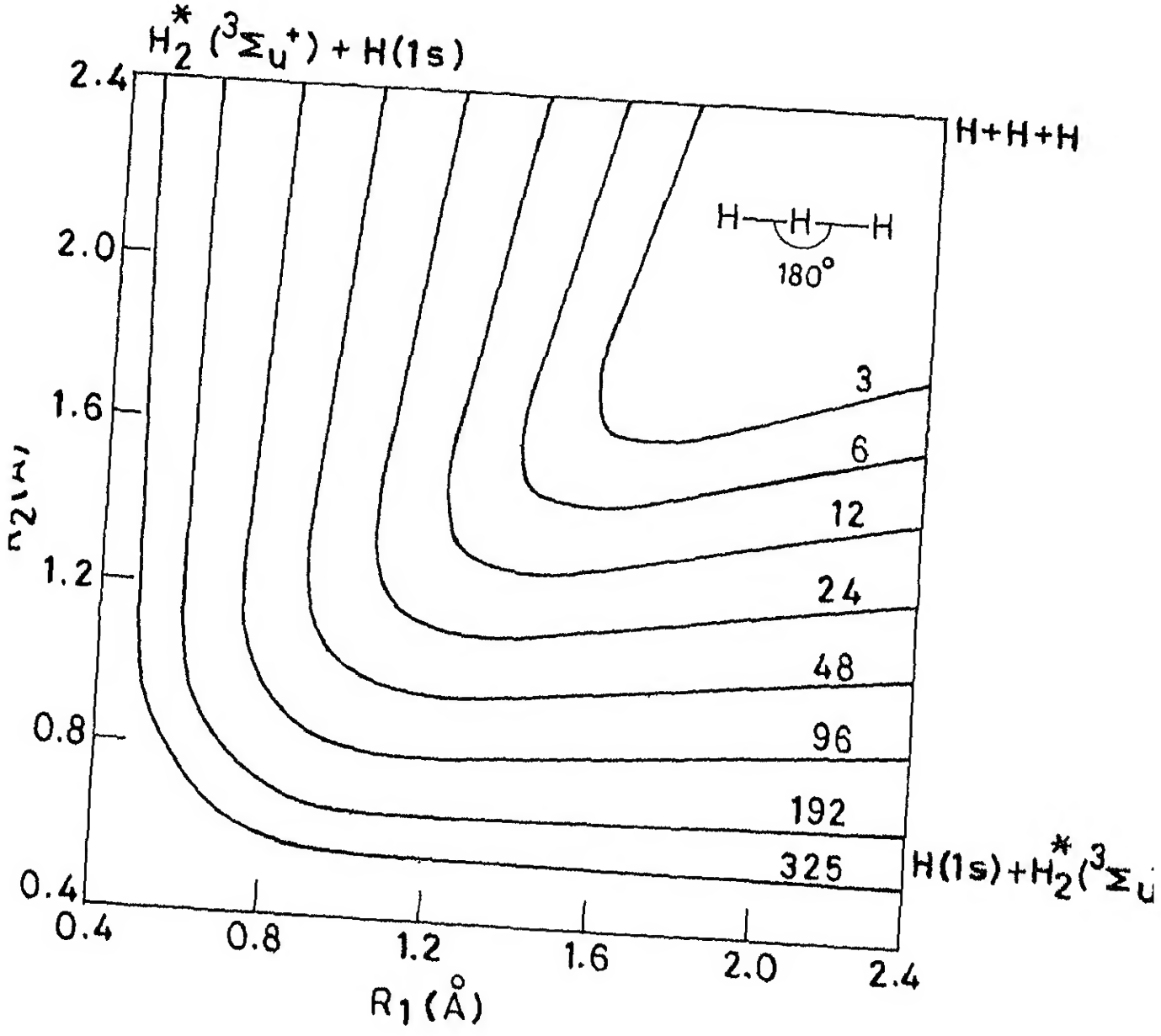

Fig. 5 PE contours for RAMCS fitted collinear H_3^* surface. The PE values are in kcal. mol^{-1} units relative to the separated atoms limit.

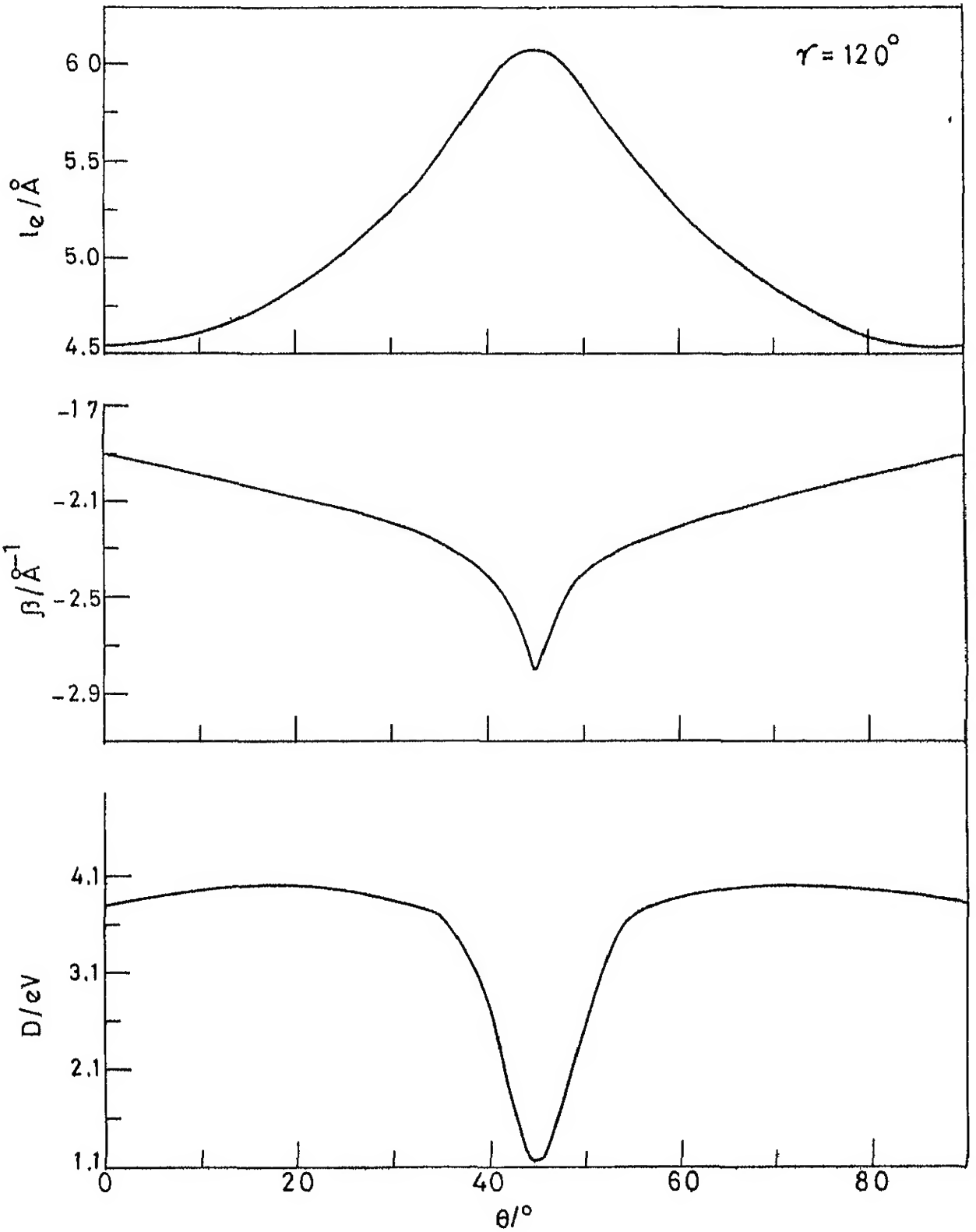

Fig. 6 Same as fig. 4 for $\gamma = 120°$.

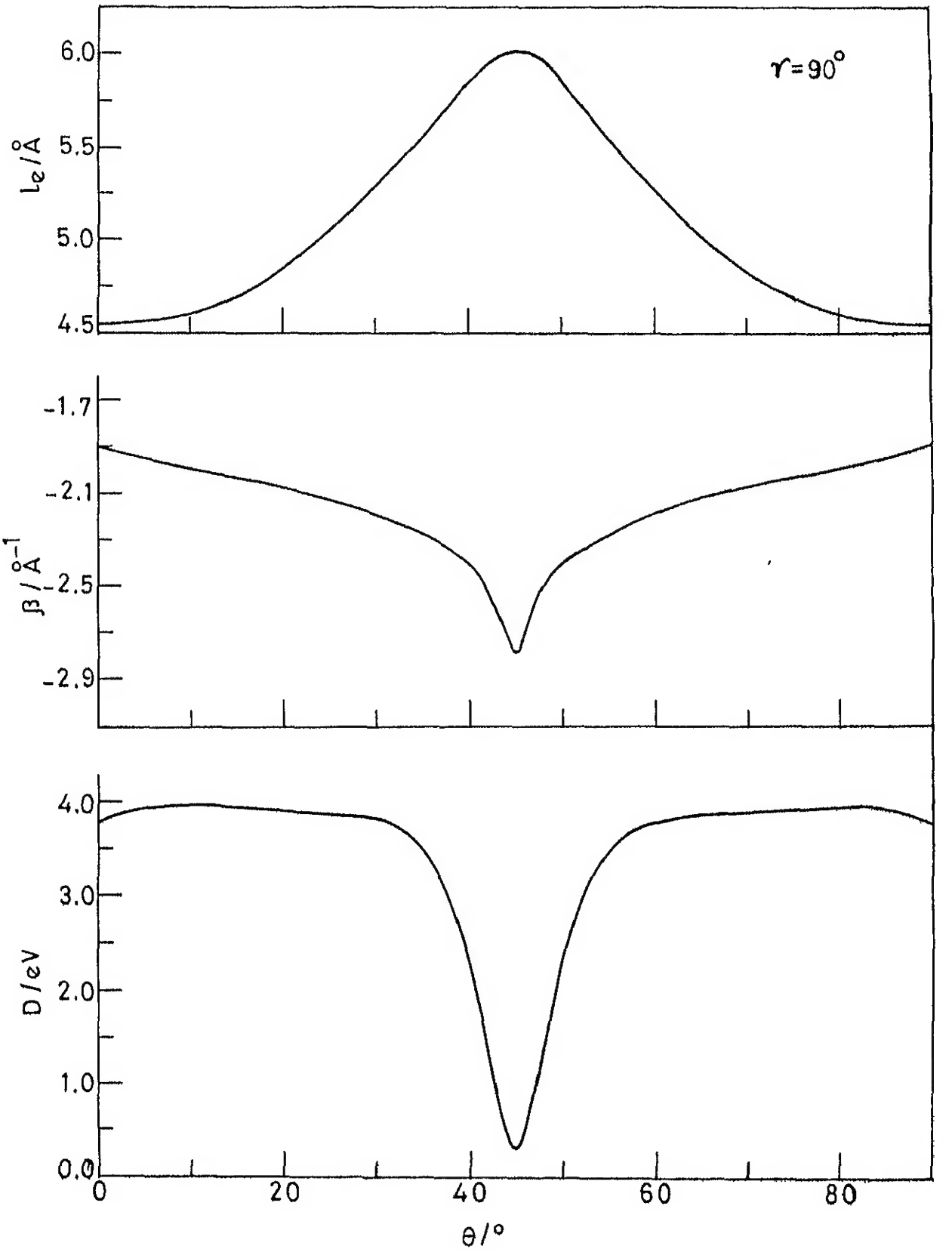

Fig. 7 Same as fig. 4 for $\gamma = 90°$.

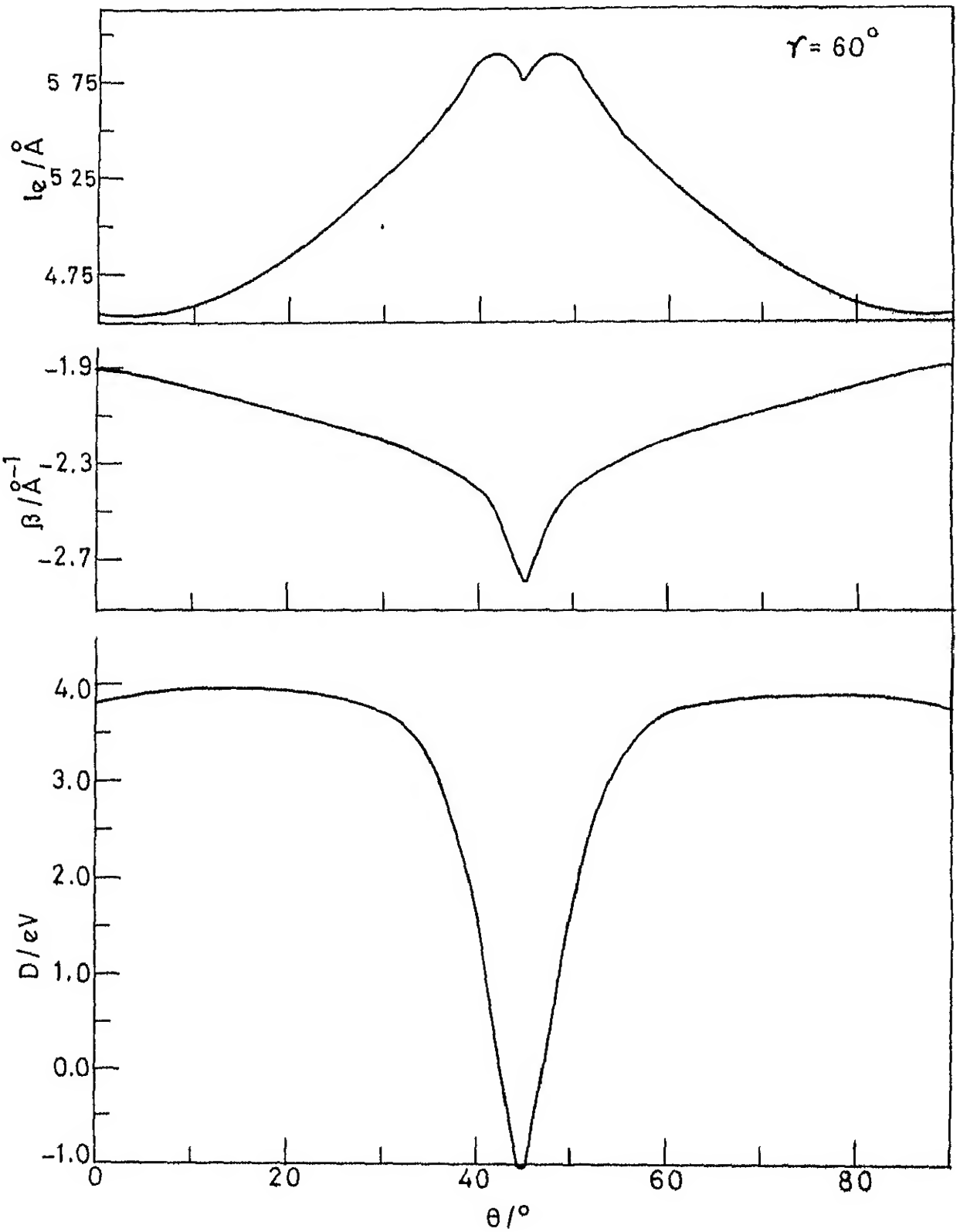

Fig. 8 Same as fig. 4 for $\gamma = 60^{\circ}$.

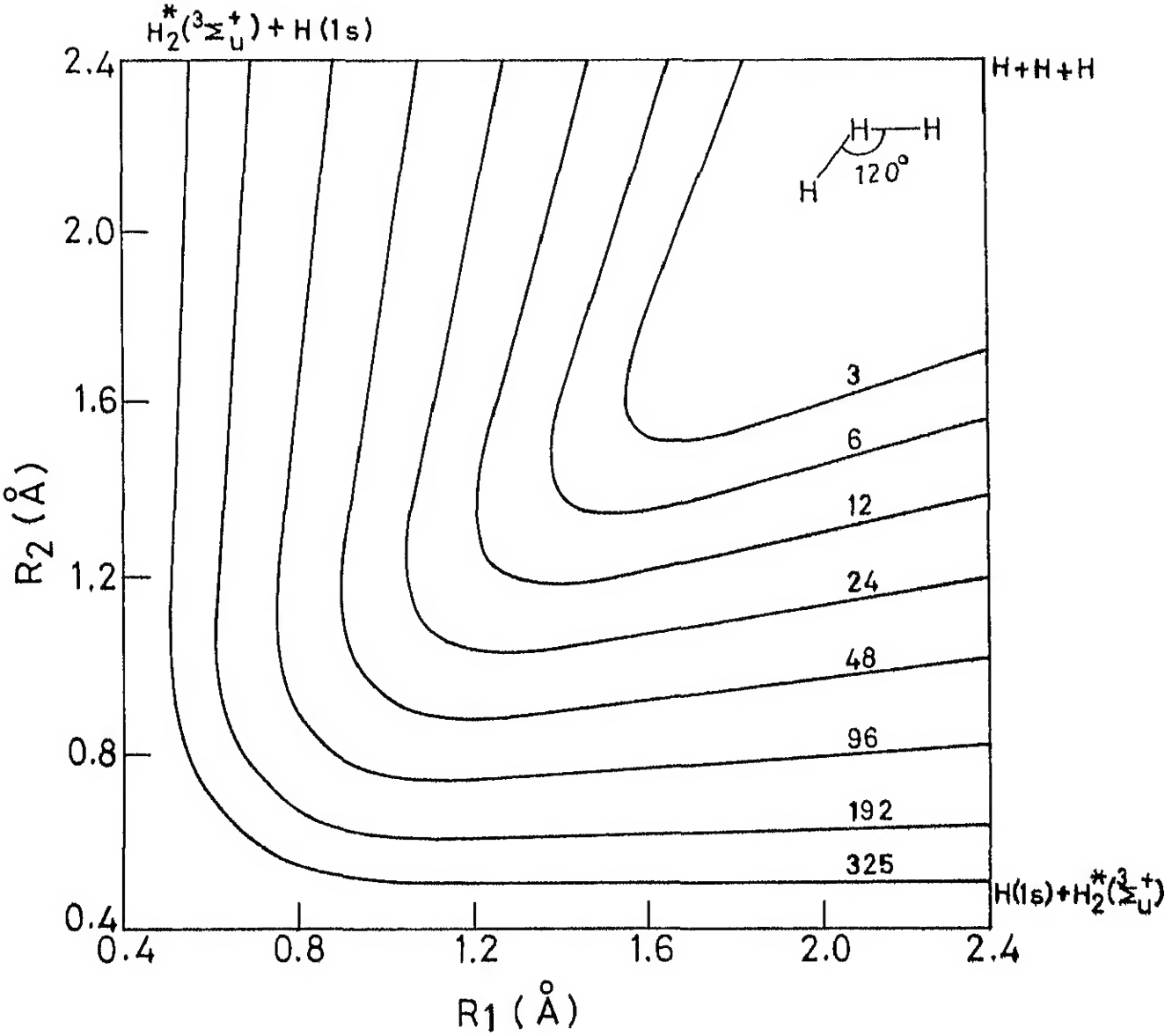

Fig. 9 Same as fig. 5 for $\gamma = 120°$.

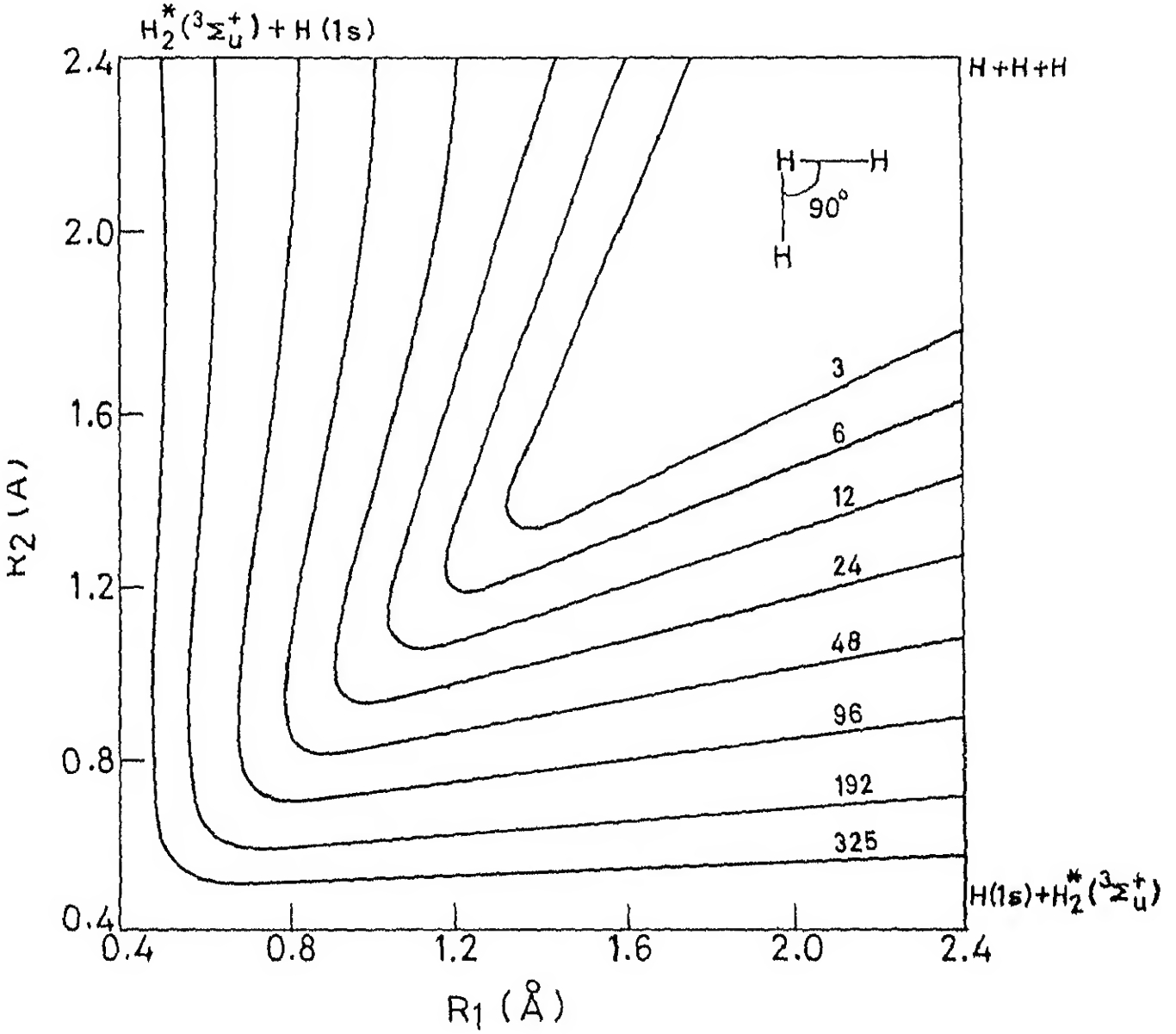

Fig. 10 Same as fig. 5 for $\gamma = 90°$.

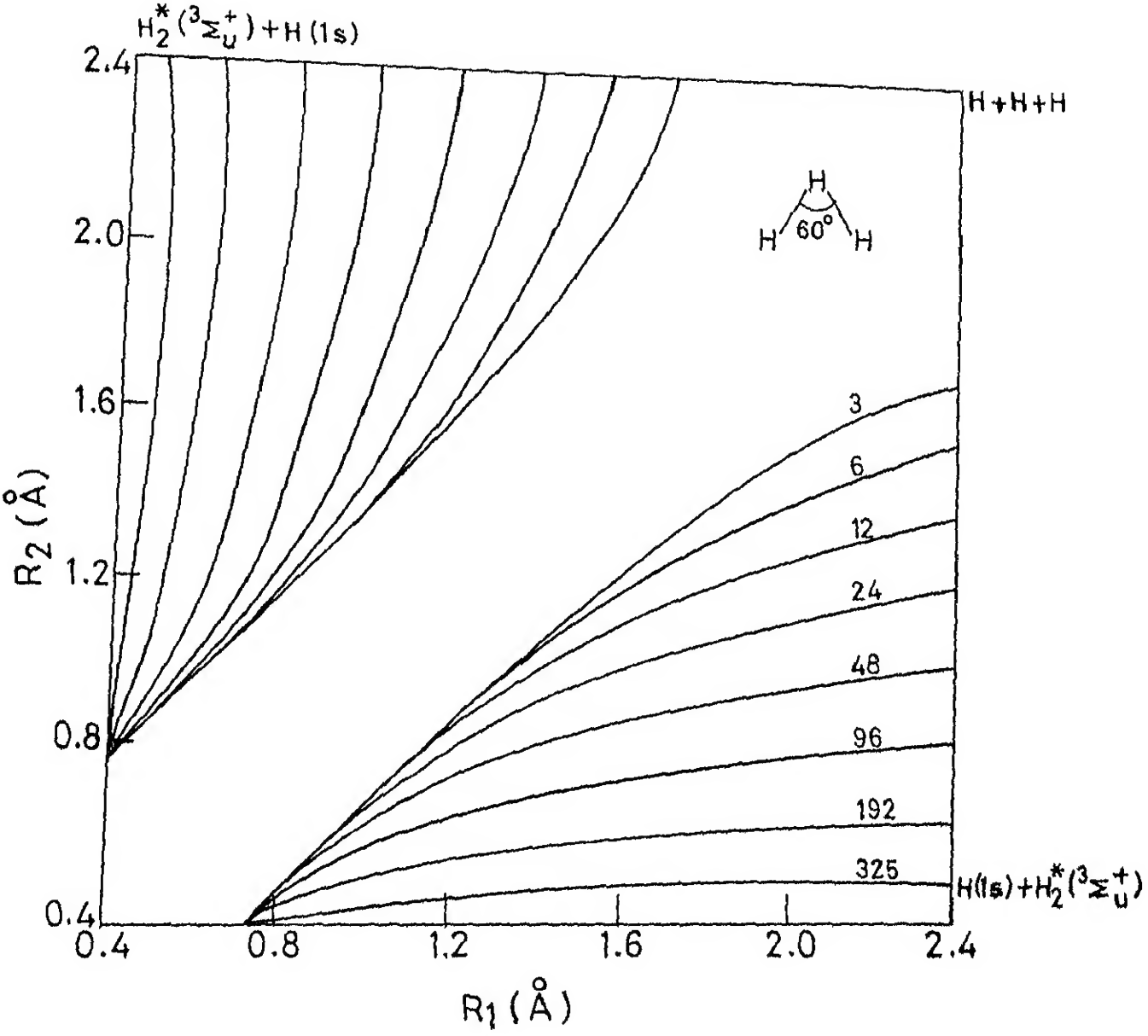

Fig. 11 Same as fig. 5 for $\gamma = 60°$.

CHAPTER THREE

SORBIE-MURRELL FUNCTIONAL FIT FOR THE PES FOR THE GROUND AND THE FIRST EXCITED STATE OF H_3

3.1 Ground State PES

For a triatomic system ABC, the SM functional representation of the PES is given by

$$V_{ABC} = V_A + V_B + V_C + V_{AB}(R_1) + V_{BC}(R_2) + V_{CA}(R_3) + V_I(R_1, R_2, R_3) \qquad (11)$$

where V_A, V_B, V_C are the monoatomic terms which can be set to zero, V_{AB}, V_{BC}, V_{CA} are the 2-body terms as a function of the bond distances R_1, R_2, R_3 respectively and V_I is the 3-body term that goes to zero as one of the $\{R_i\}$ values goes to infinity. We have used the FR function (eq.(7) in Chapter 2) to fit the 2-body potential, that is, the PE values of Kolos and Wolniewicz[13] for H_2. The resulting parameters as obtained by using the nonlinear least-squares fitting subroutine E04FCF of the NAG library[59] are reported in Table 2.

The 3-body interaction term is represented by

$$V_I = (P + P')TA \qquad (12)$$

where P and P' are polynomials and TA is a range factor. Because of the symmetry of the H_3 system, we use symmetry-

Table 2 · Parametersfor the Extended Rydberg Functional fit for $H_2(^1\Sigma_g^+)$

D /eV	4 747733
$r_e/\mathring{A}$	0 74139
$a_1/\mathring{A}^{-1}$	3.6720
$a_2/\mathring{A}^{-2}$	2.9869
$a_3/\mathring{A}^{-3}$	2.7045
$a_4/\mathring{A}^{-4}$	-1.0972

adapted displacement coordinates $\{Q_i\}$

$$\begin{bmatrix} Q_1 \\ Q_2 \\ Q_3 \end{bmatrix} = \begin{bmatrix} \sqrt{1/3} & \sqrt{1/3} & \sqrt{1/3} \\ 0 & \sqrt{1/2} & -\sqrt{1/2} \\ \sqrt{2/3} & -\sqrt{1/6} & -\sqrt{1/6} \end{bmatrix} \begin{bmatrix} \rho_1 \\ \rho_2 \\ \rho_3 \end{bmatrix} \qquad (13)$$

where $\rho_i = R_i - R_i^o$, R_i^o being a reference point, treated as an adjustable parameter We use a fourth order polynomial for P:

$$P = \alpha_o + \alpha_1 Q_1 + \alpha_2 Q_1^2 + \alpha_3 q_r^2 + \alpha_4 Q_1^3 + \alpha_5 Q_1 q_r^2 + \alpha_6 q_s^3 + \alpha_7 Q_1^4 + \alpha_8 Q_1^2 q_r^2 + \alpha_9 Q_1 q_s^3 + \alpha_{10} q_r^4 \qquad (14)$$

where $\{\alpha_i\}$, $i = 0, 10$ are adjustable parameters and

$$q_r = \pm \sqrt{Q_2^2 + Q_3^2} \qquad (15)$$

and

$$q_s^3 = Q_3^3 - 3Q_2^2 Q_3 \qquad (16)$$

The additional polynomial P' was introduced[19] to reproduce the Jahn-Teller intersection for the D_{3h} geometries, as

$$P' = q_r \{\beta_1 + \beta_2 Q_1 + \beta_3 Q_1^2 + \beta_4 q_r^2 + \beta_5 Q_1^3 + \beta_6 Q_1 q_r^2 + \beta_7 q_s^3\} \qquad (17)$$

with $\{\beta_i\}$, $i = 1\text{-}7$, and q_r the positive root of eq. (15). We took TA to be $(1-\tanh(\gamma Q_1/2))$ in which γ is yet another

parameter to be determined.

Omission of the polynomial P' led to an rms deviation of 3.0 kcal.mol^{-1}, and a maximum deviation of 15 kcal.mol^{-1} for noncollinear geometries. Therefore we included P' and obtained the 20 parameters by a nonlinear least squares fit of the function to the 267 PE values of Siegbahn and Liu[6-8] The result was an analytic fit with an rms deviation of 0.78 kcal.mol^{-1}. But there was a spurious potential well of about 4 kcal.mol^{-1} depth at R_1 = 2.12 Å and R_2 = 0.74 Å in the entrance channel and a similar one in the exit channel for the collinear configuration This was mainly due to inadequate ab initio data at large separations of H from H_2. An addition of 14 PE values, generated from the SLTH surface for geometries with R_1 = 2.12-2.91 Å and R_2 = 0.71-0.77 Å to the ab initio data resulted in a lowering of the well depth to 1 kcal.mol^{-1}. Therefore we decided to add yet another 28 PE values generated from the SLTH surface in the same (R_1,R_2) range. We also added the exact location and energy of the saddle point of the SLTH surface to the data. Thus the function was fitted to a total of 310 input points and the resulting rms deviation was 0.825 kcal.mol^{-1} and the well depth was only 0.50 kcal.mol^{-1}. The classical barrier height, however, was only 9.42 kcal.mol^{-1}. Therefore we added a correction term 0.013 (1-tanh(Q_1-1.33774)) to the function, to make the barrier height 9.8 kcal.mol^{-1}. We also added a gaussian in the form of

$$V_{gauss} = 0.47 \exp\{-1.92 (Q_1 - 2.87796)^2\} \qquad (18)$$

to remove the well. The overall fit now has the correct classical barrier height of 9 8 kcal.mol^{-1} and an rms deviation of 0.9 kcal mol^{-1}. The well in the entrance channel for the collinear configuration is only 0.12 kcal.mol^{-1} deep. For an approach angle of 90^{o} between H and H_2, there is a well of 1.7 kcal.mol^{-1}. But it is unlikely to affect the dynamics as the reaction is dominated by the collinear geometry. The parameters of the final fit are given in Table 3.

Before proceeding to a detailed dynamical calculation it is essential to ensure the quality of the fitted PES using criteria other than the rms deviation. Therefore we have plotted the PE contours for collinear and different fixed non-collinear geometries in figs. 12-16.

The variation of the classical barrier height for the reaction (R1) with γ is illustrated in fig. 17. For a comparison, results obtained by the SLTH fit are included in the same figure. The minimum energy path (MEP) and the variation of the potential along the MEP as obtained by the SM fit, for the collinear conformation, are illustrated in figs. 18 and 19. We have computed the stretching force constants $K_s = (\partial^2 E/\partial g_1^2)$ and $K_a = (\partial^2 E/\partial g_2^2)$ for collinear H_3 at the saddle point ($g_1 = g_2 = 0$) where $g_1 = (\sqrt{3}/2)(R_1 + R_2 - 2R^{\neq})$ and

Table 3 · Parameters for the SM fit for the ground and the first excited state of H_3. Distances are in Å and energy in eV units

Parameter	Ground State	First Excited State
α_o	13.045	-16.615
α_1	1.7038	- 8.2855
α_2	-0.79314	-15.927
α_3	-0.89915	125.54
α_4	0.89972	- 2.7462
α_5	-9.1007	-2581.4
α_6	6.3079	-57.961
α_7	0.03498	-10.528
α_8	0.01479	704 28
α_9	3.3866	76.219
α_{10}	-12.484	-298.05
β_1	- 6.6106	90.794
β_2	- 2.3982	-787.63
β_3	2.7970	- 5.4865
β_4	13.547	-265.62
β_5	-1.9411	471.29
β_6	10.431	-1594.6
β_7	-7.6274	- 78.548
γ	1.4739	2.8683
R^o	0.7937	0.7937

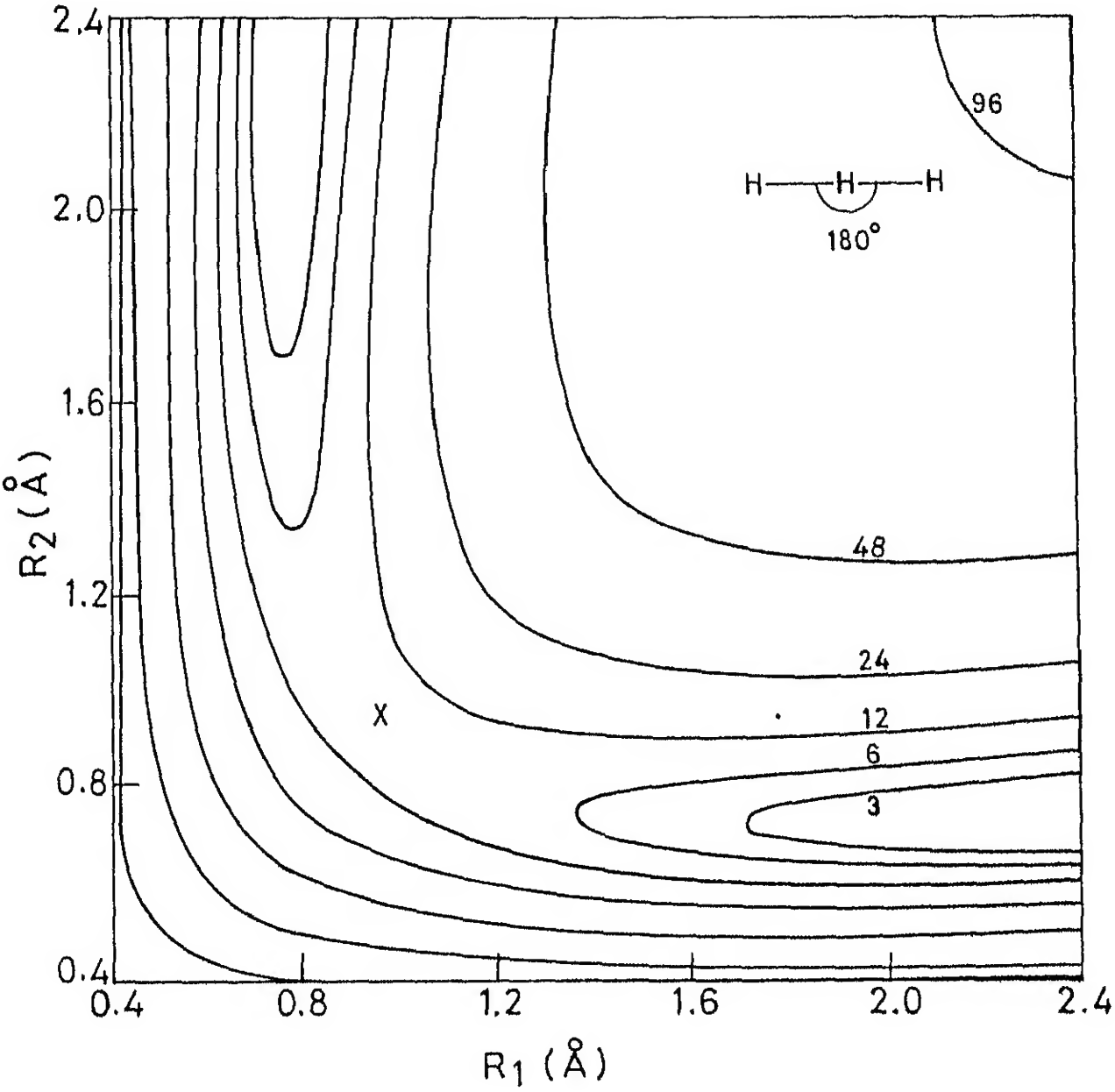

Fig.12 PE contours for the collinear ($\gamma = 180^{\circ}$) conformation from the SM fit. The numbers give the PE values in kcal.mol^{-1} units relative to the separated H and H_2.

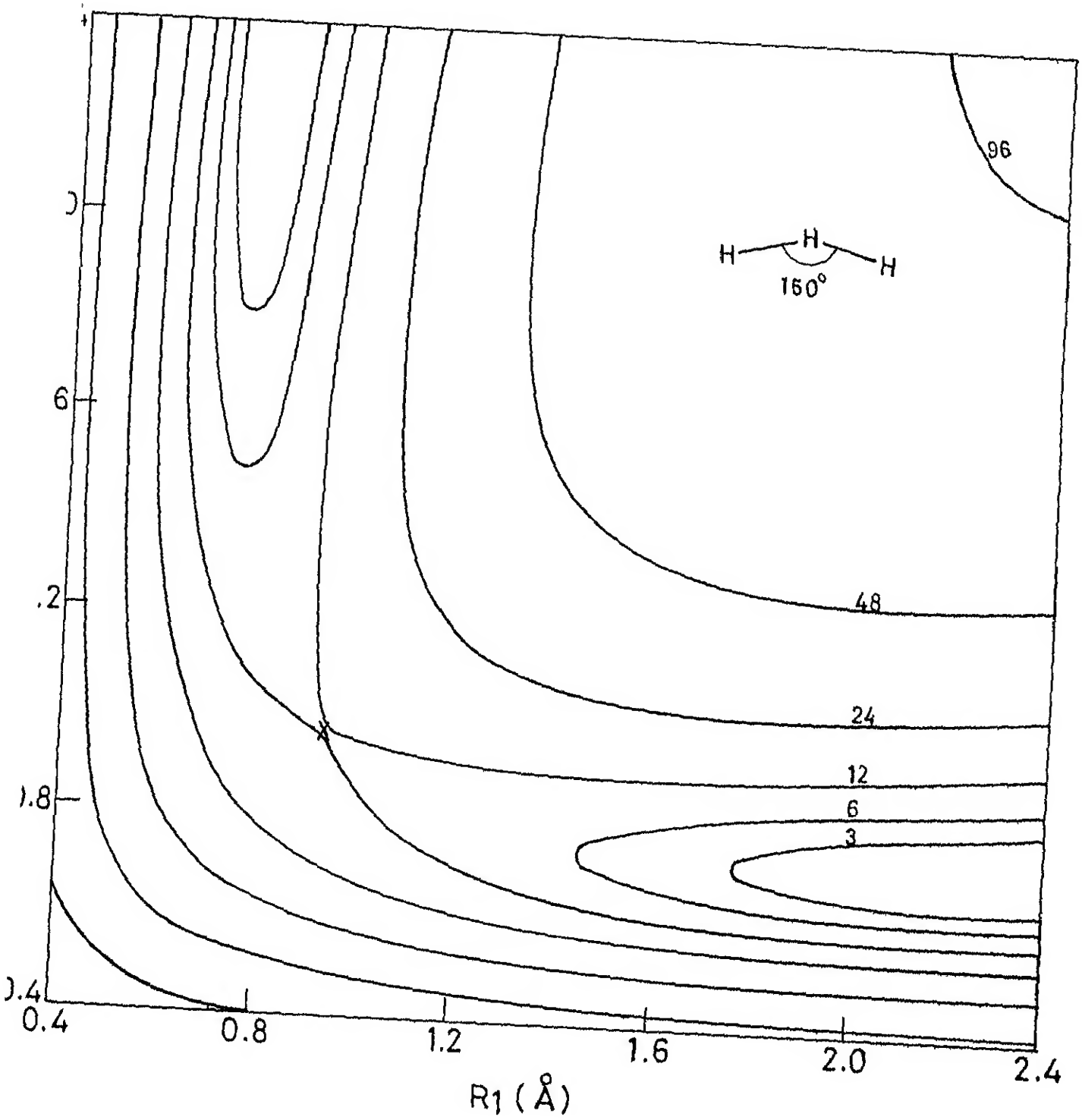

Fig. 13 Same as fig. 12 for $\gamma = 150°$.

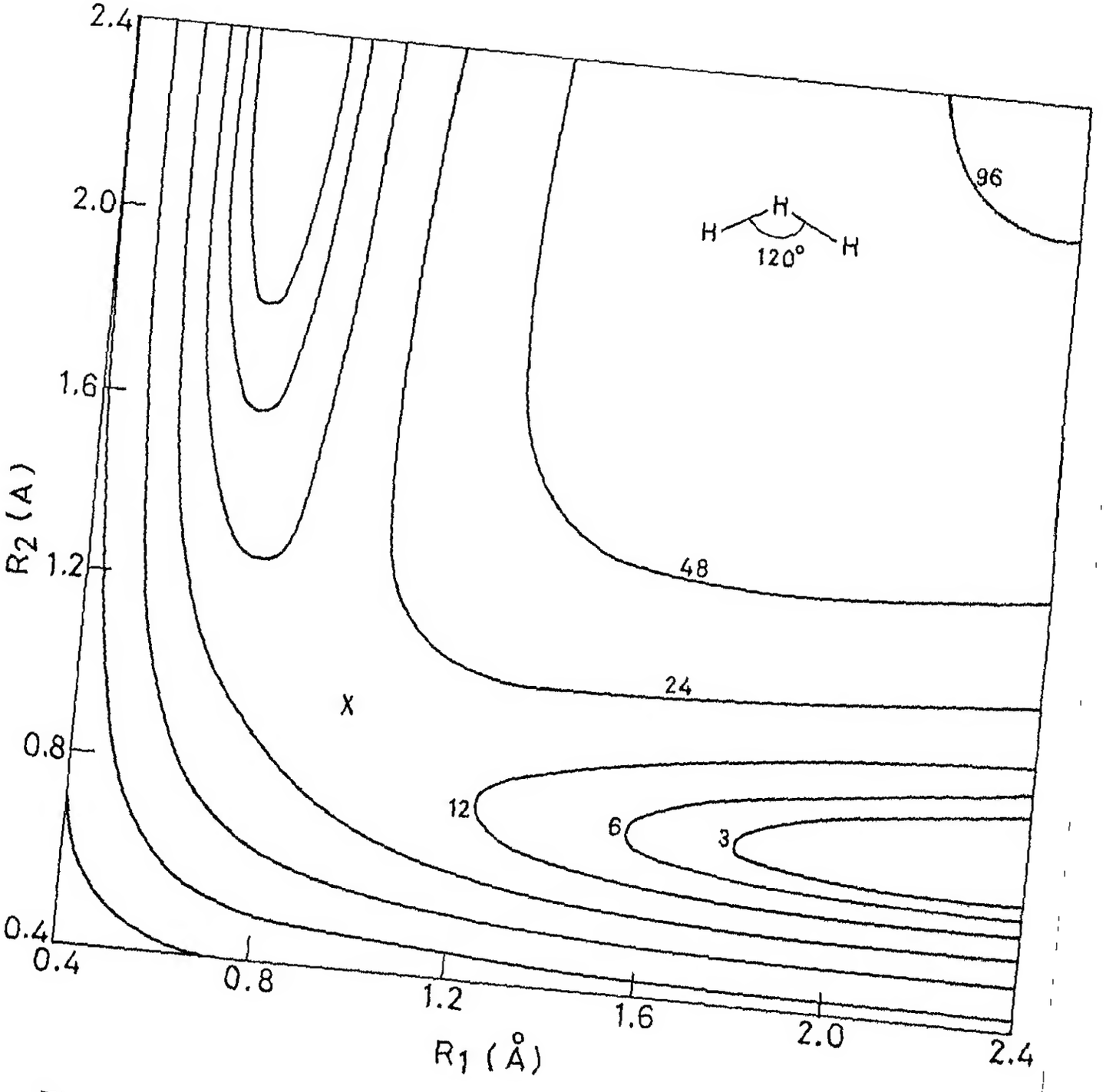

Fig. 14 Same as fig. 12 for $\gamma = 120°$.

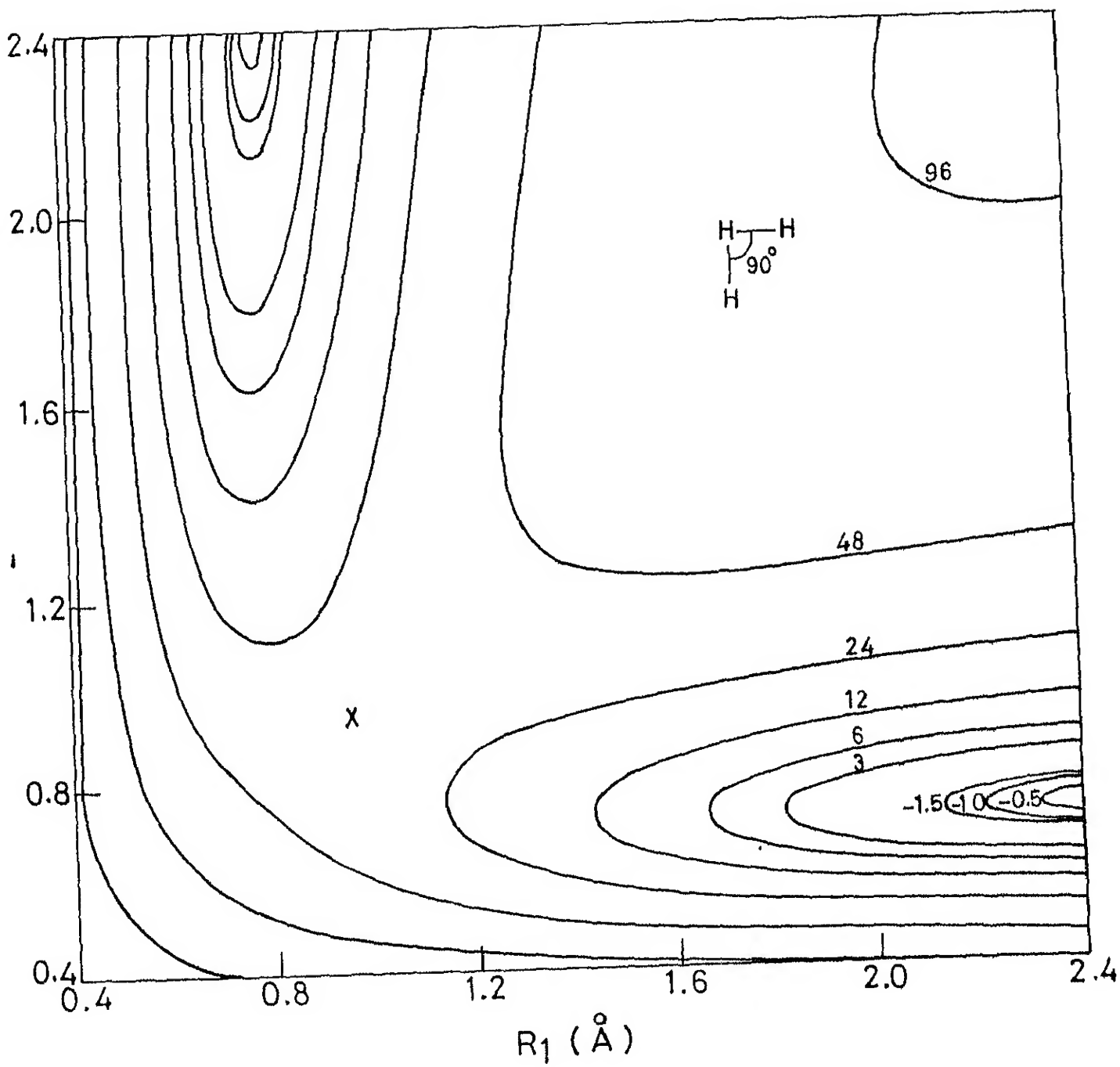

Fig. 15 Same as fig. 12 for $\gamma = 90°$.

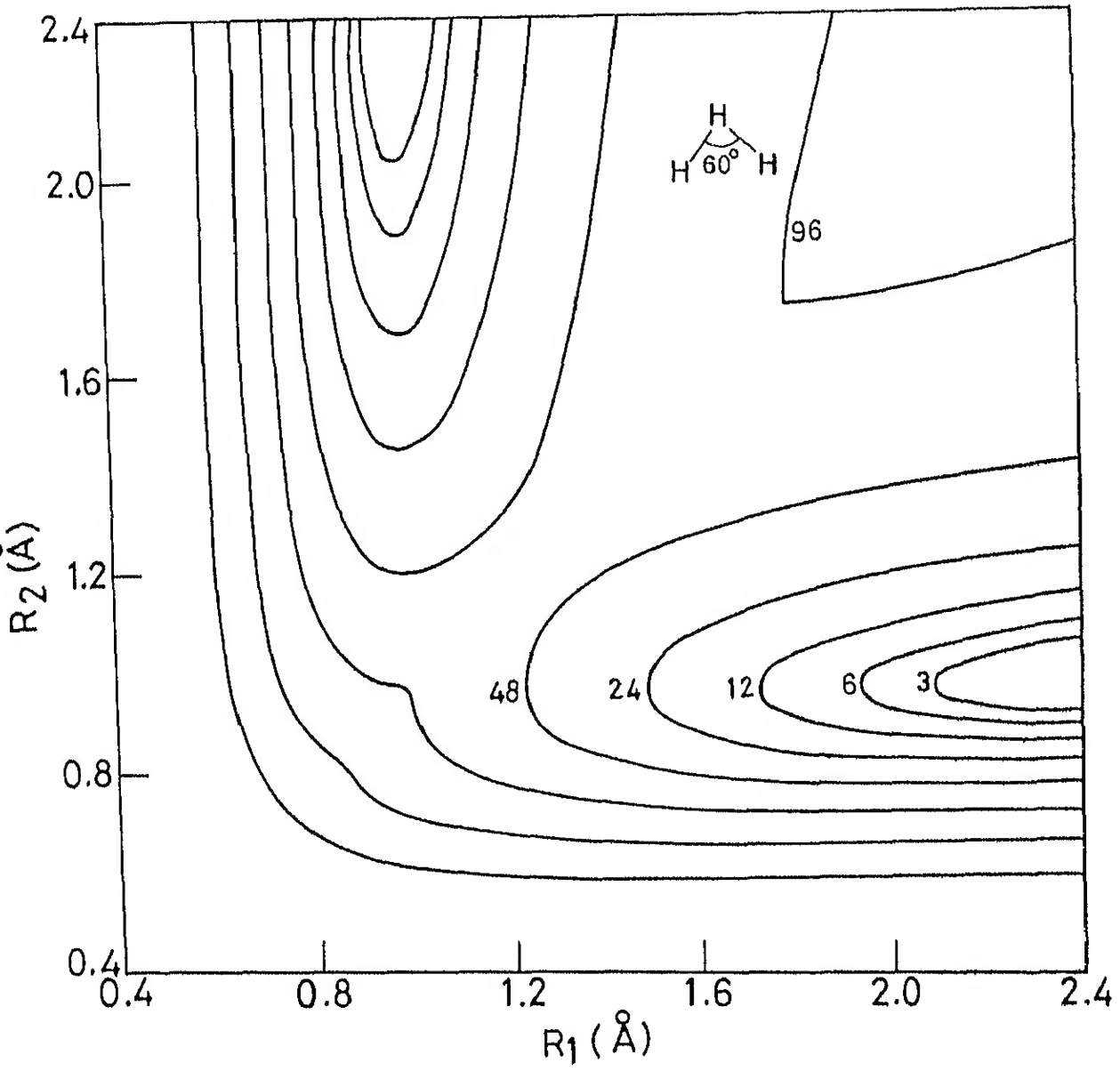

Fig. 16 Same as fig. 12 for $\gamma = 60^{\circ}$.

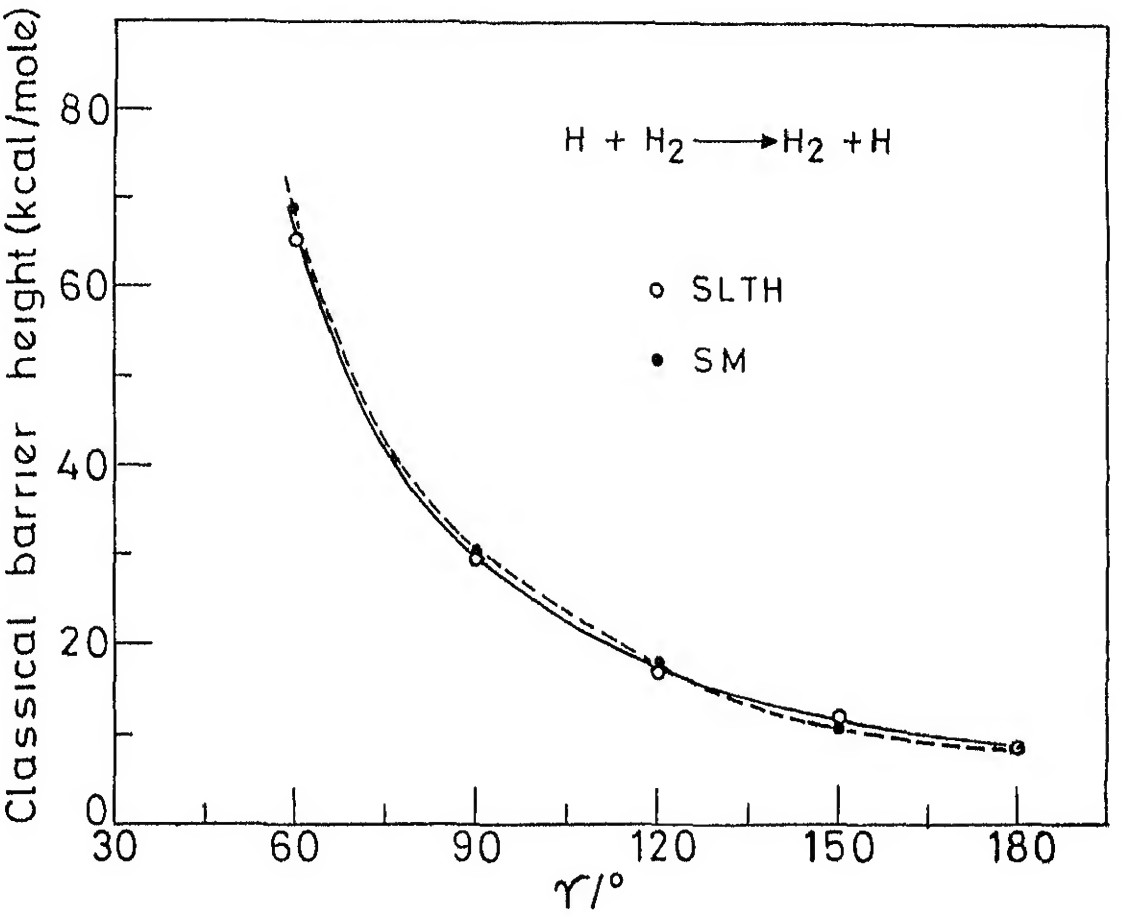

Fig. 17 Variation of the classical barrier height with γ for SM and SLTH surfaces.

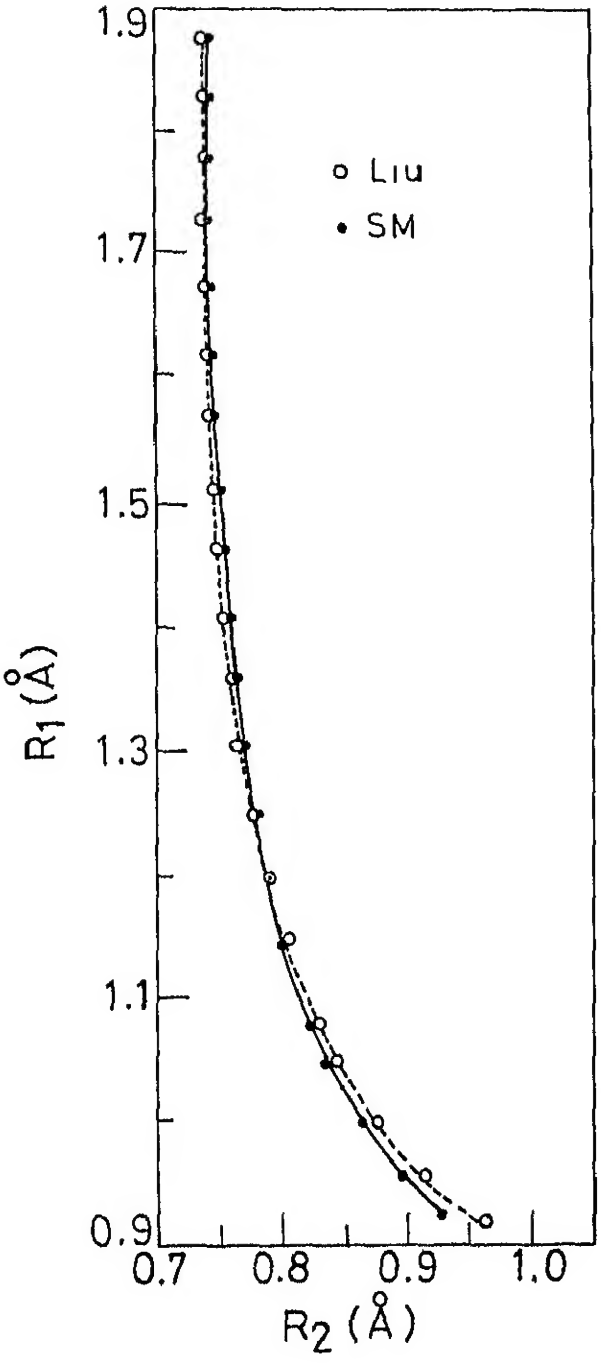

Fig. 18 Minimum-energy path for the collinear reaction from the SM and SLTH fits.

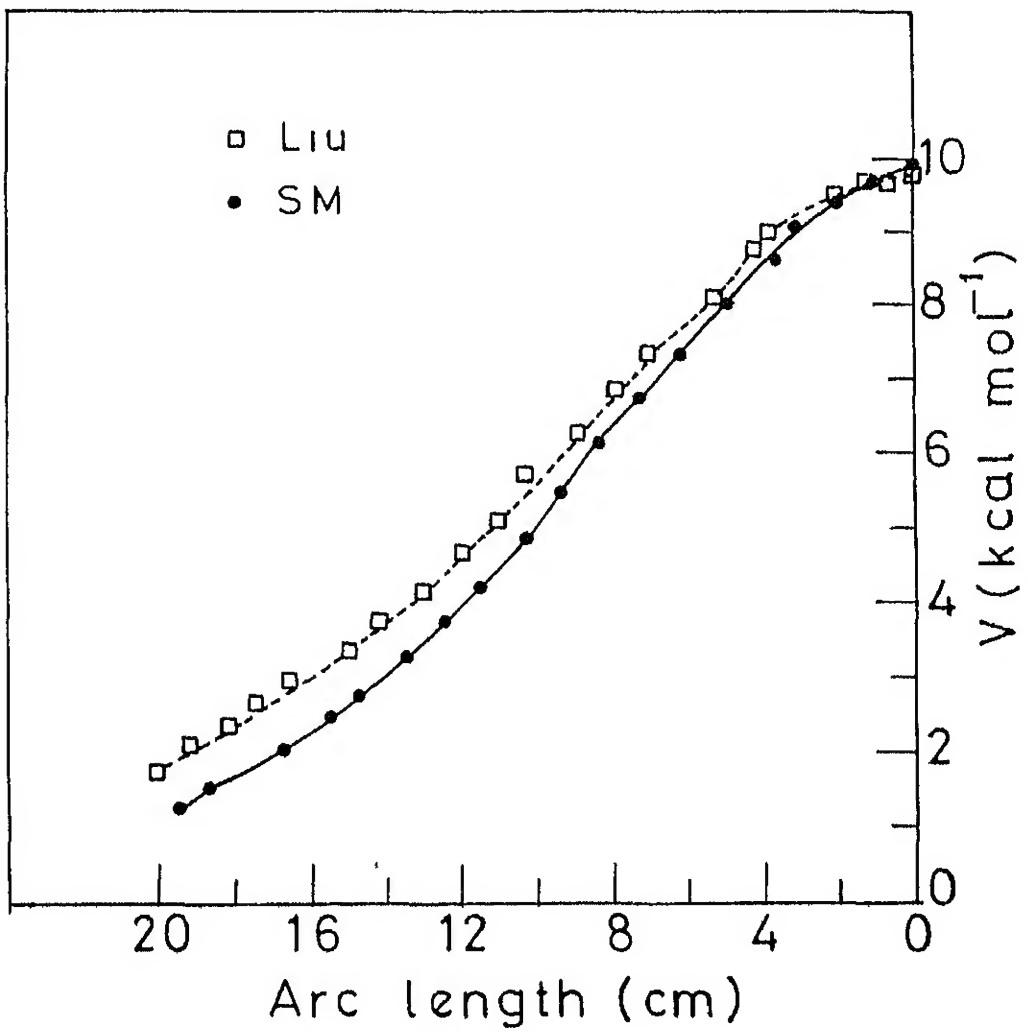

Fig.19 PE for the collinear reaction (R1) as a function of distance along the minimum-energy path.

$g_2 = (1/2)(R_1 - R_2)$ and compared with the values for the SLTH surface A summary of the saddle point properties is given in Table 4.

From the above figures it is clear that the fit does not have any unphysical behaviour except for the well of 1.7 kcal.mol^{-1} at $\gamma = 90^{o}$. In addition it meets many other criteria required of an accurate analytic fit:

(i) It is symmetric with respect to an interchange of R_1 and R_2.

(ii) It has a correct barrier height for the collinear reaction and it fits the ab initio data satisfactorily. Asymptotically it gives an accurate description of the diatom.

The angular variation of the potential as obtained by the SM fit is illustrated in figs.20 and 21 for $r_{H_2} = 0.74$ Å and 1.48 Å respectively. For comparison, the plot for $r_{H_2} = 0.74$ Å obtained from the SLTH surface is shown in fig.22.

It is instructive to expand the potential as

$$V(R_1, R_2, R_3) = \sum_L V_L(R_2, R_{H-H_2}) P_L(\cos\chi_2) \qquad (19)$$

where R_2 is one fixed bond distance and χ_2 is the angle

Table 4 : Saddle Point Properties

Property	Siegbahn-Liu	SLTH	Present fit
$R_1^{\neq}$ (Å)[a]	0.9297	0.9297	0.9432
E_b (kcal.mol^{-1})[b]	9.80	9.802	9.80
K_s (eV Å^{-2})[c]	31.09	31.40	34.78
K_a (eV Å^{-2})[d]	5.63	-5.60	-8.31

a $R_1^{\neq}$ is the distance between adjacent hydrogen nuclei at the linear symmetric saddle point

b E_b is the classical barrier height taken with respect to the corresponding H and H_2 results.

c K_s is symmetric stretch constant.

d K_a is asymmetric stretch constant.

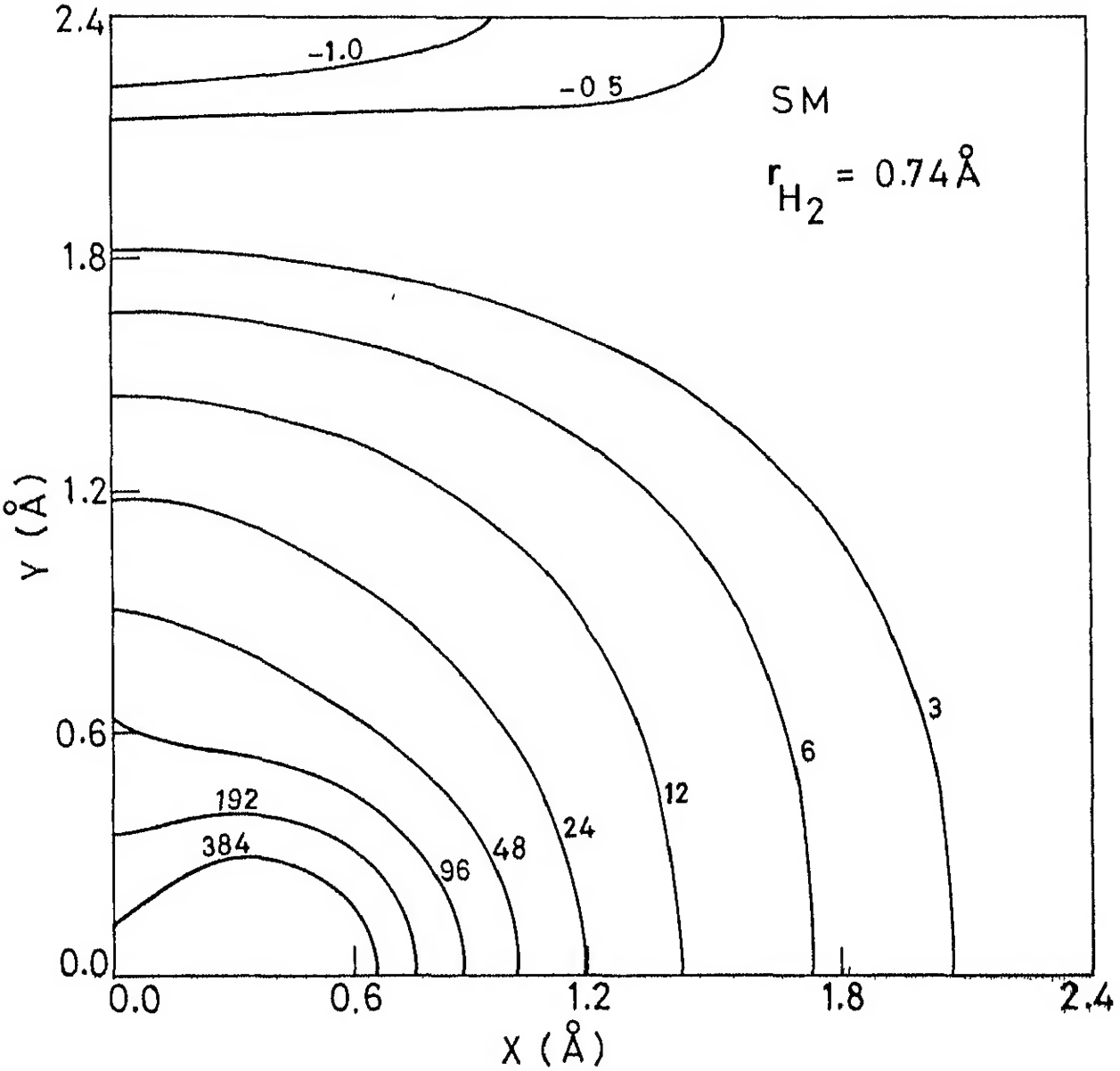

Fig. 20 Fixed-molecule PE contours at r_{H_2} = 0.74 Å for the SM surface.

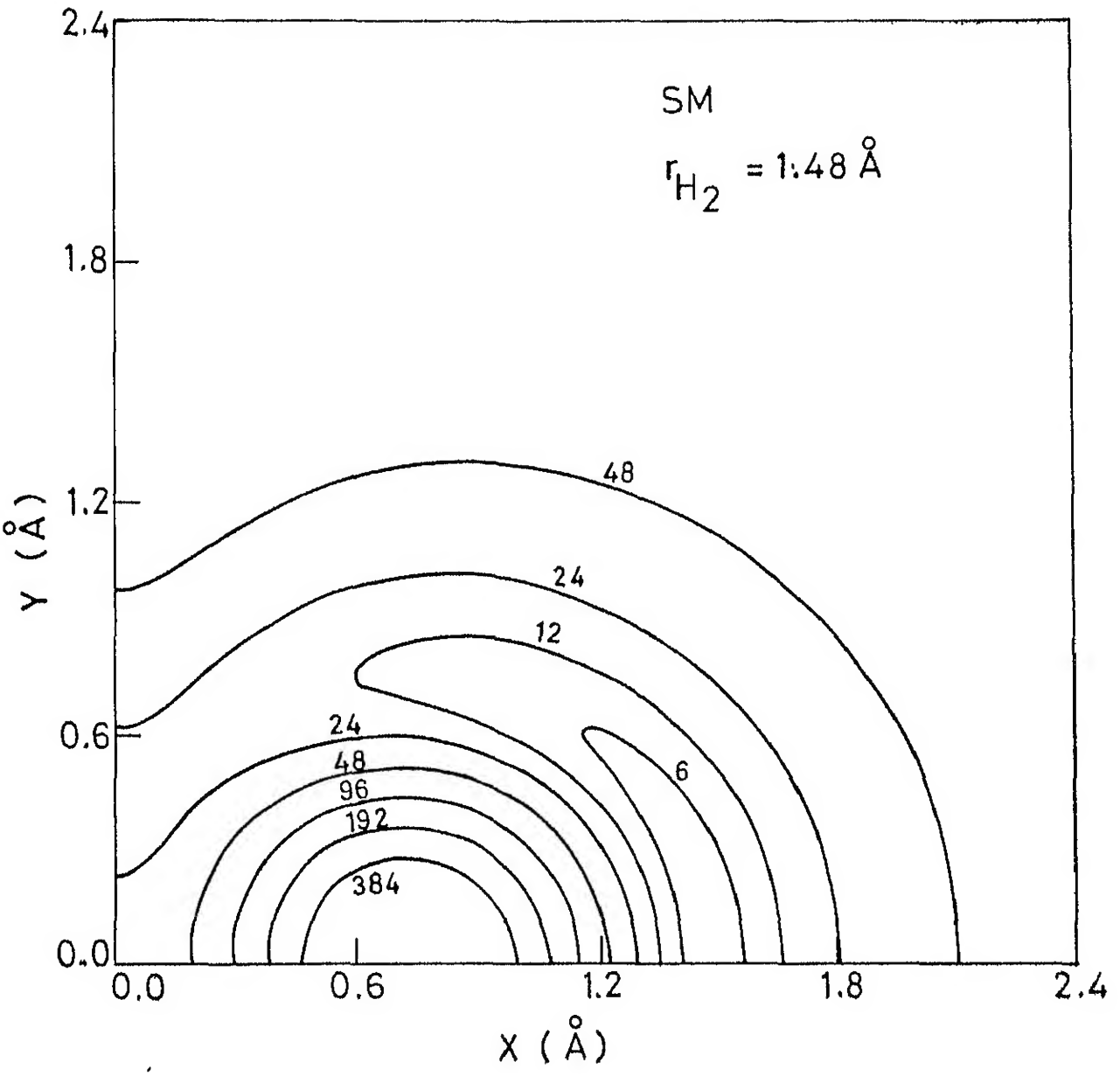

Fig. 21 Same as fig. 20 for r_{H_2} = 1.48 Å.

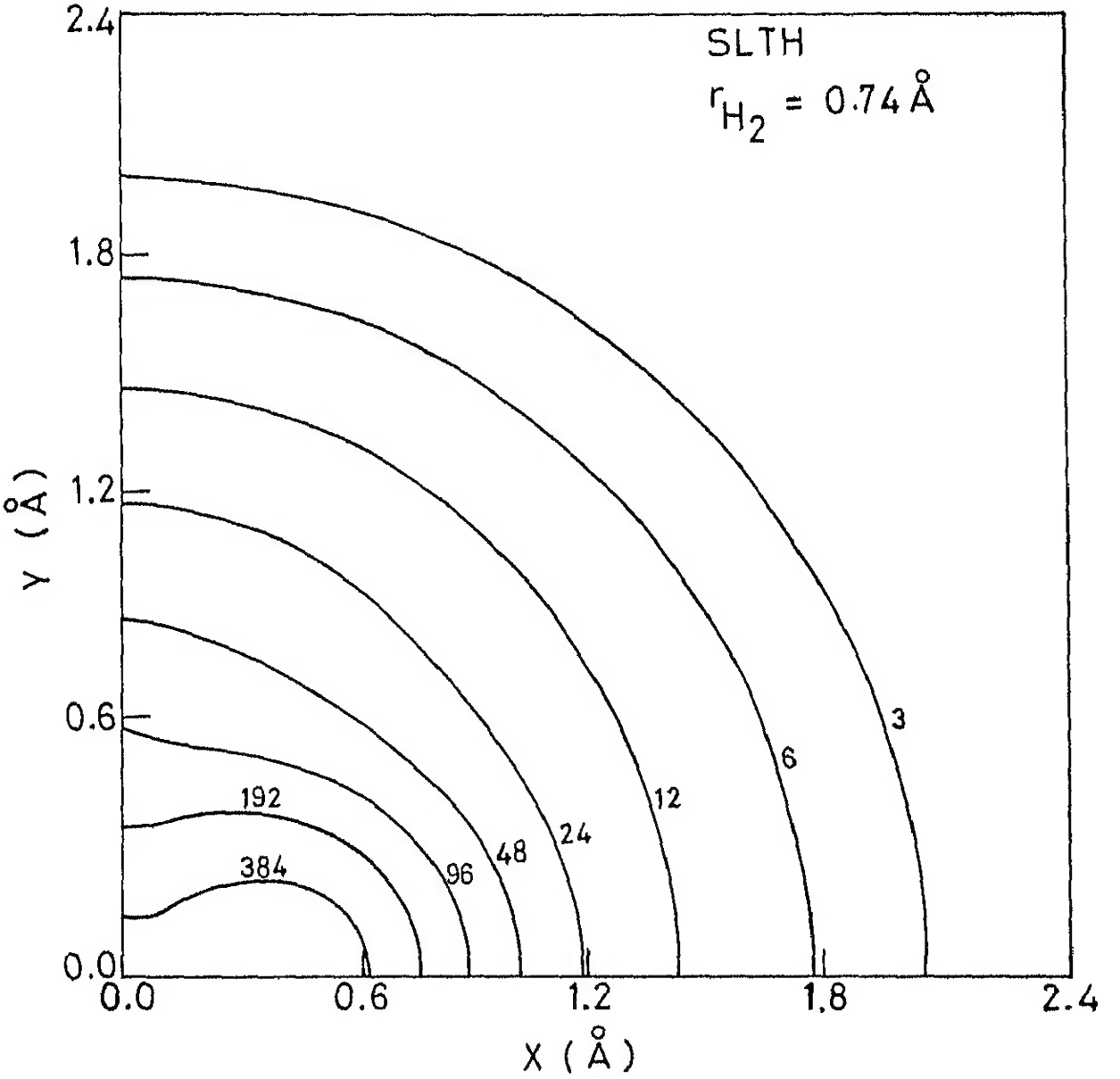

Fig. 22 Same as fig. 20 for the SLTH surface.

between the bond vector and the center-of-mass separation vector. At a given R_{H-H_2} the V_L values are obtained by integrating $V(R_2, R_{H-H_2})$ weighted by the appropriate Legendre polynomial

$$V_L(R_2, R_{H-H_2}) = \left(\frac{2L+1}{2}\right) \int_{-1}^{1} P_L(\cos\chi_2)\, V(R_2, R_{H-H_2})\, d(\cos\chi_2) \tag{20}$$

We have computed and presented in Table 5, V_o and V_2 for $R_{H-H_2} = 1.6\text{-}3.5\ a_o$.

Over the entire range, V_o of the SM fit is in good agreement with that of the SLTH, V_2 of SM is also in agreement with that of SLTH at $R_{H-H_2} = 1.6\ a_o$. But the former is larger in magnitude than the latter at $R_{H-H_2} = 3.5\ a_o$. Similar to the SLTH fit, the SM fit also yields a V_2 that changes sign thrice along the R_{H-H_2} axis. It is positive for $R_{H-H_2} = 1.6\ a_o\text{-}2.1a_o$ and becomes negative at $2.1a_o$ and becomes positive again at $2.9a_o$ similar to the results of Varandas[63]. It becomes negative again at larger R_{H-H_2}. The occurrence of the middle zero of SLTH V_2 at a larger R_{H-H_2} need not be accurate and ours may be better in this respect.

The ultimate test of the reliability of a fitted surface would be to carry out dynamics on it and compare the results

Table 5 : Legendre coefficients $V_L(R_e, R_{H-H_2})$ in $kcal.mol^{-1}$ units for the SM and the SLTH fits

R_{H-H_2} (a_o)	SM	SLTH
	L=0	
1.6	61.50	61.60
2.0	32 61	31.67
2.5	17.065	16.32
3.0	8.867	8 699
3.5	4.063	4.477
4.0	1 290	2.100
4.5	-0.124	0.838
5.0	-0 600	0.266
	L=2	
1.6	25.92	26.48
1.8	7.473	-
2.0	0.546	-0.922
2.1	-0.831	-
2.5	-1.255	-2.597
2.8	-0.102	-
2.9	0.291	-
3.0	0.663	-0.911
3.5	2.025	-0.170
4.0	2.498	-0.041
4.5	2.239	-0.004
5.0	1.644	-0.006
6.4	0.121	-ve
7.1	-0.207	-
10.0	-0.193	-ve

with those on the exact surface Since a TDQM study of a collinear reaction can be carried out almost routinely (for example, see ref.{(60c)}) and the reaction (R1) is dominated by the collinear approach, we carried out a TDQM calculation on the SM surface and also on the SLTH surface for the collinear geometry. A comparison of the results on the two surfaces is presented in fig.23 in the form of the reaction probability as a function of time for H_2 in its first excited vibrational state at a translational temperature of 1000 K. It is clear that the SM fit not only has the static properties similar to those of SLTH but it is also able to reproduce the dynamical results as obtained on the SLTH. Therefore we can say that the SM fit is an adequate representation of the Siegbahn-Liu surface for the ground state of H_3.

3.2 Excited State PES

A correlation diagram of the first few states of H_3 as given in ref.60(b) is reproduced in fig.24. We have undertaken to fit the available ab initio data for the lowest excited state (2pE') that conically intersects with the ground state in the D_{3h} geometry. Nager and Jungen[27] reported the binding energy (ε) values for the third electron, in the frozen core approximation for the metastable Rydberg states of H_3 upto the principal quantum number $n^* = 4$ in the neighborhood of the equilibrium geometry of the parent

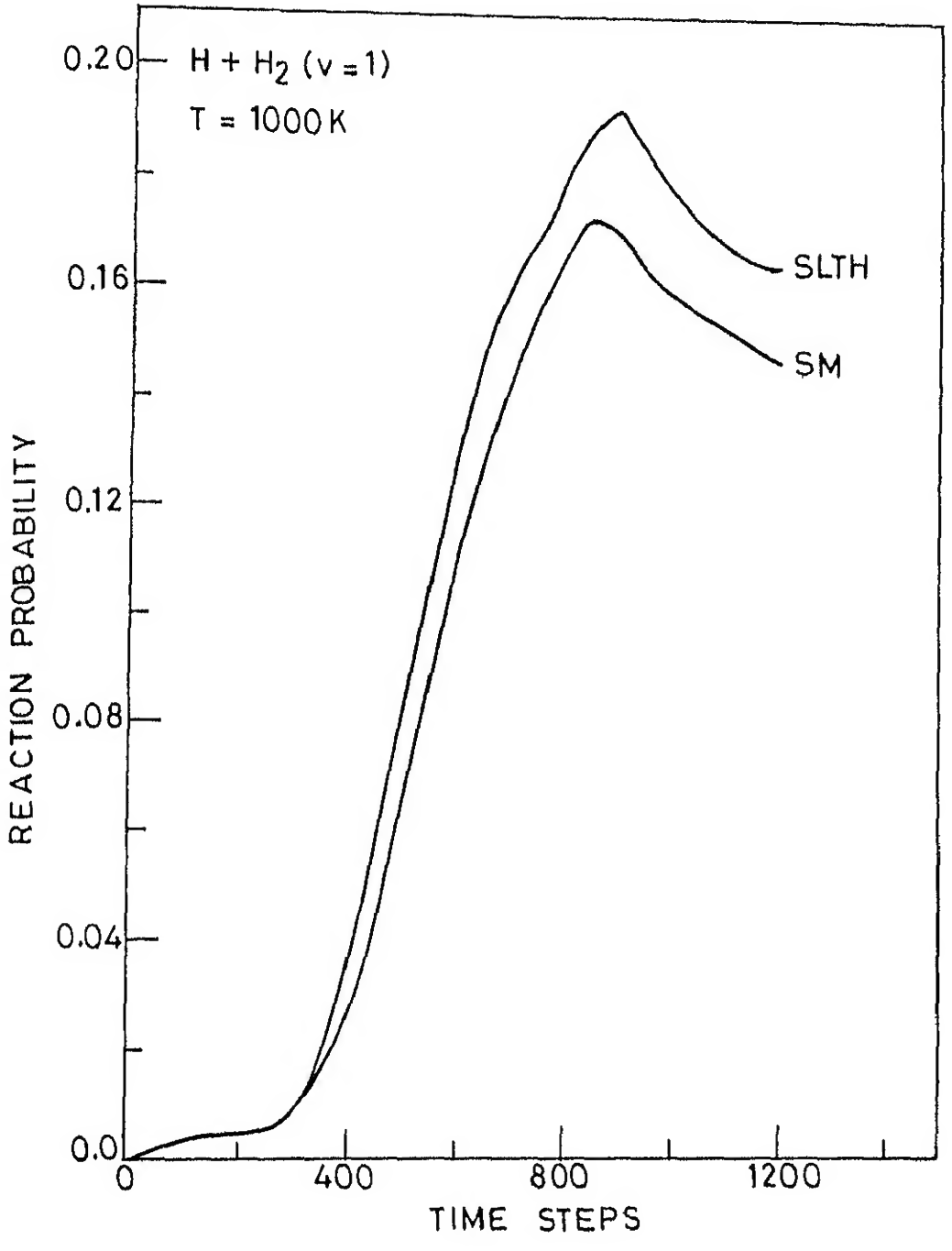

Fig. 23 Reaction probability as a function of time with each time step equal to 0.53875×10^{-16}s on SLTH and SM surfaces.

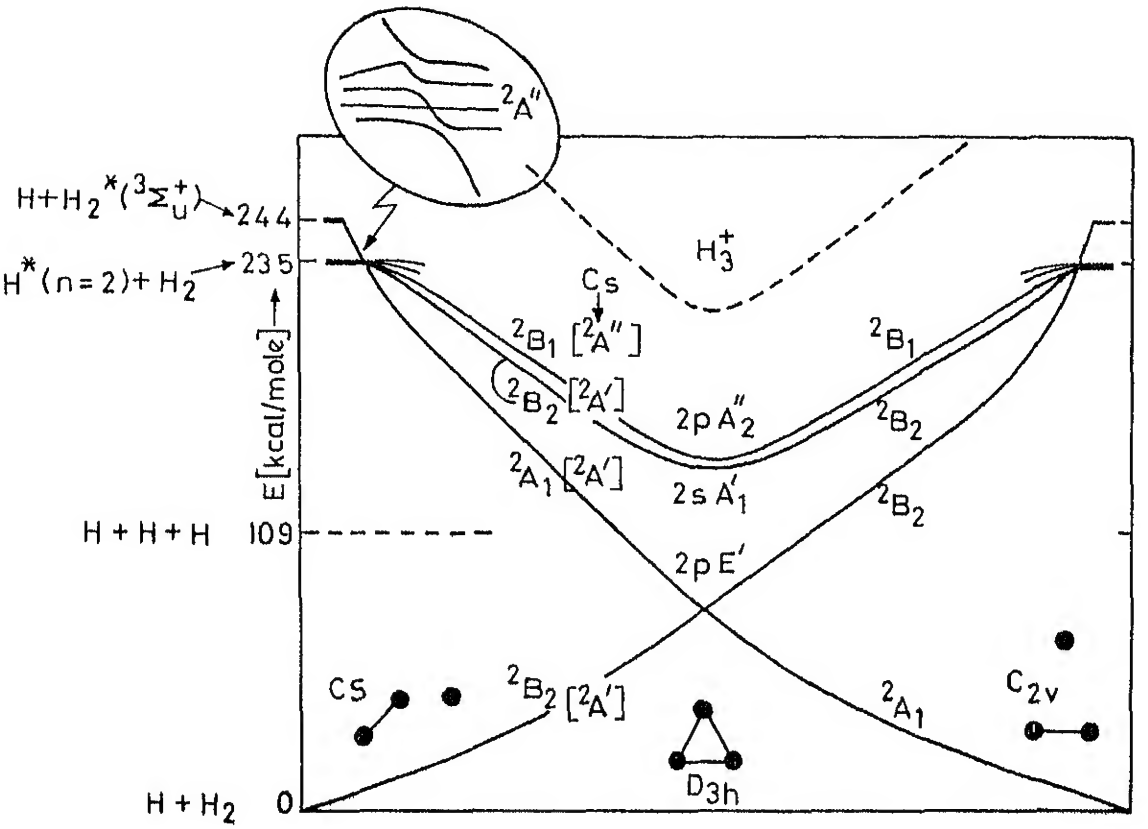

Fig.24 Correlation energy diagram for the four lowest potential-energy surfaces of H_3^* together with the ground-state surface, as a function of nuclear geometry. The lowest excited-state and ground-state surfaces meet in a conical intersection at D_{3h} geometry.

ion H_3^+. For $n^* = 2$, they reported values of the total energy (that is a sum of ε and the core energy for H_3^+) for C_s, C_{2v} and D_{3h} geometries. For $D_{\infty h}$ and $C_{\infty v}$ geometries, however, they reported only the ε values and we added the core energy for H_3^+ as obtained from the Giese-Gentry[64] fit of the ab initio results of Csizmadia et al[65] in order to obtain the total energy. In toto, there are 67 PE values available for the $H_3^*(2pE')$.

We followed essentially the same strategy as we employed for the ground state in fitting the SM function to the PE values for the first excited state of H_3. Asymptotically, $H_3^*(2pE')$ goes to $H(1s) + H_2^*(^3\Sigma_u^+)$. We used the exponential-poly function (eq (5) in Chapter 2) To fit the ab initio PE values of Kolos and Wolniewicz[13] for the repulsive state of $H_3^*(^3\Sigma_u^+)$ and the parameters are listed in Table 6.

The 3-body interaction potential was represented by eq.12 with the P' defined in terms of the negative root for q_r in eq.(15). The resulting functional fit had an rms deviation of 3.1 kcal.mol^{-1}. An examination of the variation of the PE as a function of the side length of the equilateral triangle for D_{3h} geometries as illustrated in fig.25 reveals the difference between the fits for the ground and the excited state PES of H_3. The two fits do not yield identical PE values for the D_{3h} geometry. Part of the reason

Table 6 : Parameters for the exponential-poly fit of the respulsive PE curve for $H_2^*(^3\Sigma_u^+)$

a_o	4.9986
$a_1/\mathring{A}^{-1}$	-8.3407
$a_2/\mathring{A}^{-2}$	9.0983
$a_3/\mathring{A}^{-3}$	-6.4784
$a_4/\mathring{A}^{-4}$	2.1694
$a_5/\mathring{A}^{-5}$	-0.2802

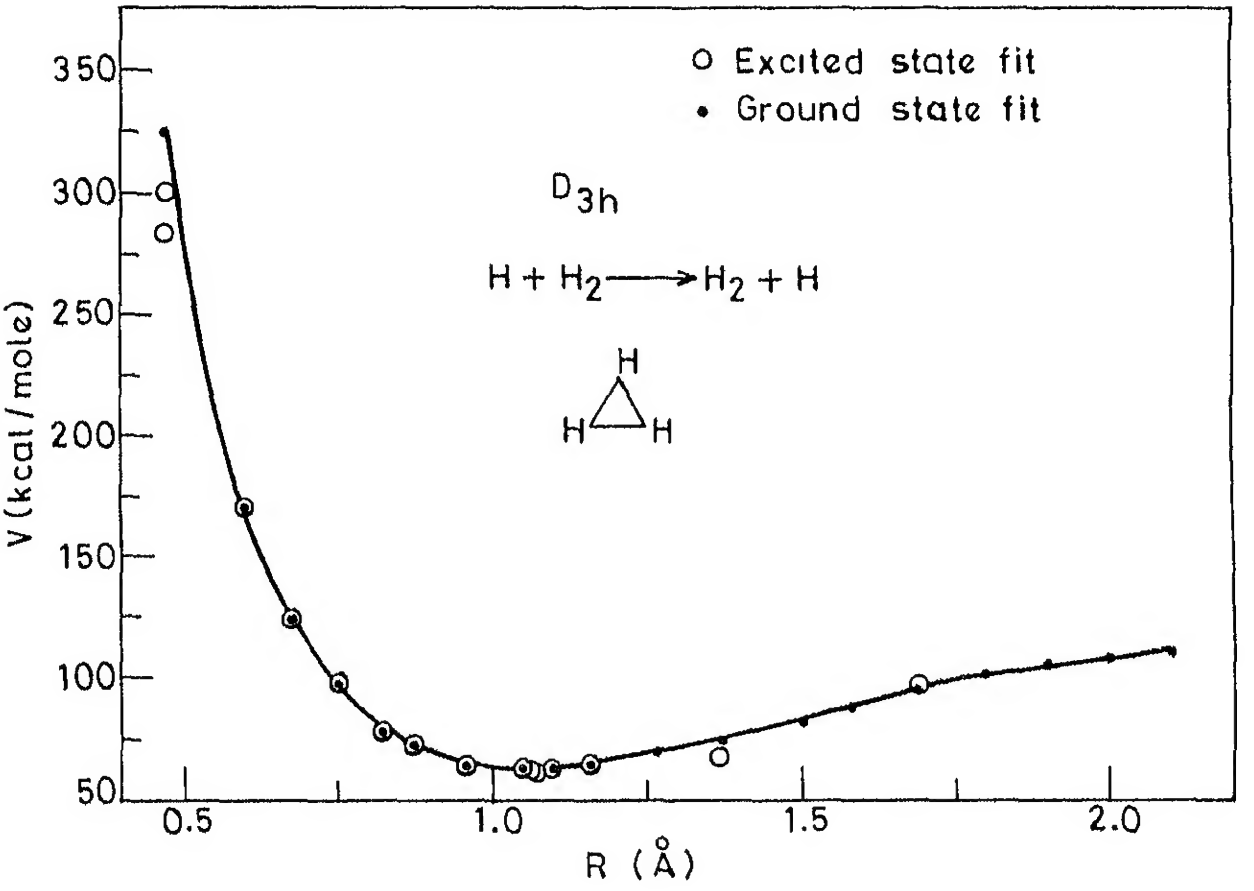

Fig.25 PE in kcal.mol^{-1} units as a function of the side length of the D_{3h} geometry R(Å) for the SM fitted ground and excited state PESs.

for the discrepancy is the difference in the quality of the results of Siegbahn and Liu[6-8] results and those of Nager and Jungen[27]. Since the former values are more accurate than the latter, we replaced the Nager-Jungen PE values for twelve D_{3h} geometries by the values generated from our SM fit of the Siegbahn-Liu surface. The resulting fit had an acceptable rms deviation of 2 6 kcal.mol^{-1}. The parameters for the fit are included in Table 3.

3.3 Attempts to fit a Double-Valued Surface

We have tried the approach of Varandas and Murrell[19] of using the SM function as an analytic fit for both surfaces as two roots of a polynomial. The parameters α_o, α_1, α_2, α_4, α_7 and γ were obtained by fitting seven D_{3h} ab initio values of Siegbahn and Liu[7]. We attempted to obtain the remaining twelve parameters by fitting the function to the data of Nager and Jungen for $C_{\infty v}$, $D_{\infty h}$ and C_s geometries (56 points in all). But the parameters did not converge.

For systems like FH_2[22], OH_2[66] and CH_2[67-68] the SM approach has been extended to fit the double valued surfaces. The basic philosophy has been to fit each diabat to an SM function and the nonadiabatic interaction term to a trigonometric function and to obtain the lower and upper surfaces as the roots of a 2x2 determinant. Such approach would be successful if equal number of ab initio values are available

for both the surfaces. Unfortunately, sufficient number of data points are not available for the excited PES at this stage. Work is in progress to arrive at a double valued function for H_3.

CHAPTER FOUR

DYNAMICS OF A MODEL SIX-CENTER EXCHANGE REACTION

A quasiclassical trajectory study of a model six-center exchange reaction between a van der Waals (VDW) dimer $A_2...B_2$ and a monomer C_2

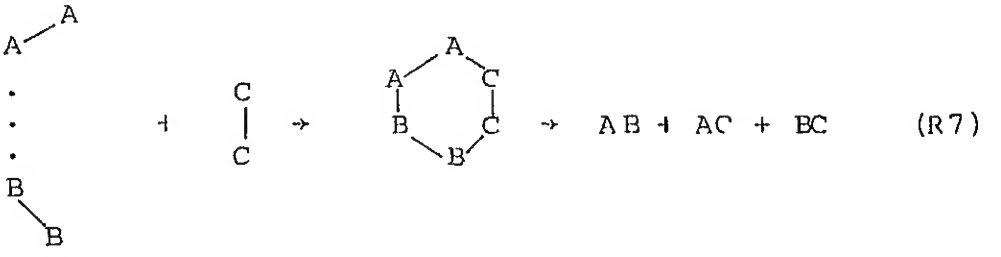

$$A_2...B_2 + C_2 \rightarrow \text{(cyclic intermediate)} \rightarrow AB + AC + BC \qquad (R7)$$

was initiated earlier in our group (The study yielded only nonreactive trajectories)[69]. We have followed it up to obtain results like reaction cross section and rate constant data which can be compared with the available experimental results and also an insight into the details of the dynamical pathway. We give below a brief description of the methodology.

4.1 Methodology

We have used three types of coordinate systems (each being cartesian) in our study.

(i) Space-fixed coordinates XYZ with the center-of-mass (c.m.) of the whole hexa-atomic system as the origin.

(ii) Space-fixed coordinates X'Y'Z' with the c.m. of the tetra-atomic species (VDW molecule) as the origin.

(iii) Molecule-fixed coordinates xyz for A_2, x'y'z' for B_2 and x"y"z" for C_2 with the c.m. of the respective molecule as the origin.

Figure 26 shows the coordinates and their conjugate momenta in the space-fixed frame XYZ and Fig.27 the space-fixed X'Y'Z'.

We assume that the motion of the atoms can be described by Hamilton's[70] equations. In order to solve these equations we need the derivatives of the potential with respect to the coordinates in addition to the initial conditions (coordinates and momenta).

Based on the London equation, Eyring and coworkers[71,72] derived the secular equation for a six-electron system to evaluate the PE:

$$|H_{ij} - E\, S_{ij}| = 0 \qquad (21)$$

where $H_{ij} = \langle \chi_i | H | \chi_j \rangle$ and $S_{ij} = \langle \chi_i | \chi_j \rangle$ with $\{|\chi_i\rangle\}$ the basis functions. Thompson and Suzukawa[39] applied the same approach to the 6C reaction. We have extended it to get a value of E_b equal to that of the ab initio value of Dixon et al[40].

We have evaluated the individual terms in the secular determinant[71] which consists of Coulombic integral Q_{ij} and

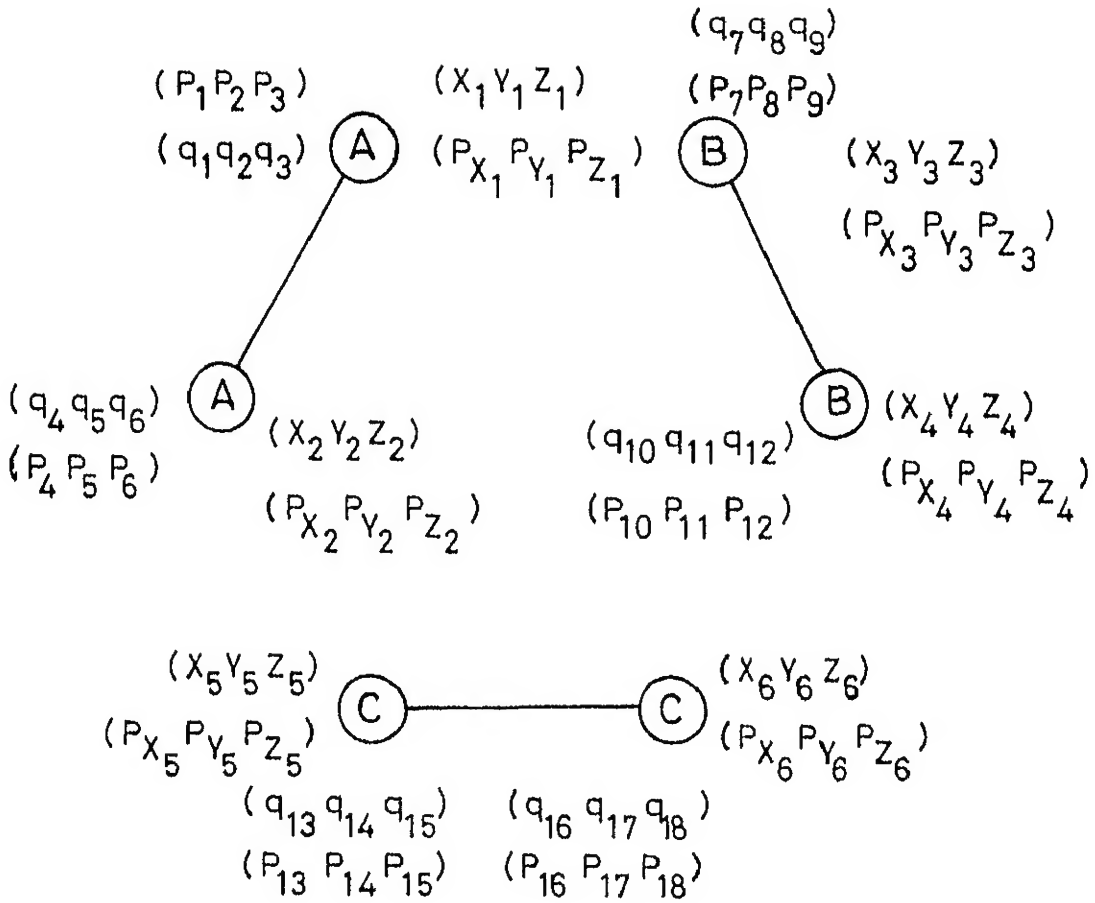

Fig. 26 Coordinates and their conjugate momenta in the space-fixed frame XYZ.

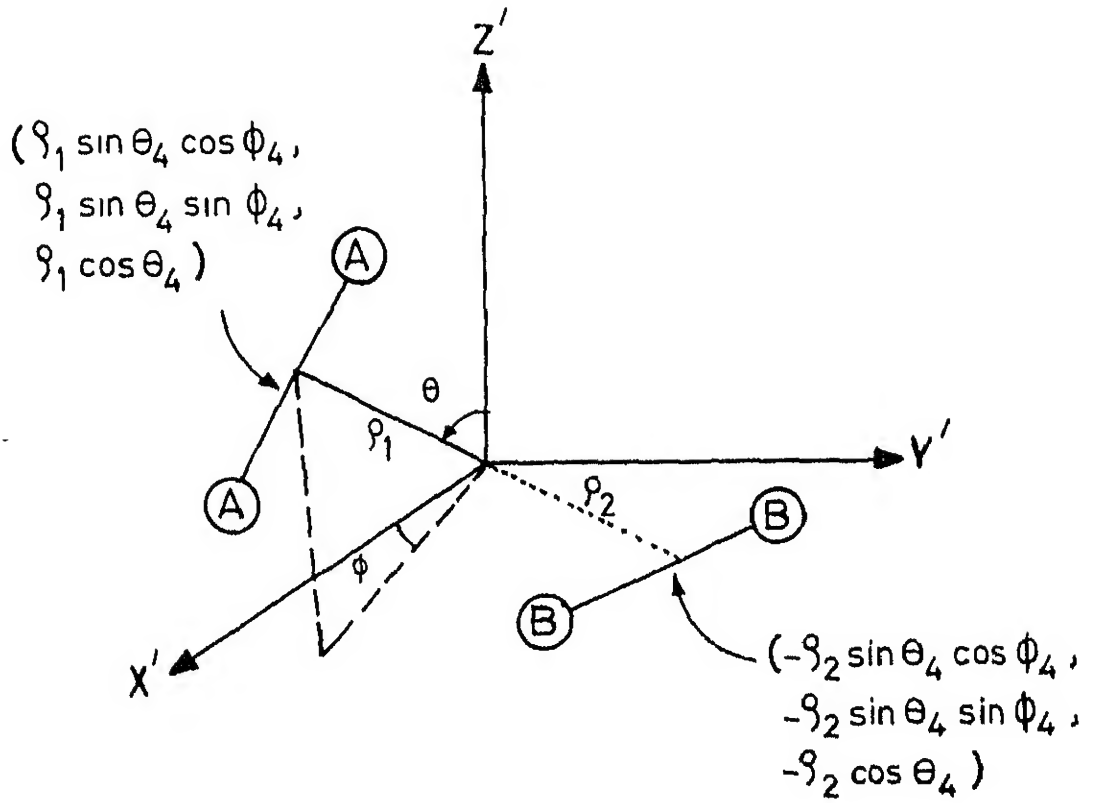

Fig. 27 Orientation of the VDW bond and the coordinates of the c.m. of A_2 and B_2 in the $(X'Y'Z')$ frame.

exchange integral J_{ij}, which are functions of the corresponding internuclear distances. We have used the London-Eyring-Polanyi-Sato (LEPS) formalism[73] to evaluate these integrals

$$^1E_{ij} = \frac{Q_{ij} + J_{ij}}{1 + S} \tag{22}$$

$$^3E_{ij} = \frac{Q_{ij} - J_{ij}}{1 - S} \tag{23}$$

where $^1E_{ij}$ and $^3E_{ij}$ are the singlet and triplet energies for the diatomic molecule given by

$$^1E_{ij} = {}^1D_{ij} \{\exp\{-2\alpha_{ij} (r_{ij} - r^e_{ij})\} - 2 \exp(-\alpha_{ij} (r_{ij} - r^e_{ij}))\} \tag{24}$$

r^e_{ij} is the equilibrium internuclear distance and α_{ij} is the Morse parameter. The triplet state curve for the atom pair ij is represented by the Pedersen-Porter[44] function

$$^3E_{ij} = {}^3D_{ij} (\exp\{-2\beta_{ij}(r_{ij}-r^e_{ij})\} + 2 \exp\{-\beta_{ij}(r_{ij}-r^e_{ij})\}) \tag{25}$$

for $r_{ij} \leq R_c$ and

$$^3E_{ij} = C_{ij} (r_{ij} + A_{ij}) \exp(-\sigma_{ij} r_{ij}) \tag{26}$$

for $r_{ij} > R_c$.

The parameters computed by Raff et al[74] for H_2 had been used in a number of trajectory calculations for three- and four-atom systems results of which were in satisfactory agreement with the experimental results Hence we made use of these parameters, except for the Sato parameter S, which was varied till E_b for the reaction (R7) through a regular hexagonal geometry agreed with the ab initio value of 69 kcal.mol^{-1}.The parameters are listed in Table 7.

The derivative of E with respect to any specific internuclear distance has been calculated by making use of the Hellmann-Feynman theorem (HFT)[75]. It can be expressed[76] as

$$\frac{\partial E_k}{\partial r_1} = \frac{\vec{C}_k^{+} \left(\frac{\partial H}{\partial r_1}\right) \vec{C}_k}{\vec{C}^{+} \vec{S} \vec{C}_k} \qquad (27)$$

where $\vec{C}_k$ are the eigenvectors corresponding to the lowest eigenvalue E_k. $\vec{C}_k$ and E_k were calculated by using the NICER[77] subroutine. These derivatives were then converted into derivatives with respect to the coordinates using the chain rule.

Initial coordinates and momenta[69] of the molecules involved in the reaction were calculated as follows. Initially the molecule A_2 was aligned along the Z-axis with its c.m. as the origin. Hence in the molecule-fixed system the coordinates of A_2 are given by

Table 7 : Potential-energy Parameters for H_2

^1D (kcal.mol^{-1})	109 46086
r^e (Å)	0.74127
α (Å^{-1})	1 97357
^3D (kcal.mol^{-1})	45.35618
β (Å^{-1})	1 88999
C (kcal.mol^{-1}.Å^{-1})	1113.59090
A (Å)	0.529167
σ (Å^{-1})	3.166560
R_c (Å)	0.84667
S	0.32000

$$x_1 = y_1 = x_2 = y_2 = 0$$
$$z_1 = r_1/2$$
$$z_2 = -r_1/2 \qquad (28)$$

where r_1 is the internuclear distance of A_2. The initial x,y,z components of the total momentum conjugate to the molecule-fixed coordinates are

$$P_{x_1} = m_1 z_1 \omega_y (A_2)$$
$$P_{y_1} = -m_1 z_1 \omega_x (A_2)$$
$$P_{z_1} = |\vec{P}_v| \qquad (29)$$
$$P_{x_2} = m_1 z_2 \omega_y (A_2)$$
$$P_{y_2} = -m_1 z_2 \omega_x (A_2)$$
$$P_{z_2} = -|\vec{P}_v| \qquad (30)$$

where ω_x (A_2) and ω_y (A_2) are the angular velocities of A_2 in x and y directions respectively and $\vec{P}_v$ is the vibrational momentum.

The initial coordinates and momenta of the molecule in any position in 3D-space can be calculated by multiplying by the appropriate combination of the rotation matrices

$$R_z(\beta) = \begin{bmatrix} \cos\beta & \sin\beta & 0 \\ -\sin\beta & \cos\beta & 0 \\ 0 & 0 & 1 \end{bmatrix}$$

$$R_y(\beta) = \begin{bmatrix} \cos\beta & 0 & -\sin\beta \\ 0 & 1 & 0 \\ \sin\beta & 0 & \cos\beta \end{bmatrix} \qquad (31)$$

The coordinates of the molecule $A_2(x,y,z)$ and of $B_2(x'y'z')$ transformed into space-fixed coordinates (X'Y'Z') can be evaluated by the following transformations (see fig.27)

$$\begin{bmatrix} X'_i \\ Y'_i \\ Z'_i \end{bmatrix} = \begin{bmatrix} \rho_1 \sin\theta_4 \cos\phi_4 \\ \rho_1 \sin\theta_4 \sin\phi_4 \\ \rho_1 \cos\theta_4 \end{bmatrix} + R_z(\phi_1).R_y(\theta_1) \begin{bmatrix} x_i \\ y_i \\ z_i \end{bmatrix}, \quad i=1,2 \qquad (32a)$$

$$\begin{bmatrix} X'_i \\ Y'_i \\ Z'_i \end{bmatrix} = \begin{bmatrix} -\rho_2 \sin\theta_4 \cos\phi_4 \\ -\rho_2 \sin\theta_4 \sin\phi_4 \\ -\rho_2 \cos\theta_4 \end{bmatrix} + R_z(\phi_2)R_y(\theta_2) \begin{bmatrix} x'_i \\ y'_i \\ z'_i \end{bmatrix}, \quad i=3,4 \qquad (32b)$$

θ_1, ϕ_1, θ_2, ϕ_2, θ_3 and ϕ_3 are the orientation angles of A_2, B_2 and C_2 in the molecule-fixed frames xyz, x'y'z' and x"y"z" respectively. ρ_1, ρ_2 are the distances between the c.m. of A_2B_2 and that of A_2 and the c.m. of A_2B_2 and that of B_2 respectively.

θ_4 and ϕ_4 are the orientation angles for the VDW bond, of distance ρ

The corresponding momenta in the space-fixed frame will be given by

$$\begin{bmatrix} P_{X_i'} \\ P_{Y_i'} \\ P_{Z_i'} \end{bmatrix} = R_z(\phi_1)\, R_y(\theta_1) \begin{bmatrix} P_{x_i} \\ P_{y_i} \\ P_{z_i} \end{bmatrix}, \quad i = 1,2$$

$$\begin{bmatrix} P_{X_i'} \\ P_{Y_i'} \\ P_{Z_i'} \end{bmatrix} = R_z(\phi_2)\, R_y(\theta_2) \begin{bmatrix} P_{x_i'} \\ P_{y_i'} \\ P_{z_i'} \end{bmatrix}, \quad i = 3,4 \qquad (33)$$

The collision between (A_2B_2) and C_2 was studied by transforming the coordinates X'Y'Z' to XYZ. If the c.m. of $(A_2B_2C_2)$ is taken as the origin of the XYZ frame, we have

$$2(m_1+m_2)\,\vec{c} + 2m_3\vec{v} = 0$$

where m_2 and m_3 are the atomic masses of B and C respectively, $\vec{V} = \vec{v}-\vec{c}$ is assumed to be the relative velocity, as $\vec{v}$ is the c.m. velocity of C_2 and $\vec{c}$ the c.m. velocity of (A_2B_2), lies along the Z-direction. Hence it follows that

$$(m_1+m_2)\ \vec{C} + m_3\ (\vec{V} + \vec{C}) = 0$$

$$\vec{C} = \frac{-m_3\ \vec{V}}{m_1+m_2+m_3}$$

and

$$\vec{v} = \frac{(m_1+m_2)\vec{V}}{m_1+m_2+m_3}$$

The position and momenta of the C_2 molecule in the XYZ frame (Fig. 28) are:

$$\begin{bmatrix} X_1 \\ Y_1 \\ Z_1 \end{bmatrix} = \begin{bmatrix} 0 \\ \frac{-(m_1+m_2)b}{(m_1+m_2+m_3)} \\ \frac{-(m_1+m_2)(R_s^2-b^2)^{1/2}}{(m_1+m_2+m_3)} \end{bmatrix} + R_{z''}(\phi_3)\ R_{y''}(\theta_3) \begin{bmatrix} x_1'' \\ y_1'' \\ z_1'' \end{bmatrix}$$

$$\begin{bmatrix} P_{X_i} \\ P_{Y_1} \\ P_{Z_1} \end{bmatrix} = \begin{bmatrix} 0 \\ 0 \\ \frac{m_3(m_1+m_2)\vec{V}}{(m_1+m_2+m_3)} \end{bmatrix} + R_{z''}(\phi_3)\ R_{y''}(\theta_3) \begin{bmatrix} P_{x_1''} \\ P_{y_1''} \\ P_{z_1''} \end{bmatrix}, i=5,6 \qquad (34)$$

where b is the impact parameter and R_s the distance between the c.m. of C_2 and the c.m. of (A_2B_2). In the above transformation, Z is assumed to be the direction of approach of the C_2 molecule to the (A_2B_2) system and the c.m. of (A_2B_2) and C_2 lie in the YZ plane.

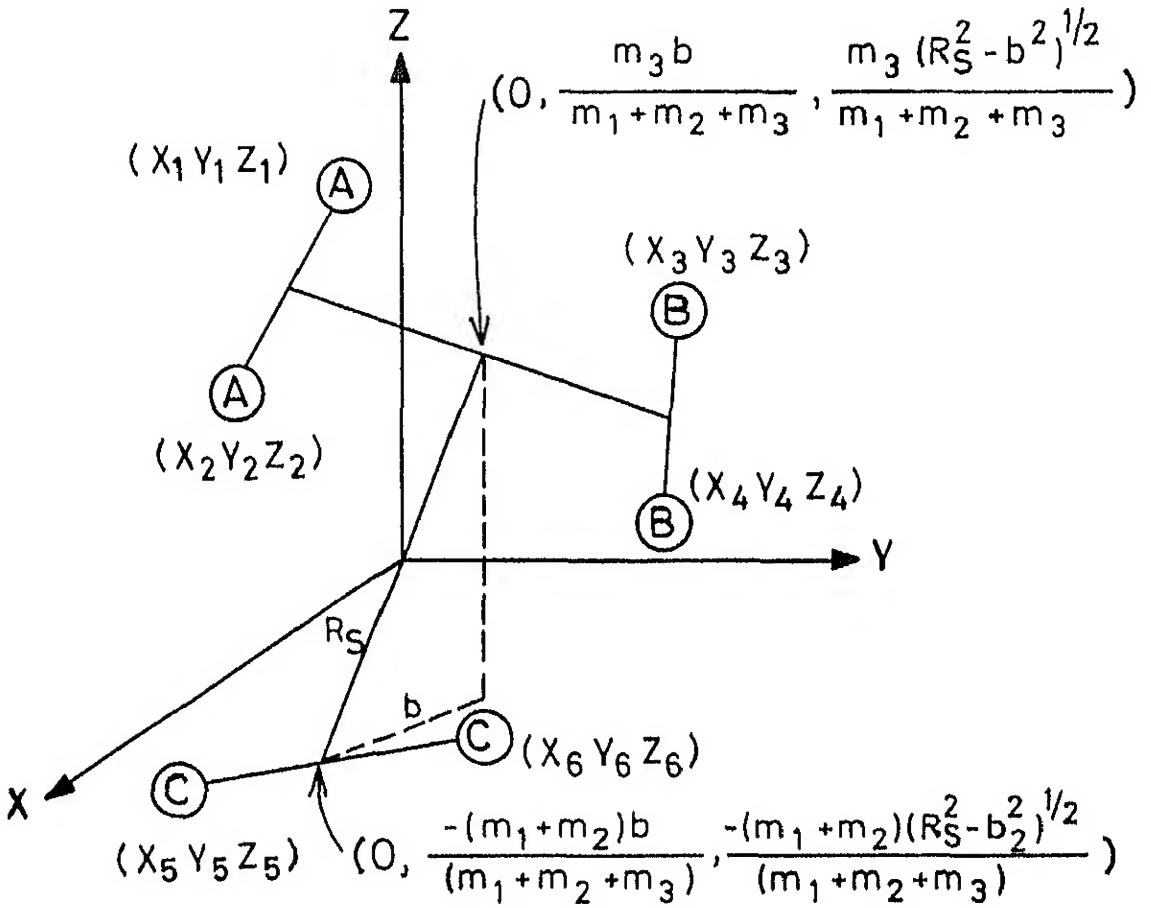

Fig. 28 Coordinates of the molecules A_2, B_2 and C_2 in the space-fixed frame X Y Z.

In the XYZ coordinate frame the initial coordinates and momenta are given as follows:

$$\begin{bmatrix} X_i \\ Y_i \\ Z_i \end{bmatrix} = \begin{bmatrix} 0 \\ \dfrac{m_3 b}{(m_1+m_2+m_3)} \\ \dfrac{m_3 (R_s^2-b^2)^{1/2}}{(m_1+m_2+m_3)} \end{bmatrix} + \begin{bmatrix} X_i' \\ Y_i' \\ Z_i' \end{bmatrix}$$

$$\begin{bmatrix} P_{X_i} \\ P_{Y_i} \\ P_{Z_i} \end{bmatrix} = \begin{bmatrix} 0 \\ 0 \\ \dfrac{m_k m_3 \vec{V}}{m_1+m_2+m_3} \end{bmatrix} + \begin{bmatrix} P_{X_i'} \\ P_{Y_i'} \\ P_{Z_i'} \end{bmatrix}, \quad i=1-4 \qquad (35)$$

$m_k = m_1$ when $i = 1$ and 2, and $m_k = m_2$ for $i = 3$ and 4.

In the present study we have fixed the values of the vibrational and rotational quantum numbers v, J and the relative translational energy (E_T) while b has been selected in a stratified manner from the appropriate distribution function. The orientation angles have been selected randomly in the interval {-1,1} generated by the IMSL subroutine GGUB[78]. After selecting initial conditions corresponding to coordinates and momenta the equations of motion were solved using the fifth-order predictor-corrector subroutine adapted from the REACTS package[79]. A step-size of $t=(0.5-1.0)\times10^{-16}$ s

was used for the integration

We analysed the final state of the trajectories as described below. In the collision between (A_2B_2) and C_2 the possible channels are:

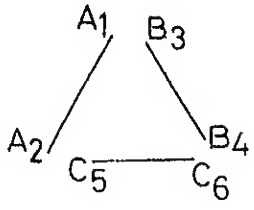

$\rightarrow A_2 + B_2 + C_2$ (R8)

$\rightarrow AB + AC + BC$ (R9)

$\rightarrow 2AB + C_2$ (R10)

$\rightarrow 2AC + B_2$ (R11)

$\rightarrow 2BC + A_2$ (R12)

(R8) is a nonreactive process,[69] (R9) a 6C reaction and in (R10), (R11) and (R12), C_2, B_2 and A_2 act as mediating partners respectively. The various possible products formed during the reaction, along with their identifications are listed in Table 8.

To identify which products have been formed, we made use of the internuclear distance criterion. All the fifteen internuclear distances were compared and the integration was continued until only three of the fifteen distances were less than a specific distance R_s. The molecules corresponding to these three distances were identified and their internal energies analysed.

Table 8 : Species Labels for Different Reactive Channels

Process	Combination of atoms in sets of three	
Nonreactive (R8)	12, 34, 56	
	AA, BB, CC	
Six-centered reaction (R9)	13, 25, 46	13, 26, 45
	AB, AC, BC	AB, AC, BC
	14, 25, 36	14, 26, 45
	AB, AC, BC	AB, AC, BC
	15, 23, 46	15, 24, 36
	AC, AB, BC	AC, AB, BC
	16, 23, 45	16, 24, 35
	AC, AB, BC	AC, AB, BC
C_2 acts as a mediating partner (R10)	13, 24, 56	14, 23, 56
	AB, AB, CC	AB, AB, CC
B_2 acts as a mediating partner (R11)	15, 26, 34	16, 25, 34
	AC, AC, BB	AC, AC, BB
A_2 acts as a mediating partner (R12)	12, 35, 46	12, 36, 45
	AA, BC, BC	AA, BC, BC

The c m. velocity in the space-fixed frame for product molecules was calculated as follows

$$(V'_{ij})_X = \frac{(P'_X)_i + (P'_X)_j}{(m_i + m_j)}$$

$$(V'_{ij})_Y = \frac{(P'_Y)_i + (P'_Y)_j}{(m_i + m_j)}$$

$$(V'_{ij})_Z = \frac{(P'_Z)_i + (P'_Z)_j}{(m_i + m_j)} \qquad (36)$$

x,y,z components of the linear momentum in the molecule-fixed coordinates are

$$P'_{x_k} = P'_{X_k} - m_k(V'_{ij})_X$$

$$P'_{y_k} = P'_{Y_k} - m_k(V'_{ij})_Y$$

$$P'_{z_k} = P'_{Z_k} - m_k(V'_{ij})_Z \quad , \; k = i,j. \qquad (37)$$

The internal angular momentum is calculated by transforming the space-fixed co-ordinates to molecule-fixed coordinates as follows:

$$x_k = X_k - \frac{(m_1 X_1 + m_j X_j)}{(m_1 + m_j)}$$

$$y_k = Y_k - \frac{(m_1 Y_1 + m_j Y_j)}{(m_1 + m_j)}$$

$$z_k = Z_k - \frac{(m_1 Z_1 + m_j Z_j)}{(m_1 + m_j)} \quad , \; k = 1,j. \qquad (38)$$

For diatomic species ij, the final internal angular momentum is given by

$$(M'_{ij})_x = (y_1 P'_{z_1} - z_1 P'_{y_1}) + (y_j P'_{z_j} - z_j P'_{y_j})$$

$$(M'_{ij})_y = (z_1 P'_{x_1} - x_1 P'_{z_1}) + (z_j P'_{x_j} - x_j P'_{z_j})$$

$$(M'_{ij})_z = (x_1 P'_{y_1} - y_1 P'_{x_1}) + (x_1 P'_{y_j} - y_j P'_{x_j})$$

(39)

The corresponding rotational energy $E'_{rot}(ij) = (M'_{ij})^2/2I$ where $I = \mu r_{ij}^2$ with $\mu = m_1 m_j/(m_1+m_j)$ and $r_{ij} = \{(x_1-x_j)^2 + (y_1-y_j)^2 + (z_1-z_j)^2\}^{1/2}$ and $(M'_{ij})^2 = (M'_{ij})_x^2 + (M'_{ij})_y^2 + (M'_{ij})_z^2$. The vibrational energy of the product molecule (ij) is calculated from

$$E'_{vib}(ij) = E'_{int}(ij) + V_{ij} - E'_{rot}(ij) \qquad (40)$$

where E'_{int} is the internal kinetic energy:

$$E'_{int} = (1/2)\ \{(P'^2_{x_i} + P'^2_{y_i} + P'^2_{z_i})/m_i + (P'^2_{x_j} + P'^2_{y_j} + P'^2_{z_j})/m_j\} \qquad (41)$$

and V_{ij} the Morse potential. The final translational energy E'_T is

$$E'_T = E_{TOT} - E'_{vib} - E'_{rot} \qquad (42)$$

4.2 Results and Discussion

For initialising the trajectories, we set the VDW bond distance $\rho_1 + \rho_2 = 3.0$ Å and $R_s = 6.5$ Å. We set $J = 0$ for all the trajectories We chose fixed values of v and E_T as described below. Trajectories were computed for different b-strata with b_{max} chosen differently for different (v, E_T). Generally, about 100-200 trajectories were run in each stratum. On the whole, about 3000 trajectories were run, with each trajectory taking about 3 min cpu time on the DEC-1090 computer Details of the number of the trajectories run for different initial conditions and the reaction

cross section (σ^R) are given in Table 9

The accuracy of integration of each trajectory was monitored by energy and angular momentum conservation measures. In many test cases, we plotted the different bond distances as a function of time to determine the outcome of the collision. This helped us in ascertaining the mechanism of the reaction as well. We find that for $(v_{A_2}, v_{B_2}, v_{C_2})=(0,0,0)$ at E_T = 90-135 kcal.mol^{-1}, the reactions (R11) and (R12) take place through a 4C pathway with the third diatom acting as a mediating partner as is illustrated for a typical trajectory in fig.29. For higher vibrational states like (11,8,8) at E_T = 130-150 kcal.mol^{-1}, we observe a 6C reaction. That is, the three (reactant) diatoms lead to three different (product) diatoms as is shown in fig 30 for a single trajectory. At such high energies, we also find that invariably only one or two diatoms are formed with the remaining atoms flying apart. That is, collision-induced dissociation occurs as is clear from the sample trajectories plotted in figs.31 and 32.

We tried to follow the molecular collision in 3D by making different types of plots. In the absence of animation facilities in our computer, we plotted 'stills' of the six atoms at different intervals of time. The composite diagram showing the time evolution became messy. Therefore we decided to show in one frame the molecules at the 'beginning' and at

Table 9 : Details of the number of trajectories for different initial conditions and the total reaction cross section results. N_R indicates the number of reactive trajectories. The error estimates of σ^R are of 68% confidence level

$v_{A_2}, v_{B_2}, v_{C_2}$	E_T (kcal.mol^{-1})	b (Å)										σ^R (Å^2)
		0 - 0.5		0.5 - 1.0		1.0 - 1.5		1.5 - 2.0		2.0 - 2.5		
		N	N_R	N	N_R	N	N_R	N	N_R	N	N_R	
0,0,0	90	128	1	100	0	-	-	-	-	-	-	0.01±0.01
0,0,0	100	156[a]	2	102	2	108	0	-	-	-	-	0.06±0.03
0,0,1	100	114[a]	5	104	1	194	3	103	1	100	0	0.16±0.07
0,0,2	100	174[a]	2	120[a]	4	115	8	114	0	-	-	0.39±0.10
0,0,0	120	100[a]	9	116[a]	4	117[a]	4	135	0	-	-	0.30±0.09
0,0,0	135	141	9	103	8	125	4	-	-	-	-	0.33±0.09

[a] In these cases, strata of 0-0.55, 0.55-1.0 and 1.0-1.55 were used.

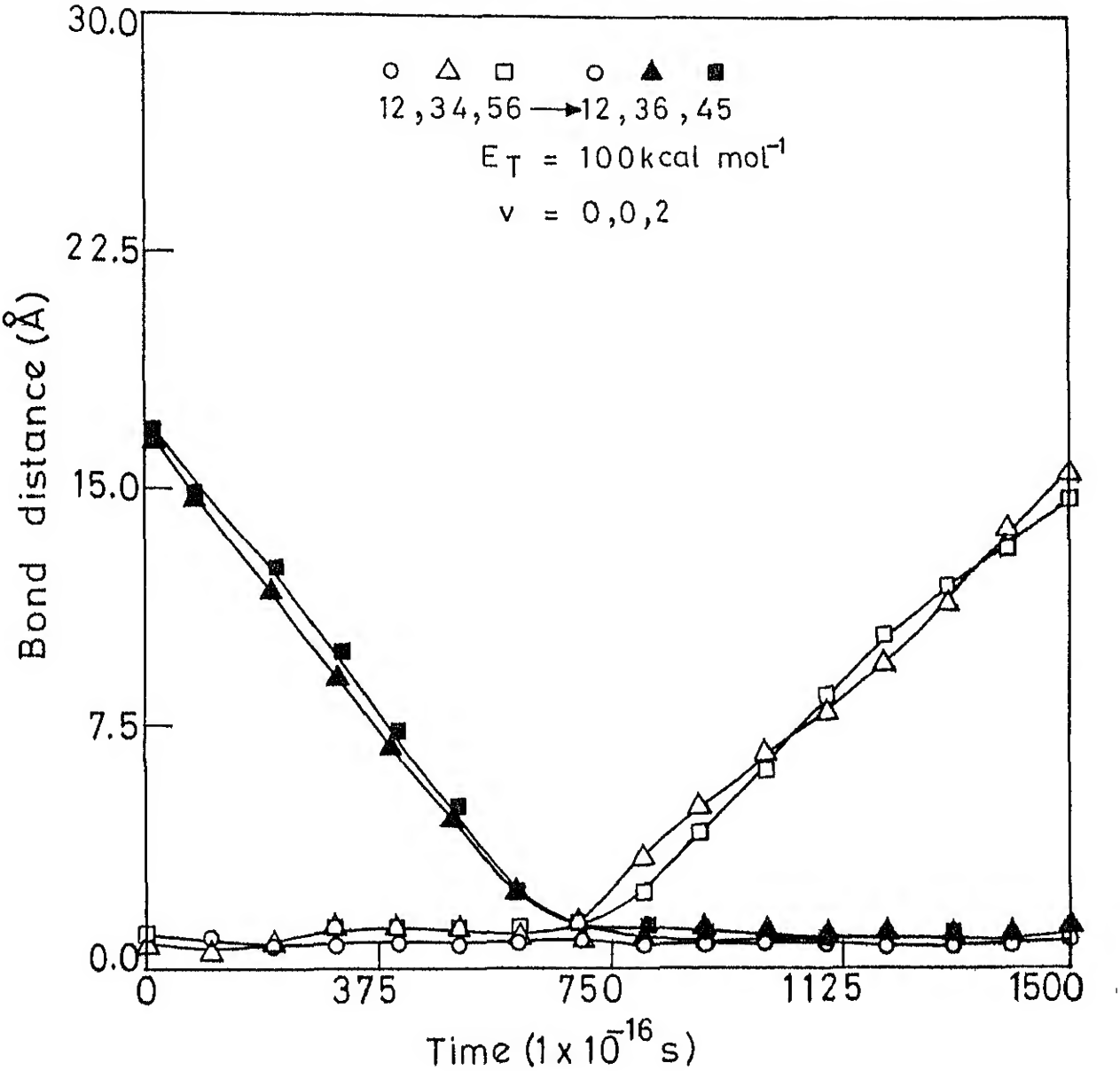

Fig.29 Bond distance versus time plot for a typical trajectory showing reaction (R12)

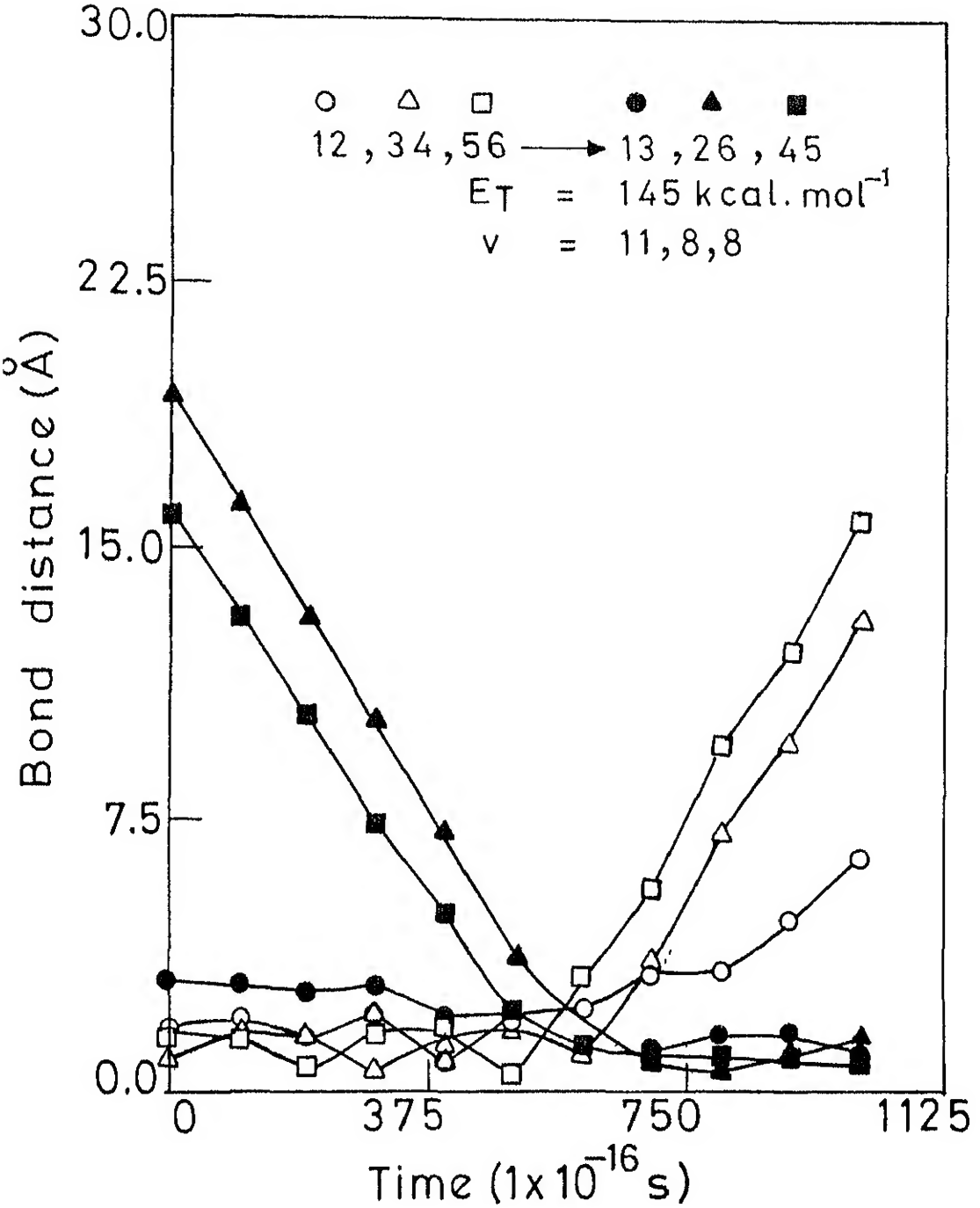

Fig.30 Same as fig.29 for a reaction of the type (R 9).

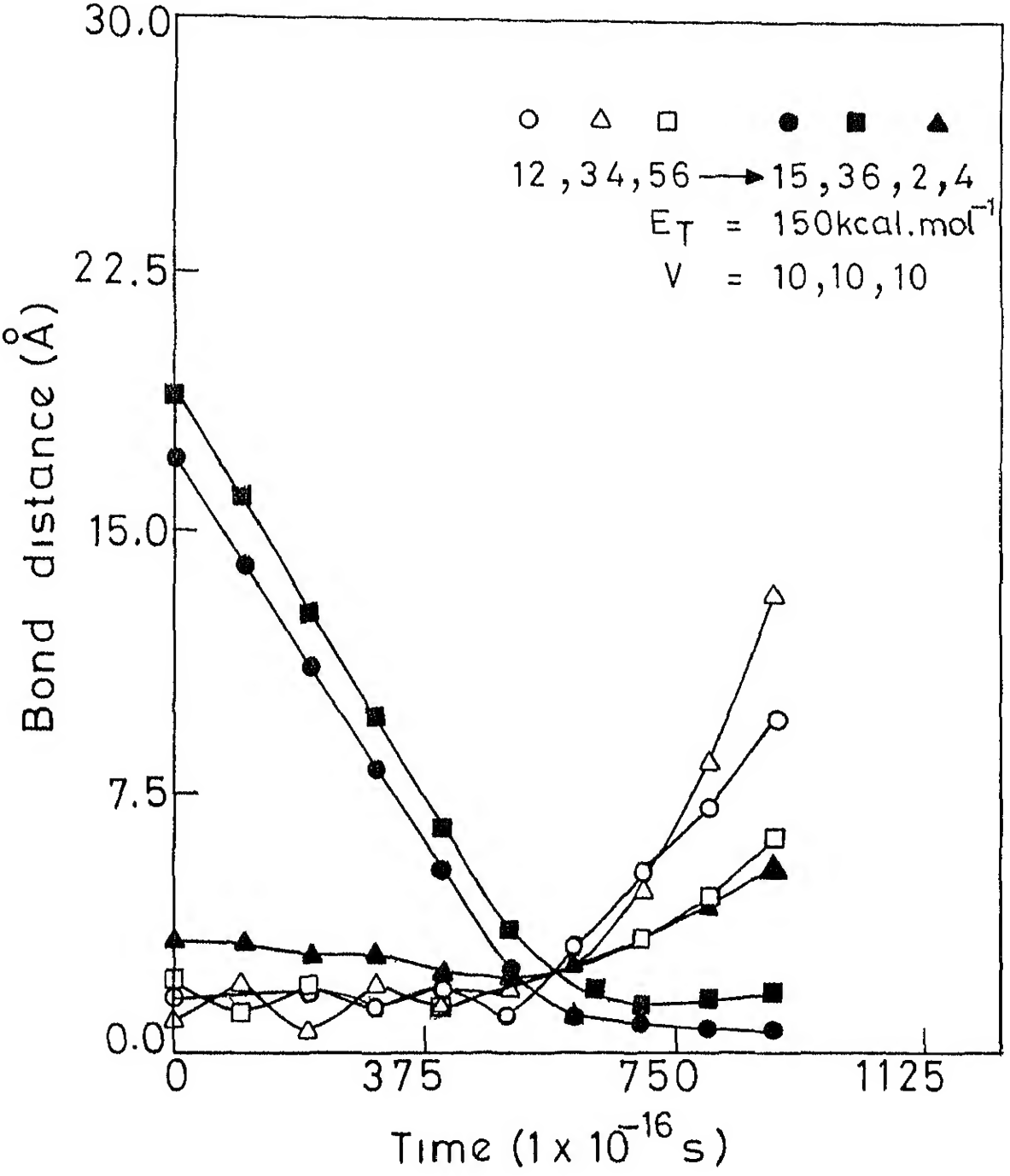

Fig. 31 Same as fig. 29 with only two diatomic molecules as the products.

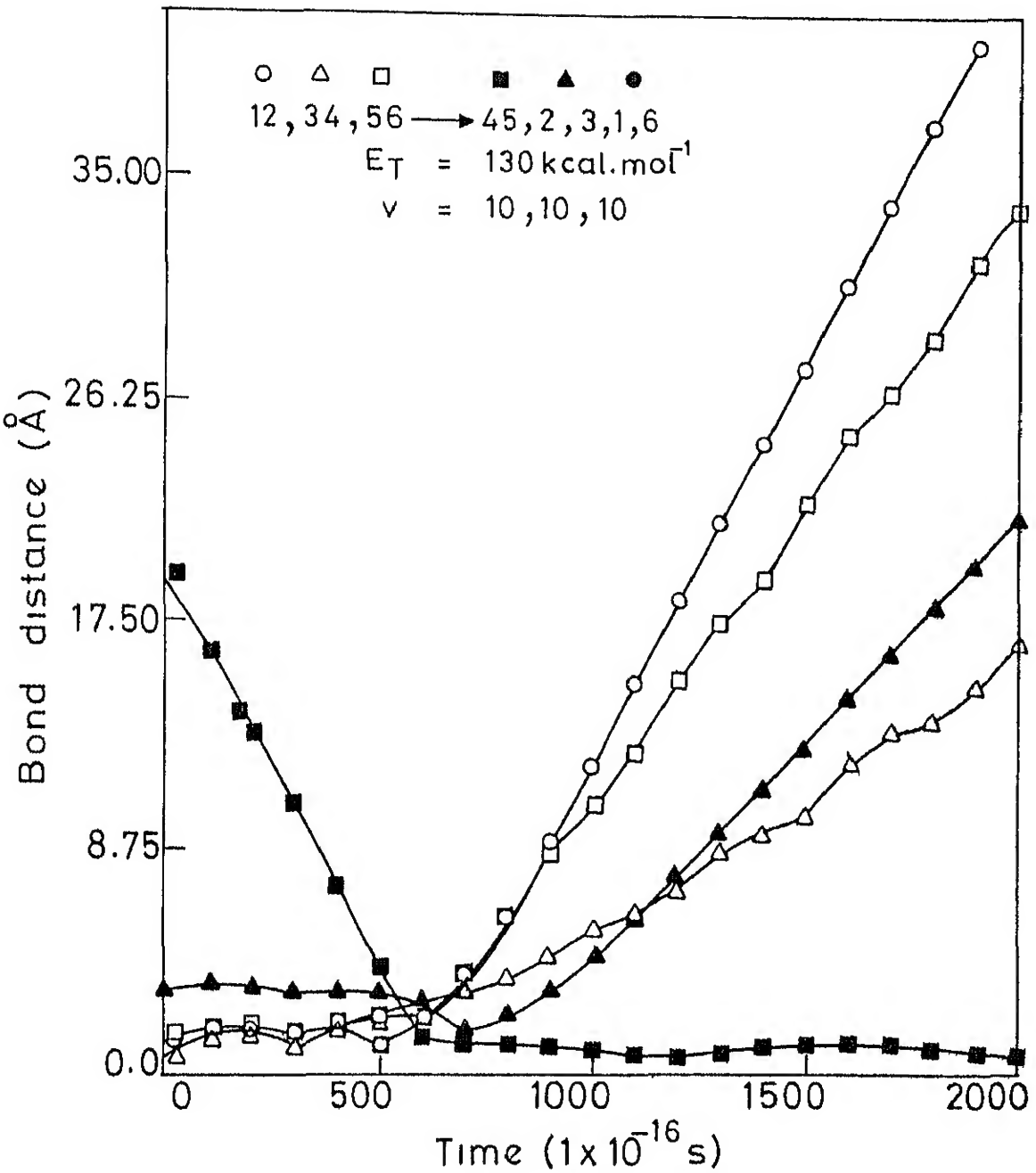

Fig.32 Same as fig. 29 with one stable diatomic molecule as a product.

the 'end' of the collision. A perspective view is shown in figs.33 and 34 for the above two types of collisions

We have investigated the effect of E_T and v on σ^R in a limited way. The summary presented in fig.35 shows that for (0,0,0), the threshold energy $E_{th} \leq$ 90 kcal.mol^{-1}, to be compared with the classical E_b of 69 kcal.mol^{-1} for the 6C pathway. It is clear that there is a substantial increase in σ^R with increase in E_T. At a fixed E_T, σ^R increases with v. Considering the fact that E_v = 6.31, 18.38 and 31.20 kcal.mol^{-1} for v = 0,1,2 respectively, it is clear that energy partitioning in the vibrational mode of the attacking diatom enhances σ^R. The fact that, as for atom-diatom systems, the increase in σ^R with E_T arises mainly from an increase in P^R in each b-stream while the vibrational enhancement arises significantly from an increase in the b_{max} is illustrated with the aid of $P^R(b)$ and $2\pi b.P^R(b)$ plots in fig.36-39.

We have computed the state-selected rate constant for the reactions (R9)-(R12) at 1000 K using the relation

$$k(T) = \langle v.\sigma^R \rangle \qquad (43)$$

We interpolated $\sigma^R(E_T)$ graphically and obtained k as 4.5×10^{-31} cm^3.molecule^{-1}s^{-1}, which is 3.0×10^{13} times smaller than the observed value of Bauer and Ossa[29] for the

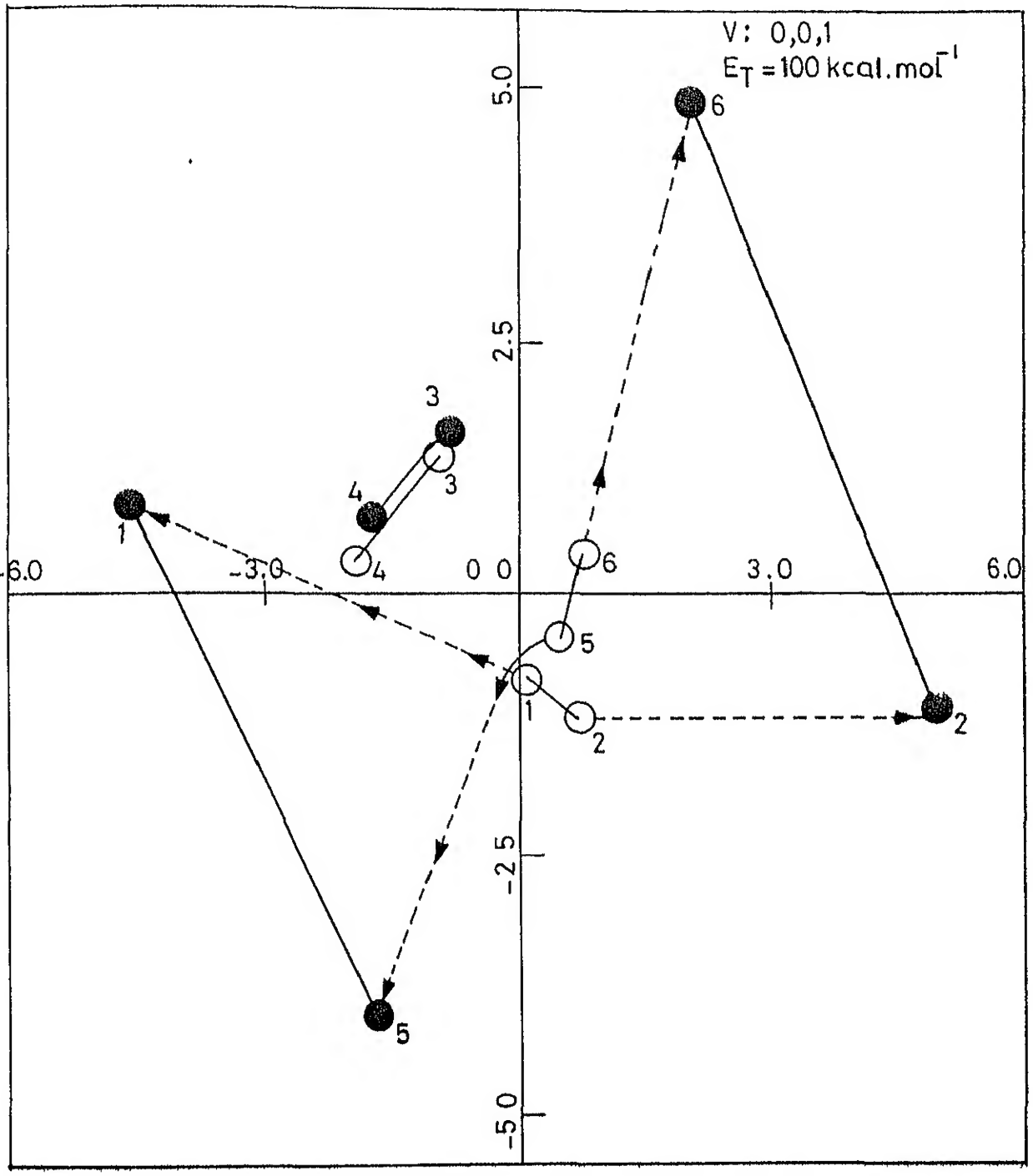

Fig.33 3D perspective view of reaction (R11).

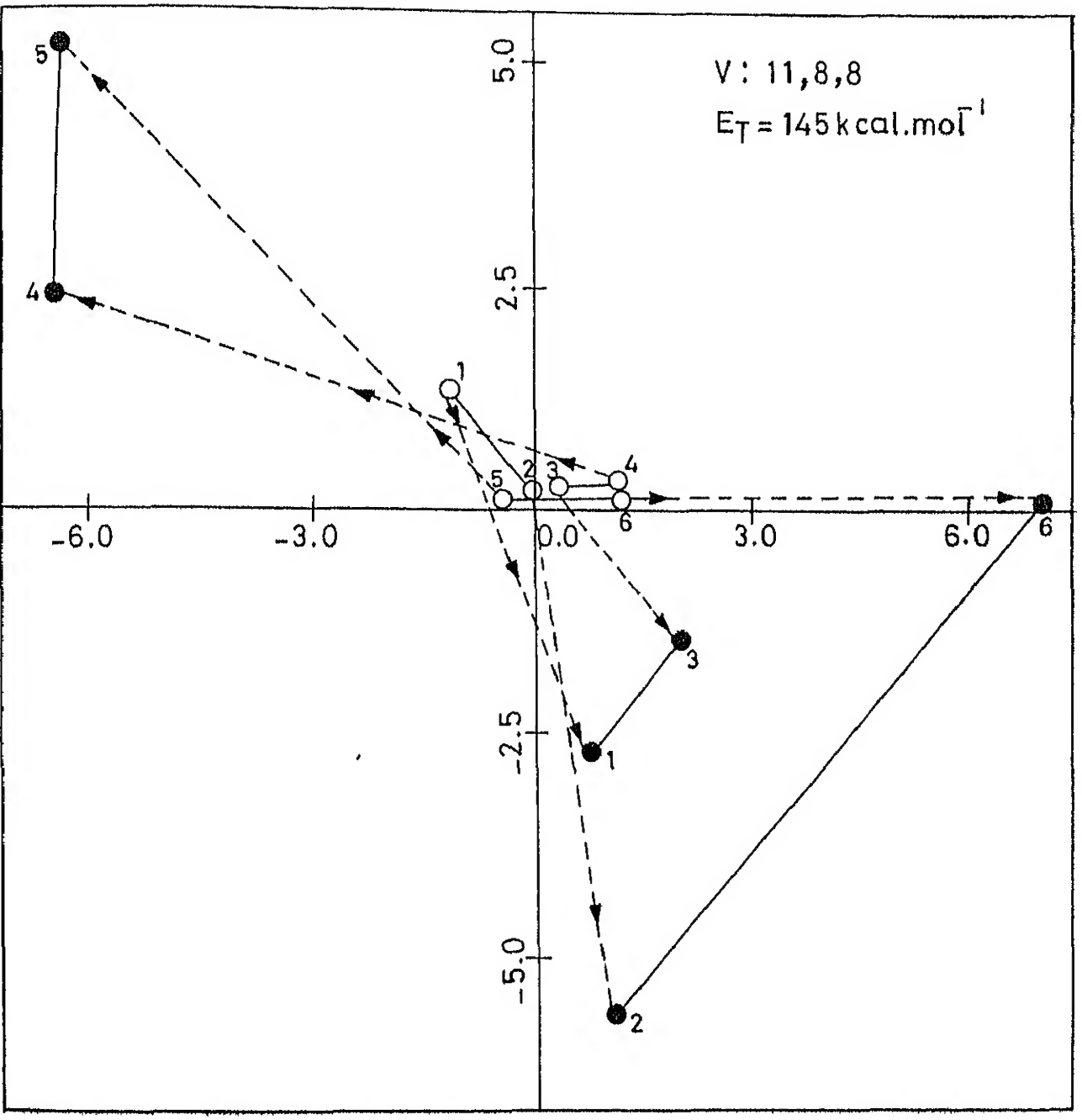

Fig. 34 Same as fig. 33 for (R9).

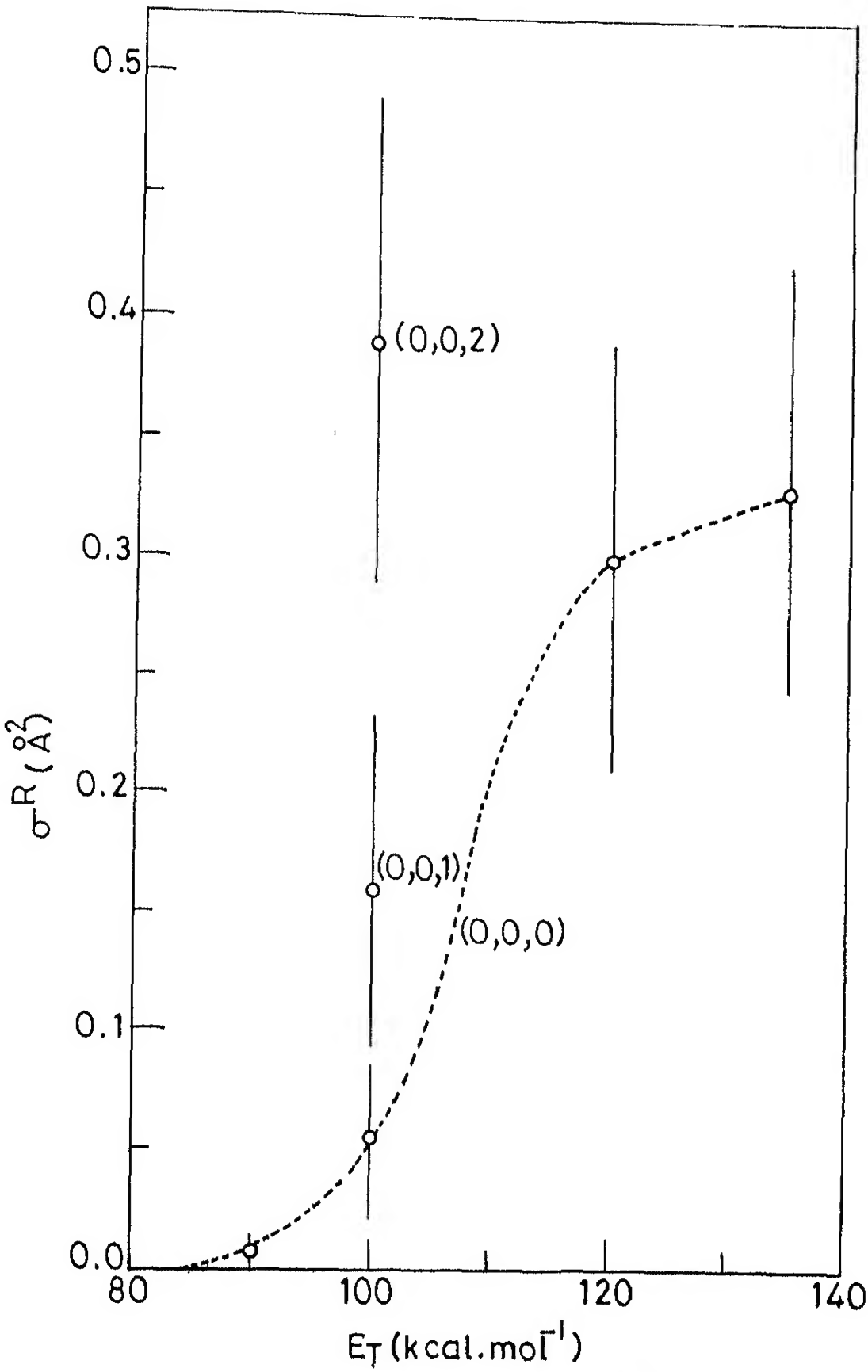

Fig.35 Dependence of σ^R on E_T and v. The error bars are of 68% confidence level.

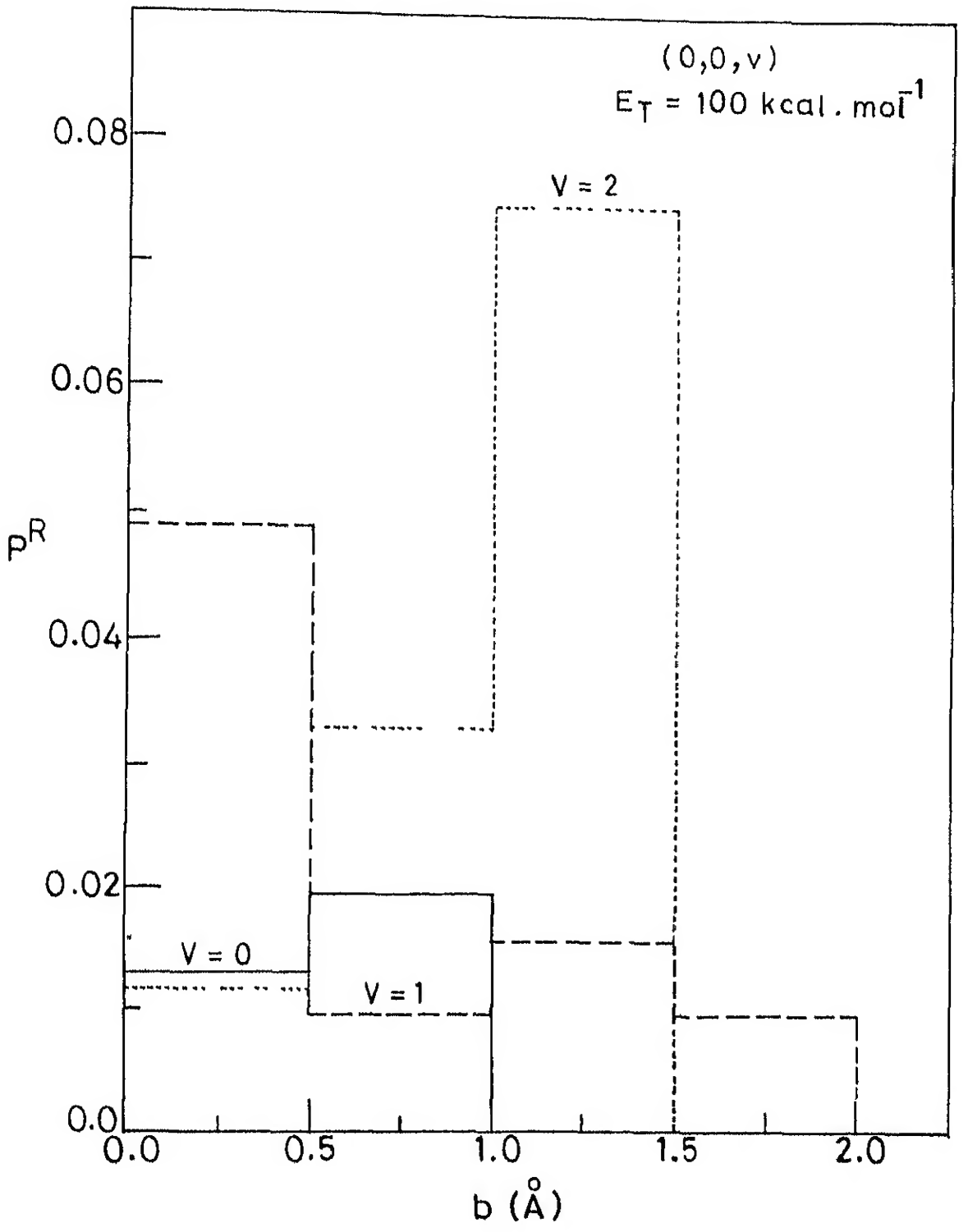

Fig. 36 Reaction probability as a function of impact parameter for different (0,0,v) at E_T = 100 kcal.mol^{-1}.

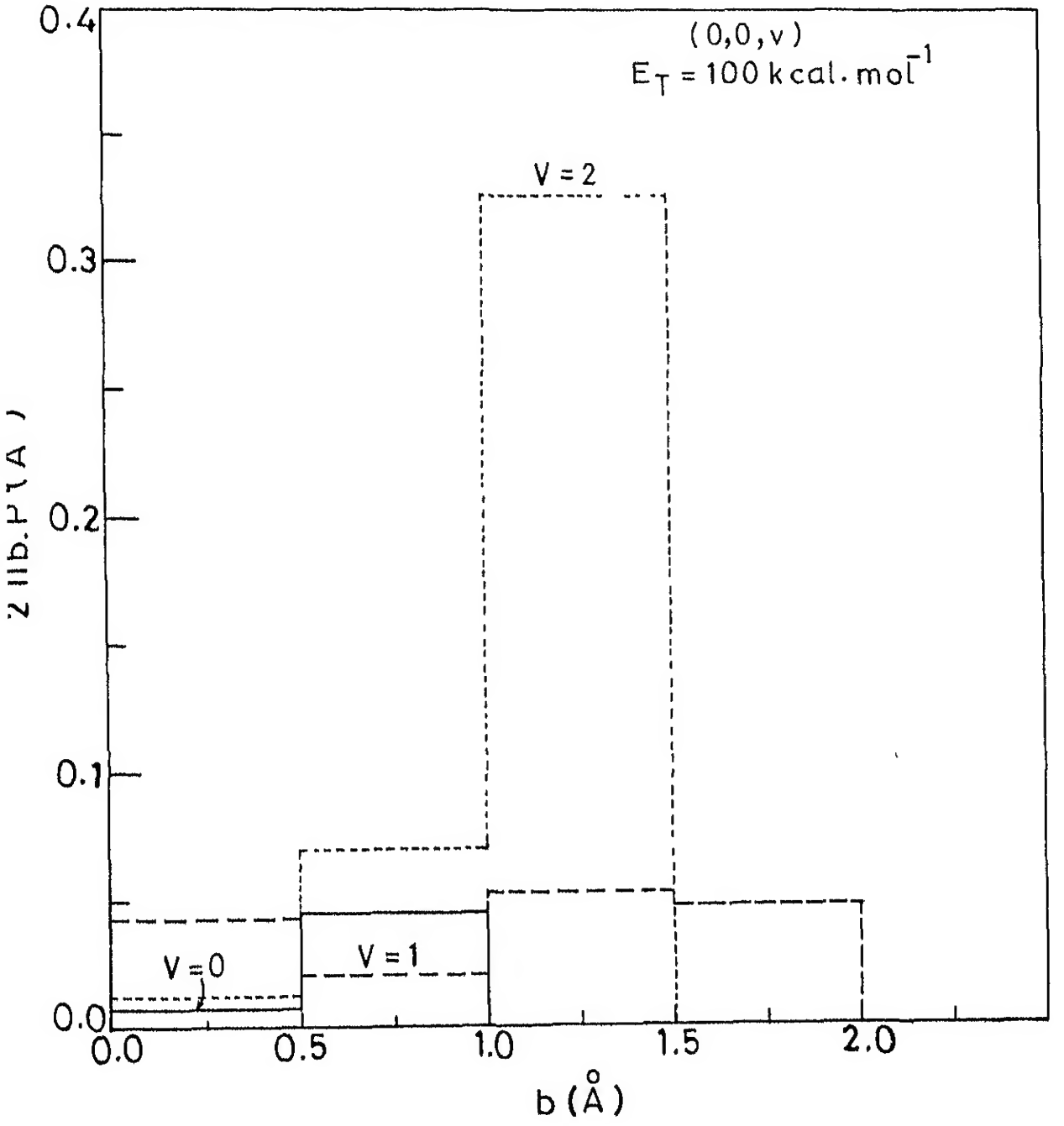

Fig. 37 Partial cross section as a function of b for different (0,0,v) at E_T = 100 kcal.mol^{-1}.

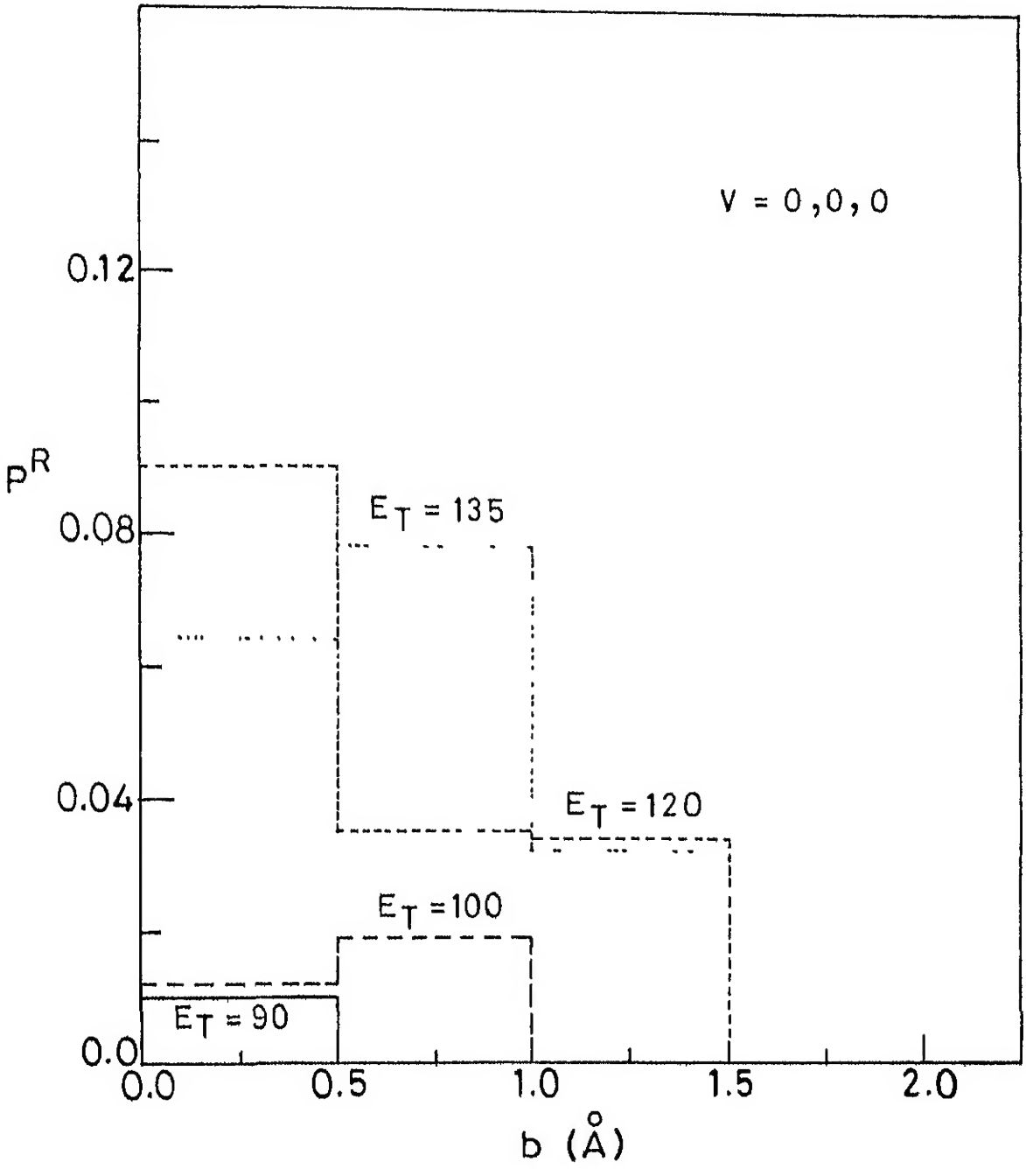

Fig. 38 Same as fig.36 for v= 0,0,0 at four different E_T.

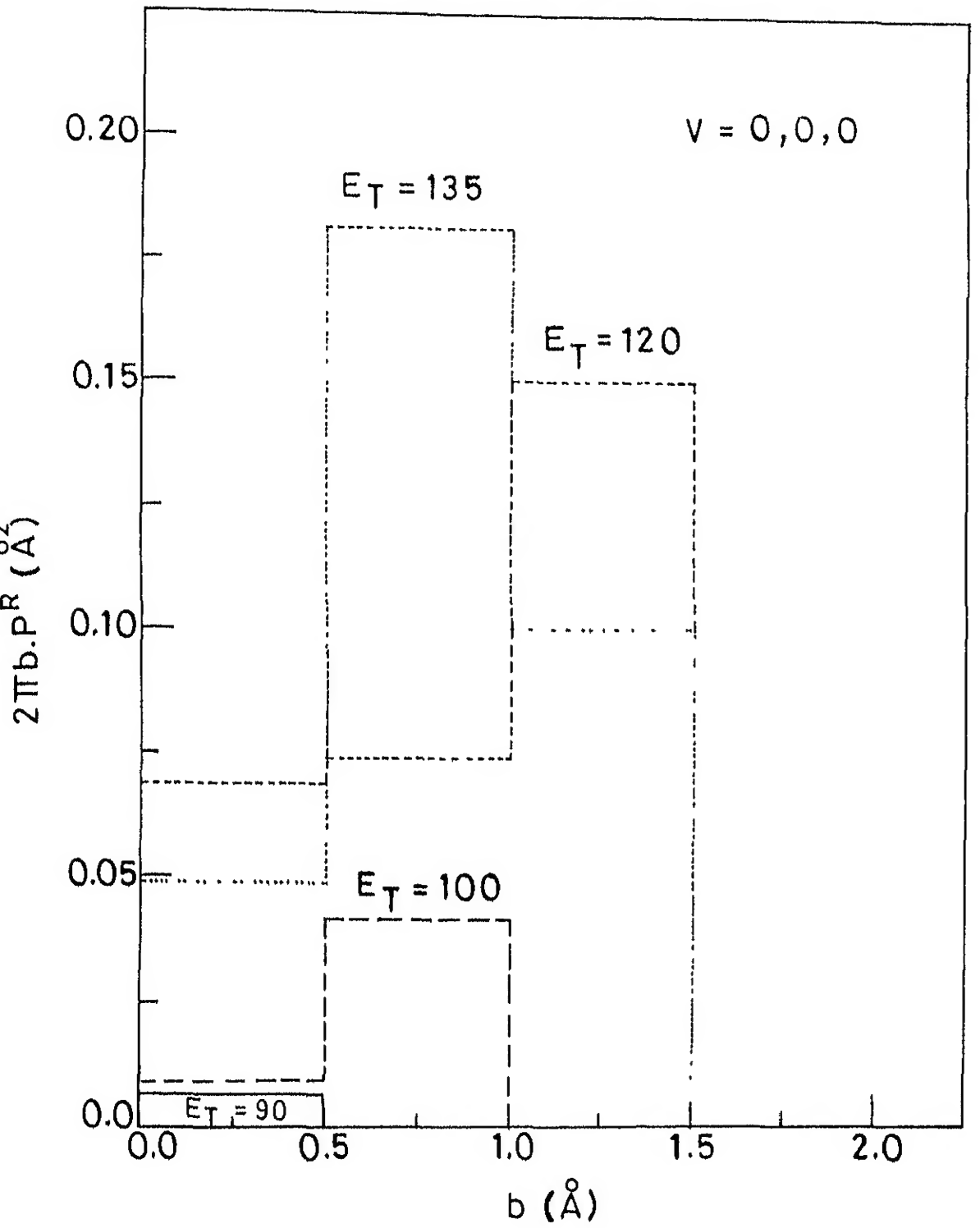

Fig.39 Same as fig.37 for V = 0,0,0 at four different E_T .

reaction (R3) in the presence of argon Despite the fact that a 6C pathway is energetically favored over the 4C pathway, the former has a dynamical threshold of ~90 kcal.mol^{-1}, nearly twice the experimental E_a of 42 kcal.mol^{-1}. Thus our computed k is bound to be several orders of magnitude less than the experimental k. As a matter of fact, if an E_a of 90 kcal.mol^{-1} is used instead of 42 kcal.mol^{-1} in the rate expression of Bauer and Ossa, k becomes comparable to ours emphasizing the role of the third body in the 4C exchange reaction.

CHAPTER FIVE

SUMMARY AND CONCLUSION

We have tested the utility of various different analytic functions in fitting repulsive potential-energy curves for $H_2(^3\Sigma_u^+)$, He_2, HeH and NaLi. A comparison of the different analytically fitted potentials for the test case of H_2 was presented in Chapter 2 with the help of 'ln V vs r' and residual plots. We have extended the study to 3-dimensions by fitting the limited amount of data available on the PES for the linear and bent geometries of $H_3^*(2pE')$ in the D_{3h} configuration by the rotated-anti-Morse-curve-spline (RAMCS) approach. The quality of the fit was illustrated with the help of contour plots, for different apex angles. We conclude that an exponential-poly function gives the best fit of the repulsive potential for $H_2(^3\Sigma_u^+)$ and HeH and close to the best for He_2 and NaLi The traditional anti-Morse function does serve as a reasonable alternative, particularly in view of the fact that it can be generalized to two and three dimensions as is the case for $H_3^*(2pE')$.

We have tested the utility of the SM function in fitting the chemically accurate ab initio data of Siegbahn and Liu for the ground state PES for H_3. Details of the fit along with a discussion of the quality of the fit with the aid of contour maps are given in Chapter 3. The SM function has been shown to

reproduce the surface with an rms deviation of 0.9 kcal mol^{-1}. A TDQM calculation for H + H_2 (v = 1) at 1000 K on the SM and SLTH surfaces vindicates the utility of the former in spite of the deficiencies like the tendency to show spurious wells in the region of the PES where there is a lack of ab initio data.

We have also reported the analytic fit of the ab initio data of Nager and Jungen for $H_3^{\wedge}(2pE')$. The SM function reproduces this surface with an rms deviation of 2.6 kcal. mol^{-1}. Unfortunately our attempts to make the two surfaces degenerate for D_{3h} geometries have not been successful. We are pursuing this aspect further.

We have presented the results of a dynamical study of a model six-center exchange reaction in Chapter 4. We have found that at low E_T (100-135 kcal.mol^{-1}) the reaction proceeds essentially as a 4C pathway with one of the diatomic molecules in the dimer acting as a mediating partner. At a higher E_T (135-155 kcal.mol^{-1} and for large v = 8-11) a 'true' 6C reaction takes place invariably leading to some dissociated molecules because of the high energies involved The computed σ^R values yield a threshold energy of ~90 kcal.mol^{-1}. While σ^R increases with E_T there is a vibrational enhancement when the energy is repartitioned from translation to vibration. We have computed the state-selected rate constant at 1000 K to be 4.5×10^{-31} cm^3 $molecule^{-1}s^{-1}$, several orders of magnitude

smaller than the experimentally observed value This discrepancy arises largely from the fact that despite the 6C pathway having a lower E_b than the 4C analog, the observed E_{th} of 90 kcal.mol^{-1} is still a factor of two larger than the experimental E_a of ~ 42 kcal.mol^{-1}. Since ours is the first 6C dynamical study, a much more elaborate study is needed and is planned for the next few months

REFERENCES

1. W.H. Miller, ed. Dynamics of Molecular Collisions, Parts A and B, Plenum, New York, 1976.
2. R.B. Bernstein, ed. Atom-molecule Collision Theory, a guide to experimentalist, Plenum, New York, 1979.
3. D.G. Truhlar, ed. Potential-Energy Surfaces and Dynamics Calculations, Plenum, New York, 1981.
4. M. Baer, ed. The Theory of Chemical Reaction Dynamics, CRC, Baco Raton, USA, in press.
5. Gaussian 80, QCPE Program No.406, Indiana University, Bloomington, Indiana U.S.A.
6. B. Liu, J. Chem. Phys. 58, 1925 (1973).
7. P. Siegbahn and B. Liu, J. Chem. Phys. 68, 2457 (1978).
8. B. Liu, J. Chem. Phys. 80, 581 (1984)
9. D.R. McLaughlin and D.L. Thompson, J. Chem. Phys. 70, 2748 (1979).
10. N. Sathyamurthy, Computer Phys. Rep. 3. 1 (1985).
11. J.N. Murrell, S. Carter, S.C. Farantos, P. Huxley and A.J.C. Varandas, Molecular Potential Energy Functions, John Wiley, Chichester (1984).
12. S. Thareja and N. Sathyamurthy, J. Chem. Soc. Faraday Trans. 2, 81, 717 (1985).

13. W. Kolos and C. Wolniewicz, J. Chem Phys 49, 404 (1968).

14. D.R. Mclaughlin and H F. Schaefer III, Chem. Phys. Lett 12, 244 (1971).

15. G. Das, A.F. Wagner and A.C. Wahl, J. Chem. Phys. 68, 4917 (1978).

16. P.J. Betroncini, G. Das and A.C. Wahl, J. Chem. Phys., 52, 5112 (1970).

17. S. Raynor, Private communication.

18. K.S. Sorbie and J.N. Murrell, Mol. Phys. 29, 1387 (1975).

19. A.J.C. Varandas and J.N. Murrell, Faraday discuss. Chem. Soc. 62, 92 (1977).

20. R. Schinke and W.A Lester, Jr., J. Chem Phys. 70, 4893 (1979); 72, 6821 (E) (1980), 72, 3754 (1980).

21. M.J. Redmon and G.C. Schatz, Chem. Phys. 54, 365 (1981).

22. S. Carter and J.N. Murrell, Mol. Phys. 41, 567 (1980)

23. M.A. Giltins, D.M. Hirst and M.F. Guest, Faraday Discuss. Chem. Soc. 62, 67 (1977).

24. E. Herbst. Chem. Phys. Lett. 47, 517 (1977).

25a) Tomi Joseph, Ph.D. Thesis, Indian Institute of Technology, Kanpur, 1983.

b) Tomi Joseph and N. Sathyamurthy, J. Chem. Phys. - to be published.

26. D.G. Truhlar and C.J. Horowitz, J. Chem. Phys.68, 2466 (1978); 71, 1514 (E) (1979).

27. Ch. Nager and M. Jungen, Chem. Phys. 70, 189 (1982).

28a) J.H. Sullivan, J. Chem. Phys. 46, 73 (1967).

b) R.N. Porter, L.B. Sims, D.L. Thompson and L.M. Raff, J. Chem. Phys. 58, 2855 (1973).

29. S.H. Bauer and E. Ossa, J. Chem Phys 45, 434 (1966).

30. A. Burcat and A. Lifshitz, J. Chem. Phys. 47, 3079 (1967).

31. R.D. Kern and G.G. Nika, J. Phys. Chem. 75, 1615 (1971); 75, 2541 (1971).

32. S.H. Bauer, Ann. Rev. Phys. Chem. 30, 271 (1979).

33. L.P. Herman, J. Chem. Phys. 72, 5777 (1980)

34. J.M. Silver and R.M. Stevens, J. Chem. Phys 59, 3378 (1973).

35. N.J. Brown and D.M. Silver, J Chem. Phys. 68, 3607 (1978)

36a) R.B. Woodward and R. Hoffmann, The Conservation of Orbital Symmetry, Verlag Chemie, Gmbh, Weinheim, 1970.

b) R. Hoffmann, J. Chem. Phys. 49, 3739 (1968).

37. J.S. Wright, Chem. Phys. Lett. 6, 476 (1970).

38. J.S. Wright, Can. J. Chem. 53, 549 (1975).

39. D.L. Thompson and H.H. Suzukawa, J. Am. Chem. Soc. 99, 3614 (1977).

40. D.A. Dixon, R.M. Stevens and D.R. Herschbach, Faraday Discuss. Chem. Soc. 62, 110 (1977).

41. D.A. Dixon and D.R. Herschbach, J. Am. Chem. Soc., 97, 6268 (1975).

42. D.A. Dixon and D.R. Herschbach, Ber Bunsenges, Phys. Chem 81, 145 (1977)

43. S. Sato, J. Chem. Phys. 23, 592 (1955).

44. L. Pedersen and R N. Porter, J. Chem. Phys.47, 4751 (1967).

45. W. Kolos and C. Wolniewicz, J. Chem. Phys. 43, 2429 (1965); 49, 404 (1968).

46. D.R. Bates, K. Ledsham and A.L Stewart, Phil. Trans Roy. Soc. (London), 246, 215 (1953).

47. P.J. Kuntz and A.C. Roach, J. Chem. Soc. Faraday Trans. 2, 68, 259 (1972).

48. D.R. Bates and R.H.G. Reid, Adv. At. Mol. Phys. 4, 13 (1968).

49. T. Berces, React. Kinet. Catal. Lett. 7, 379 (1977).

50. O. Kafri and M.J. Berry, Faraday Discuss. Chem. Soc. 62, 127 (1977).

51. J.R. Stine and J.T. Muckerman, J. Chem. Phys. 68, 185 (1978).

52a) D.R. McLaughlin and D.L. Thompson, J. Chem. Phys. 59, 4393 (1973).

b) N. Sathyamurthy and L.M. Raff, J. Chem. Phys. 63, 464 (1975).

53. S.A. Sonneleitner and C.L. Beckel, J. Chem. Phys. 73, 5405 (1980).

54. M.M. Madsen and J.M. Peek, At. Data, 2, 171 (1971).

55. A.J.C. Varandas and J. Brandão, Mol. Phys. 45,857 (1982).

56. J.N. Murrell and K.S. Sorbie, J. Chem. Soc. Faraday Trans. 2, 70, 1552 (1974).

57. P. Huxley, D.B. Knowles, J.N. Murrell and J.D. Watts, J. Chem. Soc. Faraday Trans. 2, 80, 1349 (1984).

58. H. Akima, J. Assoc. Comput. Mach. 17, 589 (1970), Commun. Assoc. Comput. Mach. 15, 914 (1972).

59. NAG : Numerical Algorithms Group, Mark 8 Library, Daresbury Laboratory, UK.

60a) H.R. Mayne, R.A. Poirier and J C. Polanyi, J Chem. Phys. 80, 4025 (1984).

b) H.R. Mayne, J.C. Polanyi, S. Raynor and N. Sathyamurthy, J. Phys. Chem. 88, 4064 (1984).

c) P.M. Agrawal, V. Mohan and N. Sathyamurthy, Chem. Phys. Lett. 114, 343 (1985).

61a) K.C. Kulander, and M.F. Guest, J. Phys. B, 12, L501 (1979).

b) S. Raynor and D.R. Herschbach, J. Phys. Chem. 86, 1214, 3592 (1982).

62. F.T. Wall and R.N. Porter, J. Chem. Phys. 36, 3256 (1962).

63. A.J.C. Varandas, J. Chem. Phys. 70, 3786 (1979).

64. C.F. Giese and W.R. Gentry, Phys Rev. A10, 2156 (1974).

65. I.G. Csizmadia, R.E. Kari, J.C. Polanyi, A.C . Roach and M.A. Robb, J. Chem. Phys. 52, 6205 (1970).

66. J.N. Murrell, S. Carter, I.M. Mills and M.F. Guest, Mol. Phys. 42, 605 (1981).

67. P. Knowles, N.C. Handy and S. Carter, Mol. Phys. 49, 681 (1983).

68. J.N. Murrell and L.J. Dunne, Chem. Phys. Lett. 102, 155 (1983).

69. I. Noor Batcha, Ph.D. Thesis, Indian Institute of Technology, Kanpur, India (1982).

70. H. Goldstein, Classical Mechanics, Addison-Wesley, Reading, Mass (1950).

71. A. Sherman and H. Eyring, J. Am. Chem. Soc. 54, 2661 (1932).

72. H.S. Taylor, H. Eyring and A. Shermann, J. Chem. Phys. 1, 68 (1933).

73. S. Glasstone, H. Eyring and K.J. Laidler, "The Theory of Rate Processes", McGraw-Hill, New York (1941).

74. L.M. Raff, L. Stivers, R.N. Porter, D.L. Thompson and L.B. Sims, J. Chem. Phys. 52, 3449 (1970).

75. R.P. Feynman, Phys. Rev. 56, 340 (1939).

76. P.O. Lowdin, J. Mol. Spectrosc. 3, 2232 (1962).

77a) Y. Beppu and T. Ninomiya, Comput. Phys. Commun. 23, 123 (1981).

b) Quantum Chemistry Program Exchange Program No. 409, Indiana University Bloomigton Ind. USA (1981).

78. IMSL: International Mathematical and Statistical Libraries, Inc., Houston, Texas, USA.

79. J.L. Schreiber, University of Toronto, Canada, 1975.

APPENDIX

J. Chem. Soc., Faraday Trans. 2, 1985, 81, 717–723

Fitting Repulsive Potential-energy Curves and Surfaces

BY SUKARMA DHARMA AND N SATHYAMURTHY*

Department of Chemistry, Indian Institute of Technology, Kanpur 208 016, India

Received 29th August, 1984

The utility of various different analytic functions in fitting repulsive potential-energy curves for a few diatomic species has been tested. An exponential function with a polynomial exponent is found to be the best. A limited number of data on the potential-energy surfaces for the linear and bent geometries of H_3^+ ($2p\pi_u$ in the $D_{\infty h}$ configuration) can be fitted reasonably well by an approach involving a rotated anti-Morse curve-spline interpolation.

Fitting an analytic function to potential-energy values continues to remain a bottleneck in going from electronic-structure calculations to detailed dynamical studies. Fitting potential-energy values as a function of one independent variable is the simplest problem. While considerable progress has been made in fitting potential-energy curves containing one minimum,[1] the problem of fitting a purely repulsive curve has received less attention. The first attempt to represent a repulsive potential-energy curve was by Sato[2] and was for the triplet state ($^3\Sigma_u^+$) of H_2. He had used an anti-Morse function of the form

$$V = \frac{D}{2}[\exp(-2\beta\rho) + 2\exp(-\beta\rho)] \tag{1}$$

where $\rho = r - r_e$ and D, r_e and β are the bond dissociation energy, the equilibrium bond distance and the curvature parameter, respectively, for the ground state ($^1\Sigma_g^+$) of H_2 and have no physical meaning for the triplet state.

Pedersen and Porter[3] extended the function by matching it with an exponential function at longer range:

$$\begin{aligned} V &= A[\exp(-2\beta\rho) + 2\exp(-\beta\rho)], && r \leq 1.6 \text{ au} \\ &\quad - b(r + c)\exp(-\alpha r), && r > 1.6 \text{ au} \end{aligned} \tag{2}$$

and were able to fit the *ab initio* potentials for H_2 and $H_2^+(^2\Sigma_u^+)$.[4,5] Kuntz and Roach[6] modified the anti-Morse function further by allowing β to be a variable.

$$\beta = \beta(1 + \gamma\rho + \delta\rho^2) \tag{3}$$

and fitted the potentials for H_2 and H_2^+ successfully.[4,7] Berces[8] has shown that

$$V = (D/\alpha)\exp(-2\beta\rho)[1 + (\beta\rho)^{2\alpha}] \tag{4}$$

is also more flexible than the anti-Morse function in fitting the triplet potential-energy curves of H_2, HI and I_2. Kafri and Berry[9] used a simple exponential with a polynomial exponent for fitting the *ab initio* data of Kolos and Wolniewicz[4]

$$V = \exp[(a_0 + a_1 r + a_2 r^2 + a_3 r^3 + a_4 r^4 + a_5 r^5)], \tag{5}$$

Stine and Muckerman[10] used a one-dimensional spline[11] for fitting the potential-energy curve for $H_2^+(^2\Sigma_u^+)$. Sonnleitner and Beckel[12] have shown that rational fractions can be used to reproduce the potential for $H_2^+(2p\sigma_u)$.[13]

More recently Varandas and Brandão[14] have proposed the use of an exponential multiplied by r^{-1}, i.e.

$$V = A\rho^{-1}\exp(-b\rho) \tag{6}$$

for alkali-metal dimers in their $^1\Sigma$ state. Almost a decade ago Murrell and Sorbie[15] had proposed the use of an extended Rydberg function

$$V = -D\exp(-a_1\rho)(1 + a_1\rho + a_2\rho^2 + \quad) \tag{7}$$

for fitting potentials with a single minimum. However, there is no reason why it cannot be used to fit a repulsive curve in the same way as an anti-Morse function. In principle, given adequate data, the potential-energy values can be fitted by a polynomial, or better still by a one-dimensional spline or Akima[16] interpolation. In practice one prefers a simple analytic function with a few parameters to be determined.

To the best of our knowledge no comparative study has been made of the validity of these various functions in fitting the data for a single system. The obvious choice for a test case would be the $^3\Sigma_u^+$ state of H_2 for which accurate *ab initio* values are available.[4] We have undertaken such a study for H_2, He_2, HeH and NaLi and the results are summarized in the next section. We must mention that we have only considered global functions in this study and not the use of piecewise interpolation methods. We have specifically considered only the anti-Morse,[2] Berces,[8] exponential-poly,[9] modified exponential[14] and extended Rydberg[15] functions, as we are interested in functions which require only limited input data and also are extendable to higher dimensions.

As a test case of a repulsive potential-energy surface with 2 or 3 independent variables we have examined the possibility of fitting the potential-energy surface for H_3^* ($2pE'$ in its D_{3h} geometry). This surface is needed in our study of the spectroscopy of the transition state in predicting the wings to the Lyman-α line in $H + H_2$ collisions.[17] The amount of *ab initio* information available on this surface is scanty.[18] Therefore, at our request Raynor[18c] has computed a diatomics-in-molecules[18b] potential-energy surface in rotated Morse coordinates[19] (l, θ) for linear as well as non-linear geometries, with three potential-energy values along each direction, for $\theta = 0$, 10, 20, 30, 35, 40, 42, 43, 44 and 45°, and hence by symmetry at $\theta = 46$, 47, 48, 50, 55, 60, 70, 80 and 90° for the bending angle $\gamma = 60$, 90, 120 and 180°. In the next section we report our successful rotated anti-Morse-curve-spline (RAMCS) fit of the potential for fixed-γ geometries.

RESULTS AND DISCUSSION

Ab initio values[4] of ln V for $H_2(^3\Sigma_u^+)$ are plotted against r in fig. 1, and for comparison the different analytically fitted potentials are shown in the same graph. The parameters for each function were determined by a non-linear least-squares fit of the *ab initio* data using the E04FCF program of NAG.[20] The root-mean-square (r.m.s.) and the maximum deviations for each function are listed in table 1.

The anti-Morse function fits the H_2 potential adequately at short range. The modification introduced by Berces improves the fit dramatically, but at the expense of adding a parameter. The exponential-poly function deviates much more than the Berces function at long range. However, the former gives the best overall fit,

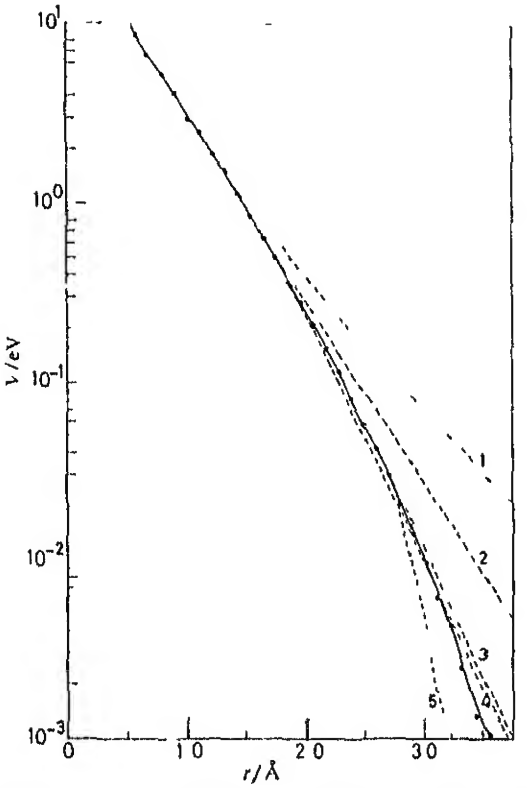

Fig. 1. Comparison of different analytic fits to the *ab initio* data The *ab initio* potential energy values[1] are connected by a solid line The dashed lines represent the different functional fits (1) modified exponential, (2) anti Morse, (3) extended Rydberg, (4) Berces and (5) exponential-poly

as is illustrated with the aid of a residual plot in fig 2 The extended Rydberg functional fit is only slightly inferior to the Berces, but involves as many parameters as the exponential-poly fit The modified exponential function gives the poorest fit

We have tried the different functional fits for the *ab initio* potentials for He_2, *HeH* and *NaLi* [21-23] The results summarized in table 1 show that while the anti-Morse function fits the potential reasonably, the exponential-poly gives a better fit for all the systems The quality of the fit obtained by using the extended Rydberg function is comparable to that of the exponential-poly for He_2 and NaLi. Berces gives the worst fit for NaLi and the extended Rydberg that for HeH

If a large number of potential-energy values are available and the number of parameters can be as large as 6, the exponential-poly fit is obviously the best or close to being the best It also offers the advantage that ln V can be fitted to a polynomial by a linear least-squares fit to yield an excellent set of initial-guess parameters for carrying out a non-linear least-squares fit (an important practical advantage over the other functional approaches) On the other hand, if the number of parameters has to be as low as three, the anti-Morse function yields reasonable results and it also promises to be the candidate when potential-energy values involving more than one independent variable are to be fitted

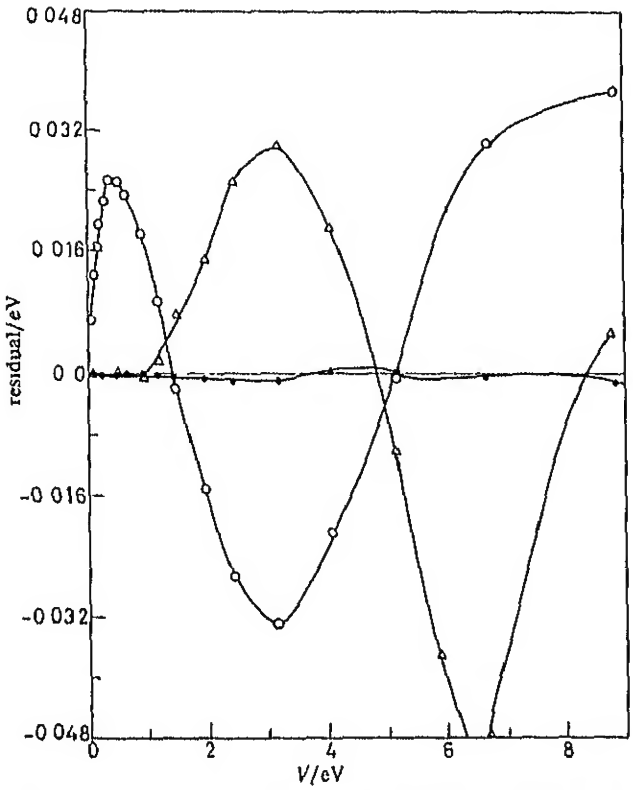

Fig. 2. Residual plots comparing the performance of the Berces (O), extended Rydberg (△) and exponential-poly (●) functions

For example, for the collinear geometry of H_3^+ we have fitted the potential[18c] along each direction for different values of θ using an anti-Morse function The θ dependence of the resulting parameters as plotted in fig 3 was reproduced by a one-dimensional spline interpolation method, and the overall RAMCS fit is illustrated with the aid of potential-energy contours in fig 4 We were also able to obtain an RAMCS fit to the potential for the bent geometries The θ-dependence of the parameters for $\gamma = 120$, 90 and 60° is comparable to that of $\gamma = 180°$ except for a double hump in $l_6(\theta)$ for $\gamma = 60°$. The potential in the range 0–6 7 eV is reproduced with r.m s deviations of 0.21, 0 19, 0 15 and 0 20 eV for $\gamma = 180$, 120, 90 and 60°, respectively The maximum deviations are correspondingly 0 35, 0 32, 0 34 and 0 30 eV When necessary, the (θ, γ) dependence of the anti-Morse parameters can be fitted by a two-dimensional spline[11] to obtain an overall three-dimensional fit

We were constrained to use only three-parameter functions in our rotated-function approach, as only three potential-energy values were available along each direction. We tried to use

$$V = \exp(a_0 + a_1\rho + a_2\rho^2) \tag{8}$$

and

$$V = Dl \exp(-a_1 l)(a_1 + a_2 l) \tag{9}$$

Table 1. Quality of fit of the different analytic functions to the *ab initio* potential of a few selected diatomic systems

system	ref for the *ab initio* data	range of r values[a] /Å	range of V values /eV	deviation[b,c] /eV				
				anti-Morse	Berces	exponential-poly	modified exponential	extended Rydberg
H_2	4	0 53–5 29 (85)	−0 002 −(+) 10 30	3 6 (−2) 14 4 (−2)	1 5 (−2) 3 8 (−2)	0 4 (−2) 1 2 (−2)	10 1 (−2) 28 6 (−2)	2 3 (−2) 17 9 (−2)
He_2	21	1 58–5 29 (26)	−0 001 −(+) 0 32	1 9 (−3) 3 0 (−3)	1 2 (−3) 1 9 (−3)	0 66 (−3) 1 0 (−3)	1 7 (−3) 2 7 (−3)	0 7 (−3) 1 1 (−3)
HeH	22	2 64–4 76 (7)	0 00001 −(+) 0 013	1 5 (−5) 3 0 (−5)	1 7 (−5) 2 0 (−5)	1 1 (−5) 15 0 (−5)	1 7 (−5) 2 9 (−5)	9 8 (−5) 16 0 (−5)
NaLi	23	2 65–7 98 (10)	0 0–0 65	6.4 (−4) 10 0 (−4)	18 0 (−4) 39 0 (−4)	1 6 (−4) 3 4 (−4)	5 0 (−4) 8 0 (−4)	1 4 (−4) 2 3 (−4)

[a] Values in parentheses give the number of r values [b] First row gives the r m s. deviation and second row the maximum deviation for each function [c] Values in parentheses give the powers of ten

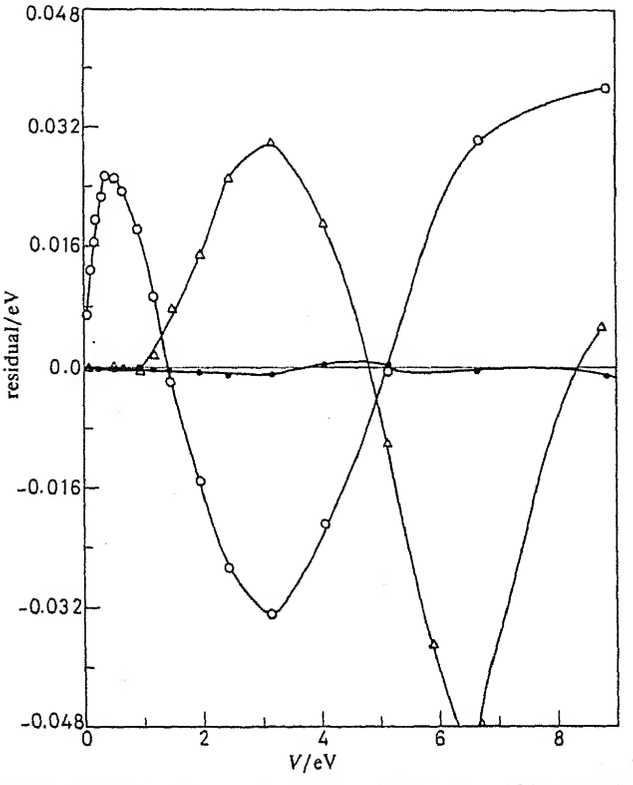

Fig. 2. Residual plots comparing the performance of the Berces (○), extended Rydberg (△) and exponential-poly (●) functions.

For example, for the collinear geometry of H_3^* we have fitted the potential[18c] along each direction for different values of θ using an anti-Morse function. The θ dependence of the resulting parameters as plotted in fig. 3 was reproduced by a one-dimensional spline interpolation method, and the overall RAMCS fit is illustrated with the aid of potential-energy contours in fig. 4. We were also able to obtain an RAMCS fit to the potential for the bent geometries. The θ-dependence of the parameters for $\gamma = 120$, 90 and 60° is comparable to that of $\gamma = 180°$ except for a double hump in $l_e(\theta)$ for $\gamma = 60°$. The potential in the range 0–6.7 eV is reproduced with r.m.s. deviations of 0.21, 0.19, 0.15 and 0.20 eV for $\gamma = 180$, 120, 90 and 60°, respectively. The maximum deviations are correspondingly 0.35, 0.32, 0.34 and 0.30 eV. When necessary, the (θ, γ) dependence of the anti-Morse parameters can be fitted by a two-dimensional spline[11] to obtain an overall three-dimensional fit.

We were constrained to use only three-parameter functions in our rotated-function approach, as only three potential-energy values were available along each direction. We tried to use

$$V = \exp(a_0 + a_1\rho + a_2\rho^2) \tag{8}$$

and

$$V = Dl \exp(-a_1 l)(a_1 + a_2 l) \tag{9}$$

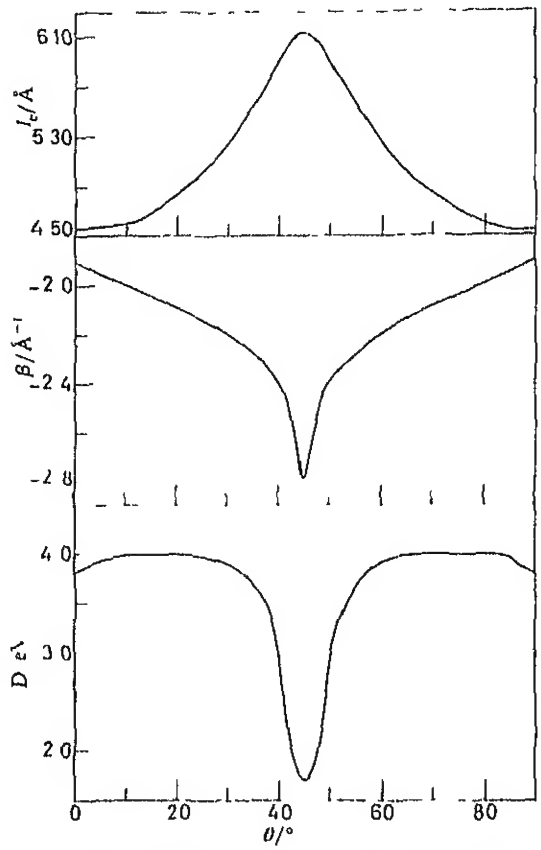

Fig. 3 Dependence on θ of the anti-Morse parameters for collinear H_3^*

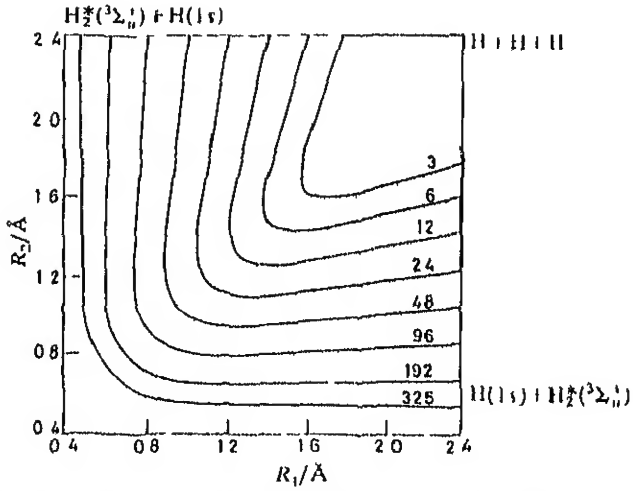

Fig. 4 Potential-energy contours for the RAMCS fitted collinear H_3^* surface The potential-energy values are in kcal mol^{-1} units relative to the separated-atoms limit

which are the truncated and modified forms of the exponential-poly and extended Rydberg functions, respectively We did not obtain satisfactory fits at low energies using eqn (8) Although eqn (9) gave a good fit along each direction, the variation of the parameters (D, a_1 and a_2) with θ was not smooth. Hence we were not in a position to fit the H_3^+ potential successfully using these two functions

CONCLUSIONS

We have shown that, while an exponential-poly function gives the best fit of the repulsive potential for $H_2(^3\Sigma_u^+)$ and HeH, and close to the best for He_2 and NaLi, the traditional anti-Morse function does serve as a reasonable alternative, particularly in view of the fact that it can be generalized to two and three dimensions as for H_3^+ ($2pE'$)

Note added in proof Huxley *et al*[24] have reported recently that an appended extended Rydberg function

$$V = A(1 + a_1 l + a_2 l^2 + a_3 l^3)\exp(-a_1 l)$$
$$-\tanh(l - l_m/2)(c_6 r^{-6} + c_8 r^{-8} + c_{10} r^{-10})$$

performs better than the extended Rydberg function in fitting repulsive potentials with a van der Waals minimum for a large number of diatomic species

The calculations reported here were carried out on a DEC-1090 Computer at the Indian Institute of Technology, Kanpur This study was supported in part by a grant from the Department of Science and Technology, New Delhi We are thankful to the referees for their comments

[1] N Sathyamurthy, *Comput Phys Rep* to be published
[2] S Sato, *J Chem Phys*, 1955, 23, 592
[3] L Pedersen and R N Porter, *J Chem Phys*, 1967, 47, 1751
[4] W Kolos and C Wolniewicz, *J Chem Phys*, 1965, 43, 2429, 1968, 49, 404
D R Bates, K Ledsham and A L Stewart, *Philos Trans R Soc London*, 1953, 246, 215
[6] P J Kuntz and A C Roach, *J Chem Soc, Faraday Trans 2*, 1972, 68, 259
[7] D R Bates and R H G Reid, *Adv Atom Mol Phys*, 1968, 4, 13
[8] T Berces, *React Kinet Catal Lett*, 1977, 7, 379
[9] O Kajri and M J Berry, *Faraday Discuss Chem Soc*, 1977, 62, 127
[10] J R Stine and J T Muckerman, *J Chem Phys*, 1978, 68, 185
[11] (*a*) D R McLaughlin and D L Thompson, *J Chem Phys*, 1973, 59, 4393, (*b*) N Sathyamurthy and L M Raff, *J Chem Phys*, 1975, 63, 464
[12] S A Sonnleitner and C L Beckel, *J Chem Phys*, 1980, 73, 5405
[13] M M Madsen and J M Peek, *Atom Data*, 1971, 2, 171
[14] A J C Varandas and J Brandão, *Mol Phys*, 1982, 45, 857
[15] J N Murrell and K S Sorbie, *J Chem Soc, Faraday Trans 2*, 1974, 70, 1553
[16] H Akima, *J Assoc Comput Mach*, 1970, 17, 589, *Commun Assoc Comput Mach.*, 1972, 15, 914
[17] P M Agrawal, V Mohan and N Sathyamurthy, *Chem Phys. Lett*, in press
[18] (*a*) K C Kulander and M F Guest, *J Phys B*, 1979, 12, L501, (*b*) S Raynor and D R. Herschbach, *J Phys Chem*, 1982, 86, 1214, 3592, (*c*) S Raynor, personal communication.
[19] (*a*) F F Wall and R N Porter, *J Chem Phys*, 1962, 36, 3256, (*b*) H Mayne, J C Polanyi, S. Raynor and N Sathyamurthy, *J Phys Chem*, 1984, 88, 4064
[20] Numerical Algorithms Group, Mark 8 Library, Daresbury Laboratory, U K
[21] D R McLaughlin and H F. Schaefer, III, *Chem Phys Lett*, 1971, 12, 244
[22] G Das, A F Wagner and A C Wahl, *J Chem Phys*, 1978, 68, 4917
[23] P J Bertoncini, G Das and A C Wahl, *J Chem Phys*, 1970, 52, 5112
[24] P Huxley, D B Knowles, J N Murrell and J D Watts, *J Chem Soc, Faraday Trans 2*, 1984, 80, 1349

(PAPER 4/1499)